MECHANIC AND FEM SIMULATION OF ACTIVE VIBRATION CONTROL IN STRUCTURAL SYSTEMS BY USING INTERNAL MASS RECONFIGURATION

A Thesis Submitted to the College of

Graduate Studies and Research

In Partial Fulfillment of the Requirements

For the Degree of Doctor of Philosophy

In the Department of Mechanical Engineering

University of Saskatchewan

Saskatoon

By

EHSAN SHARBATI

Permission to Use

In presenting this thesis in partial fulfilment of the requirements for a Postgraduate degree from the University of Saskatchewan, I agree that the Libraries of this University may make it freely available for inspection. I further agree that permission for copying of this thesis in any manner, in whole or in part, for scholarly purposes may be granted by professor W. Szyszkowski who supervised my thesis work or, in their absence, by the Head of the Department or the Dean of the College in which my thesis work was done. It is understood that any copying or publication or use of this thesis or parts thereof for financial gain shall not be allowed without my written permission. It is also understood that due recognition shall be given to me and to the University of Saskatchewan in any scholarly use which may be made of any material in my thesis.

Requests for permission to copy or to make other use of material in this thesis in whole or part should be addressed to:

Head of the Department of Mechanical Engineering

University of Saskatchewan

Saskatoon, Saskatchewan, Canada, S7N 5A9

ABSTRACT

Relative motion of different parts of a structure can affect its vibrations that may be amplified or attenuated. If such a motion is properly devised, it can lead to continuous attenuation of vibration and thus be used for eliminating vibration of the structure, as has been shown in previous works on an oscillating physical pendulum. In this thesis, the moving mass/structure interaction is investigated in order to devise a numerical tool for modeling such problems for arbitrary structures. The mass (or masses) motion patterns are synchronized such that a continuous attenuation of vibration is achieved. This is a novel technique for active vibration control especially for structures where the conventional stationary actuators are not practical.

To analyze the dynamic response of such moving mass-structure systems, a ‘composite’ beam element is introduced that permits extending the conventional finite element formulation (and software) and explicitly identifying the Coriolis and centripetal inertia effects of the moving mass. A numerical procedure is then proposed in which these inertia effects are included in the finite element model as fictitious transversal and axial forces applied to the beam element currently being traversed by the moving mass. The proposed approach is verified by comparing the results with those available in the literature as well as exact solutions possible for the pendulum.

Numerical simulations show that the periodic relative motion of the mass with a constant frequency normally tends to amplify vibration. In order to obtain a continuous attenuation, a proper synchronization method is required. It is demonstrated that such synchronization can be determined to be effective for vibration control of different structures. In particular, for structures which can be treated as uni-modal, like the pendulum, the method is quite effective with a relatively high vibration attenuation rate. For multi-modal structures, represented by beams and frames in this thesis, the vibration attenuation is less smooth and more complicated mass motion

patterns and synchronization methods are needed. It is concluded that the effectiveness of such active vibration control depends on how distinct the vibration modes to be attenuated are in the frequency spectrum.

ACKNOWLEDGMENTS

I would like to express my sincere appreciation to my supervisor, Professor Walerian Szyszkowski. I thank him for the thoughtful insights, guidance advice and for generously taking time to discuss various aspects of this research. I also would like to thank him for all the knowledge he taught me during the courses which I took with him.

My sincere thanks go to my advisory committee members: Professors R. Burton, B. Sparling and R. Fotouhi, for their invaluable suggestions and assistance during my studies and also their useful comments on the final version of my thesis.

Finally, I would like to thank the Department of Mechanical Engineering and College of Graduate Studies and Research for providing me with the financial support in form of scholarship and teaching assistantship and also my supervisor Professor W. Szyszkowski for financially supporting me with his research assistantship.

Dedication

To

my beloved parents Abbas and Zahra

TABLE OF CONTENTS

page

LIST OF TABLES

LIST OF FIGURES

Figure page

NOMENCLATURE

Roman Symbols:

A	Cross section area
a_N	Moving mass Normal acceleration
a_t	Moving mass tangential acceleration
C	Damping matrix of the element
C_e	Total damping matrix of the element
C_{eo}	Regular standard damping matrix of the element
F	External deriving force on the moving mass
f^c	Coriolis force vector
$\bar{f}_i^c$	Nodal proportional Coriolis force of the ith node
F_{cp}	Centripetal force of the moving mass
F_{cr}	Coriolis force of the moving mass
F_g	Weight of the moving mass
F_{in}	Conventional vertical inertia force of the moving mass
F_k	External concentrated force acting on the beam
F_N	Normal interaction force between the moving mass and the structure
F_t	Tangential interaction force between the moving mass and the structure
F_x	Horizontal force applied initially on the frame
F_y	Vertical force applied initially on the frame

E	Young's modulus of the beam
g	Gravity of earth
$\bar{g}$	Non-dimensional gravity of earth
I	Inertia moment of the beam's cross section
I_o	Pendulum's inertia moment about its pivot
K	Stiffness matrix of an element
J	Rotary inertia
$\bar{J}$	Non-dimensional rotary inertia
K_e^g	Total stress stiffening matrix of the element
K_{eo}	Bending stiffening matrix of the element
l_c	Distance from gravity center of the pendulum to its pivot
L	Length of the beam
L_e	Length of the element
M	Global mass matrix of the structure
M_e	Time dependent mass matrix of the element
M_{em}	Time-variant part of the mass matrix of the element
M_{eo}	Standard mass matrix of an element
$\dot{M}_e$	Rate of mass matrix of an element
m	Mass of the moving body
$\bar{m}$	Non-dimensional mass of the moving body
m_f	Total mass of the frame structure

m_p	Mass of the pendulum
n	Axial force along the beam
n_m	Axial fictitious force representing the mass centripetal force
$\mathbf{N}$	Shape functions vector of the element
N_i	ith shape functions of the element
R_s	Beam's radius of curvature at mass current position
s	Moving mass relative position
$\dot{s}$	Moving mass relative velocity
$\ddot{s}$	Moving mass relative acceleration
$\bar{s}$	Local position of the moving mass
$\hat{s}_i$	Distance from the ith node to the pendulum's pivot
s_L	Position of the guiding bar on the beam
s_0	Mean position of the moving mass sinusoidal motion
t	Time
$\bar{t}$	Non-dimensional time
T_p	Structure's current natural period
T_r	Reference time
$\bar{v}$	Non-dimensional velocity of the moving mass
v_i	ith node translational degree of freedom
w	Deflection of the beam
$\overline{w}$	Non-dimensional deflection of the beam
w_i	Deflection of the ith node

w_s Deflection of the beam at the current position of the mass

X Global nodal degrees of freedom vector

$\dot{X}$ Rate of nodal degrees of freedom vector

$\ddot{X}$ Second time derivative of nodal degrees of freedom vector

X_e Element's nodal degrees of freedom vector

$\dot{X}_e$ Element's nodal velocities vector

X_n nth modal shape of the beam

Greek Symbols:

$\delta(.)$ Dirac's function

Δt_i Integration time step

Δt_l Load step time increment

Δt_r Required time step for dynamic integration of finite element formulation

$\Delta\psi$ Phase adjustment of the moving mass sinusoidal motion

ε Dimensionless amplitude of the moving mass sinusoidal motion

φ Pendulum's angle

$\dot{\varphi}$ Pendulum's angular velocity

$\dot{\varphi}_e$ Average rotational velocity of the element

$\ddot{\varphi}$	Pendulum's angular acceleration
ρ	Material density of the element
Θ_n	Weight of nth mode shape in the beam's response
θ_i	ith node rotational degree of freedom
θ_s	Beam's slope at current mass position
θ_e	Average rotation of the element
$\dot{\theta}_e$	Average angular velocity of the element
ω	Frequency
ω_0	Initial frequency of the pendulum
ω_m	Frequency of the moving mass sinusoidal motion
ω_n	nth natural frequency of the beam
ω_P	Current frequency of the pendulum's oscillation
ψ	Phase of the moving mass sinusoidal motion
ζ	Active damping ratio

CHAPTER 1

INTRODUCTION

1.1 General Idea and Motivation

In this thesis, a novel approach for controlling vibration of a mechanical structure is proposed and applied to structures with different levels of complexity. The approach is based on moving one or more parts of the structure (or extra masses) such that its vibration is attenuated. As it has been shown in previous works, Stilling (2000), the relative motion of a mass attached to a structure can amplify or attenuate its vibration. Natural examples of such structure (or system) are when children push the swing higher by moving their body (amplifying vibration) or when gymnasts perform high bar maneuvers. The control/mechanical aspects of this concept are examined on the examples shown in Figure 1-1 starting from the simpler one (uni-modal) to more complicated (multi-modal). Figure 1-1(a) shows a rigid pendulum which is oscillating

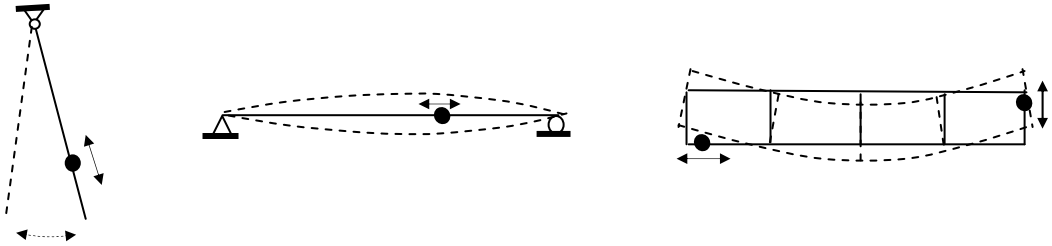

Figure 1-1 Structural systems with moving masses.

about a pivot and a mass is moving along its length to control the vibration. This problem has been analyzed analytically in Szyszkowski and Stilling (2005) and the current research is in fact an extension of this work. Figures 1-1(b) shows a beam with flexural vibration controlled by a horizontally moving mass. A frame with flexible (horizontal and vertical) sides which has in-

plane vibration (undergoing bending on the sides) is shown in Figure 1-1(c). For this case, more than one mass, as shown in the figure, is needed for fully controlling its vibration.

To the best of author's knowledge, the proposed vibration control approach has not been reported in any previous work. In addition to its novelty, the approach can be particularly useful for active vibration control of structural system for which passive dampers or standard 'stationary' actuators are either inefficient or not practical. Examples of such structures are outer space systems where the standard actuators are difficult to apply and the natural damping is usually very low.

1.2 Main Objectives

The main objectives of the current research are first to understand the dynamics of the moving mass-structure interaction. A new FEM approach is proposed and formulated for modeling such interactions properly. As will be shown in the following chapters, the relative movement of the mass makes the dynamic equations complicated and analyzing such problems is challenging, mainly due to the presence of Coriolis effects. In fact, in most of the previous works which have been done on modeling problems involving relative mass motion, the effect of the Coriolis acceleration was ignored (this will be discussed in more detail in section 1.2). It will be shown in chapter 2 and 3 that including the effect of Coriolis acceleration is essential for correct modeling of the moving mass-structure interaction for control purposes. The proposed FEM approach is then applied to a beam element and the results are verified. The significance of handling moving mass-beam interaction is that it allows us to model any other moving mass-structure interaction. For instance, for the plane structure shown in Figure 1-2, which is modeled by appropriate elements, the relative motion of the mass m can be modeled by introducing real or fictitious

beam elements along its moving path and then using the formulation for handling moving mass-beam interaction.

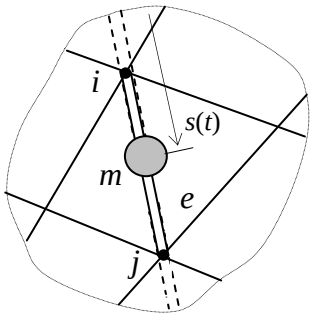

Figure 1-2 A plane structure with a moving mass.

Finally, the last objective of the research is to devise the mass (or masses) motion pattern(s) such that vibration of the main is continuously attenuated. As it will be shown later, this is quite challenging since the relative mass motion normally excites vibration (as in a child's swing). Also, for more complicated structures where more than one vibration mode is present in the dynamic response, the proper synchronization of the mass motion is harder to achieve; if the mass motion pattern is not carefully devised, the vibration attenuation is not continuous.

1.3 Literature Review

As already mentioned, the analysis and simulation of structural systems with imposed relative motion of components appears to be challenging. For instance, in the moving mass-beam interaction problem, which is the model for analyzing moving vehicle-bridge interaction, the Dirac's function is present in the dynamic equation of the system (this will be explained in more detail in Chapter 3). This complicates the equations and, thus, obtaining analytical or numerical solutions is very difficult. Due to the vast potential applications of modeling the vehicle-bridge interaction, the moving mass-beam problem has been studied in several previous works.

The most important aspect of modeling the moving mass-beam interaction problem is how the dynamic equations of the system are derived and analyzed. The critical point in deriving these equations is how the mass motion acceleration is treated. In the early works, for instance Kryloff (1905) and Timoshenko (1911), the mass is simply modeled as a moving force, where the force is representing its weight. In fact, all the inertia effects of the mass are ignored and the problem is reduced to a moving force-beam problem. Due to the relative simplicity of the dynamic equations in this case, it has also been used in more recent works where the problem is complicated in other aspects. For example, in Henchi and Fafard (1997) and Zheng et al. (1997), several moving forces travel along a multi-span beam. In Watanabe et al. (1997), the mass motion is sinusoidal. In Nguyen and Duhamel (2006), non-linear effects are included in the beam equation. Finally in Garinei and Risitano (2008) a traveling force which is varying in time is applied on the beam.

The most commonly used model for calculating the moving mass acceleration is to include the transversal acceleration of the mass in addition to its weight. In such models, the mass acceleration caused by transversal motion of the beam (to be referred to as the mass conventional acceleration) is included. This approach has been used in several previous papers, like Rieker and Trethewey (1999) and Ichikawa et al. (2000), and will be discussed in more detail in chapter 3. As will be shown in following chapters, the moving mass has an acceleration, which is referred to as Coriolis acceleration, as a result of its the relative motion. In these resources, the effect of the Coriolis acceleration is ignored and only the weight and conventional acceleration of the mass are considered.

In some of the previous works, however, the effect of Coriolis acceleration is included in addition to the effect of mass conventional acceleration. In most of these works, like Nikkhoo et

al. (2007), Siddiqui et al. (2003) and Schneider et al. (1983), the focus is limited to the constant velocity case. It is important to note that the mass is normally moving along a disturbed (and thus curved) beam. This, as will be discussed in Chapter 3, causes another component of acceleration in the mass which can be referred to as centripetal acceleration. In a few of the previous papers on the beam problem, the effect of this acceleration is, along with all other mass accelerations, including Coriolis and conventional accelerations, considered. Examples of these works are Michaltsos and Kounadism (2001), Sadiku and Leipholz (1987), Yang and Wu (2001) and Yang et al. (2004).

Another aspect of such moving mass problems is the numerical method used for solving the dynamic equations of the system. These methods vary from the finite difference method, like in Xu et al. (1997), infinite series, for instance in Jiang et al. (2003) and Yang and Lin (2005), the application of Green's function, like in Foda and Abduljabbar (1998), and the Finite Element Method, for instance in Yang and Wu (2001), Yang et al. (2004) and Lou (2004). The advantage of using Finite Element Method over the other methods is that it can be extended for modeling more complicated structures, as discussed in section 1.1. Also, the solution obtained by using infinite series does not always converge (this will be discussed in Chapter 3). Thus, this method appears to be the most effective method for solving such problems.

It is also noted that the methodology of deriving finite element formulations in Yang and Wu (2001) and Yang et al. (2004) is different than what is used in this research. In particular, the interaction force between the moving mass and the beam, as well as the geometrical constraint, are involved in their methodology. However, in the approach proposed here, the finite element formulation is handled such that there is no need for including the interaction forces and the geometrical constraint (this will be discussed in more details in the following chapters).

To the best of the author's knowledge, in all these previous works, the purpose was to model the interaction of a moving mass and the beam and no attempt to use the relative mass motion for control purposes has been done. Only in Szyszkowski and Stilling (2005) and Stilling and Szyszkowski (2002), the moving mass has been used to control oscillation of a rigid pendulum. It has been shown in these works that, normally, the relative mass motion along the pendulum results in amplification of vibration or the occurrence of parametric resonance, where the pendulum oscillation amplifies and attenuates periodically. Consequently, it was shown that synchronizing the mass motion such that the pendulum's oscillation is continuously attenuated is challenging. As it will be shown in this research, this task is even more challenging for more complicated (multi-modal) structures like beams and frames.

1.4 Outline of the Thesis

The problem of controlling oscillation of a rigid pendulum, which is rotating about a pivot point, is investigated first by the finite element. For this purpose, in Chapter 2 a combined moving mass-beam element is proposed and a new procedure to incorporate such an element into the conventional FEM formulation is presented. The results obtained by the FEM approach are verified by comparing them with an analytical solution available for the problem. This phase is vital for validation of the proposed FEM approach. Finally, a procedure for synchronizing the mass motion such that it continuously attenuates the pendulum's oscillation is devised and proven to be effective for controlling its vibration.

In Chapter 3 of the thesis, the proposed FEM formulation based on the combined beam element is extended to fully handle the interaction of a moving mass and a flexible beam. Next, for validation, the results obtained from FEM are compared to the results available in the literature and also to our numerical solutions based on an infinite series. Once verification of the

FEM results is done, the effect of including/excluding different mass acceleration terms, in particular the Coriolis and centripetal accelerations, on the solution is studied. New strategies for the mass motion pattern has to be investigated for obtaining continuous attenuation of vibration, mainly due to the presence of more vibration modes in the beam's dynamic response. These strategies are tested on examples which are presented in this chapter. Finally, for each example, the mass motion pattern is optimized for obtaining the maximum attenuation effects.

In Chapter 4, the vibration control of a frame is studied. The frame is composed of several beams which are attached to one another. The problems considered in this chapter include controlling frame's vibration when the several modes are initially excited. Also, more than one mass is used for vibration control. Various patterns of the masses' motion in different parts of the frame are investigated. Like the previous chapter, the masses' motion patterns are optimized for maximizing the attenuation effects.

CHAPTER 2

CONTROLLING VIBRATION OF A AN OSCILLATING PENDULUM

2.1 Introduction

In this chapter the proposed vibration control approach will be formulated and applied for controlling vibration of a pendulum which is oscillating about a pivot point. As shown in Figure 2-1, a pendulum is supported from a pivot point O in the gravity field and is free to oscillate about this point. Once it is disturbed from its rest vertical position, the pendulum will oscillate about the pivot point. Then, it is aimed to attenuate this vibration by moving a mass *m* along the pendulum as illustrated in Figure 2-1. As will be discussed in more detail in the following sections, the mass motion should be predefined (or synchronized) such that continuous attenuation is secured. This predefined motion is obtained by applying the external force *F*, which for instance can be applied on the mass from a motor connected to an actuator. Once the mass motion over time is known (that is $s(t)$ is defined where *s* is the location of the mass on the pendulum as shown in Figure 2-1) the force *F* can be calculated by using dynamic equilibrium of the mass along the pendulum. It is also assumed that any friction between the mass and the pendulum is included in force *F*.

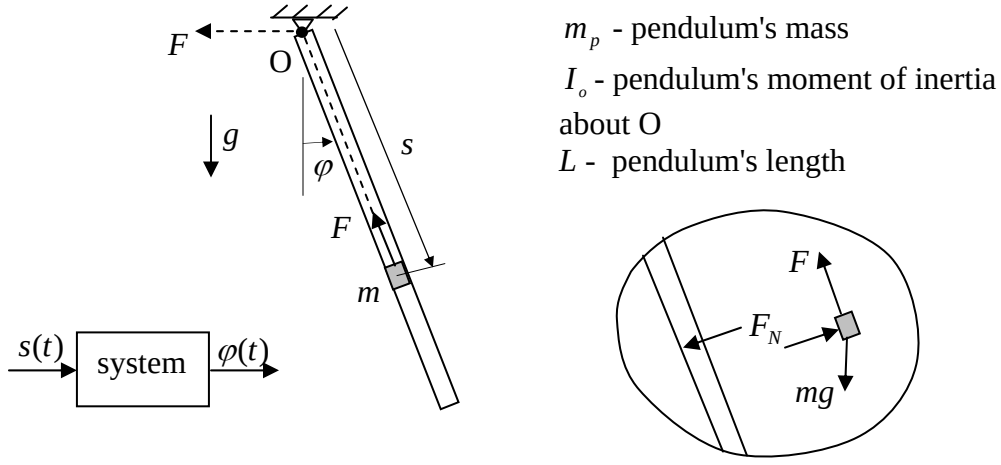

.

Figure 2-1 Scheme of an oscillating pendulum with a mass moving along its length.

In this chapter, first the dynamic equations of the moving mass-pendulum system are obtained. It will be shown that a numerical solution can be obtained by integrating these equations. This solution will be referred to as the exact solution since it's based on the exact dynamic equations. Then, a Finite Element Method (FEM) approach for solving this problem will be proposed. This approach can be verified by comparing the results obtained based on it to the exact solution. In the following chapters, this FEM approach is generalized to be used for more complex structures.

2.2. Deriving Exact Dynamic Equations

For the system shown in Figure 2-1 there are two possible approaches for obtaining the governing dynamic equations. In the first approach, the moving mass and the pendulum are separated as shown in the insert of the figure. Since we assume that the pendulum has only a rigid body rotation about the pivot, the only interacting force which should be considered is F_N, which is acting on the mass and the pendulum as illustrated in the figure. The other forces acting on the mass are mass weight and the external (driving) force F. From the kinematics of the moving mass, which states it's moving along the rotating pendulum, its acceleration along and perpendicular to the pendulum's directions can be found as:

$$a_t = \ddot{s} - s\dot{\varphi}^2 \tag{2.1}$$

$$a_N = s\ddot{\varphi} + 2\dot{s}\dot{\varphi} \tag{2.2}$$

where φ is the pendulum's angle with respect to vertical axis, a_t is the mass acceleration along the pendulum and a_N is the mass acceleration perpendicular to the pendulum. The mass dynamic equilibrium can then be written as:

$$m(\ddot{s} - s\dot{\varphi}^2) = -F + mg\cos\varphi \tag{2.3}$$

$$m(s\ddot{\varphi} + 2\dot{s}\dot{\varphi}) = F_N - mg\sin\varphi \tag{2.4}$$

where m is the mass of the moving body. The equation for the pendulum can be written by taking the moment of all the forces acting on it about the pivot point as:

$$I_0\ddot{\varphi} = -m_p g l_c \sin\varphi - sF_N \tag{2.5}$$

where m_P is the mass of the pendulum, I_0 is its inertia moment about the pivot and l_c is the distance from gravity center of the pendulum to the pivot. By eliminating F_N from Eq. (2.4) and (2.5) the governing dynamic equation for the system can be obtained as:

$$(I_o + ms^2)\ddot{\varphi} + 2m\dot{s}s\dot{\varphi} + g(m_p l_c + ms)\sin\varphi = 0 \tag{2.6}$$

It is noted that the force *F* did not appear in the derivation of Eq. (2.6) which means including or excluding the friction between the mass and the pendulum only affects the calculation of the driving force *F*. This differential equation, in which φ and s are functions of time, can be solved numerically for φ once $s(t)$ is known (the proper initial conditions should also be used). In other words, once the mass motion pattern $s(t)$, which can be considered as the input to the system, is known the system output, $\varphi(t)$, can be calculated by integrating Eq. (2.6). This solution will be referred to as the exact solution since it is based on the exact dynamic equation of the system. In the following sections, a methodology for finding a proper pattern of mass motion, such that the pendulum's vibration, φ, is attenuated over time, will be proposed.

According to Eq. (2.6), it is observed that the term $2m\dot{s}s\dot{\varphi}$ (which is directly responsible for attenuation or amplification effects of the moving mass as will be discussed in next section) can be considered as the moment caused by the force $2m\dot{s}\dot{\varphi}$ about the pivot. On the other hand, the force $2m\dot{s}\dot{\varphi}$ may be called the Coriolis force as it is the inertia force of the mass due to its

Coriolis acceleration $2\dot{s}\dot{\varphi}$. This Coriolis force will also be identified in FEM formulation and will be shown to be resisting the motion for $\dot{s} > 0$ and amplifying it for $\dot{s} < 0$.

It is also worthy to note that the dynamic equation of the system, Eq. (2.6), can also be obtained without separating the moving mass and the pendulum. In other words, the pendulum and the moving mass are considered as one body, which in turn means that force F_N is internal and consequently does not appear in the equations. On the other hand, the mass moment of inertia of the entire system will be $I_o^{new} = I_o + ms^2$ which is generally time-varying since s is a function of time. As a result, the equation of motion should be written as:

$$\frac{d}{dt}[(I_o + ms^2)\dot{\varphi}] = -m_p g l_c \sin\varphi - mgs\sin\varphi \qquad (2.7)$$

Eq. (2.7) will be identical to Eq. (2.6) once the differentiation and also rearranging of the terms are done. The significance of deriving the equation of motion through Eq. (2.7) is that the internal force F_N did not appear in the derivation; however, the time derivative of angular momentum had to be used instead of the standard inertia mass moment-acceleration product. This methodology will be in following sections for FEM formulation.

2.3. Results Based on the Exact Dynamic Equation

Prior to proposing the FEM approach for the pendulum problem, it is interesting to investigate how the pendulum responds to different mass motion. To this end, Eq. (2.6) should be solved for different patterns of mass motion, $s(t)$, while it is normally assumed that the initial conditions for the pendulum are:

$$\varphi(0) = \varphi_0, \quad \dot{\varphi}(0) = 0 \qquad (2.8)$$

which means the pendulum starts moving from a disturbed static initial position. In general, Eq. (2.6) can be rewritten as:

$$\ddot{\varphi} + 2\xi(t)\omega(t)\dot{\varphi} + \omega(t)^2 \sin\varphi = 0 \tag{2.9}$$

where we have:

$$\xi(t) = \frac{ms\dot{s}}{\sqrt{g(I_o + ms^2)(m_p l_c + ms)}} \tag{2.10}$$

$$\omega(t)^2 = \frac{m_p l_c + ms}{I_o + ms^2} g \tag{2.11}$$

For small values of φ, Eq. (2.9) can be considered as a second order linear differential equation with a time-varying coefficient. That is, the relative mass motion, $s(t)$, causes the system's 'instantaneous' frequency $\omega(t)$ and the damping ratio $\xi(t)$ to be time-varying (see Eqs. (2.10) and (2.11)). Another important aspect of Eq. (2.9) is that the damping ratio, Eq. (2.11), is proportional to $\dot{s}$ which means it is positive for $\dot{s} > 0$ and is negative for $\dot{s} < 0$. Consequently, it is expected that vibration of the pendulum be attenuated when $\dot{s} > 0$ and be amplified when $\dot{s} < 0$. As already discussed in the introduction, this conclusion (which will also be verified through numerical examples) is the main idea for attenuating vibration by moving mass (or masses). The more general form of this conclusion states that if the mass moves away from the rotation center of the main body (in this case the pendulum), it causes attenuation of vibration and when it moves toward the rotation center it causes amplification.

From mathematical point of view, Eq. (2.9) is a more general case of a of class equations called Mathieu's equations. A more detailed study of mathematical aspects of Eq. (2.9) has been presented in Szyszkowski and Stilling (2005). In this section, we will briefly present the system response obtained by numerical integration of Eq. (2.6).

A tube of length L=1.4 *m* and mass M=2.75 *kg* made of aluminum with Young modulus of 70 *GPa* and a Poisson's ratio of 0.3 is tested. The outside and inside tube's diameters are 60 *mm* and 50 *mm* respectively. The beam elements' cross-sectional properties reflect the real area and bending stiffness of the tube. A mass m=1 *kg* can slide along the tube. The dynamic simulation always starts at t=0 when the pendulum is resting at $\varphi(0) = \varphi_0 = 0.1$ *rad*. The pendulum's angular position $\varphi(t)$ is calculated by using a fourth order Runge-Kutta's numerical integration procedure.

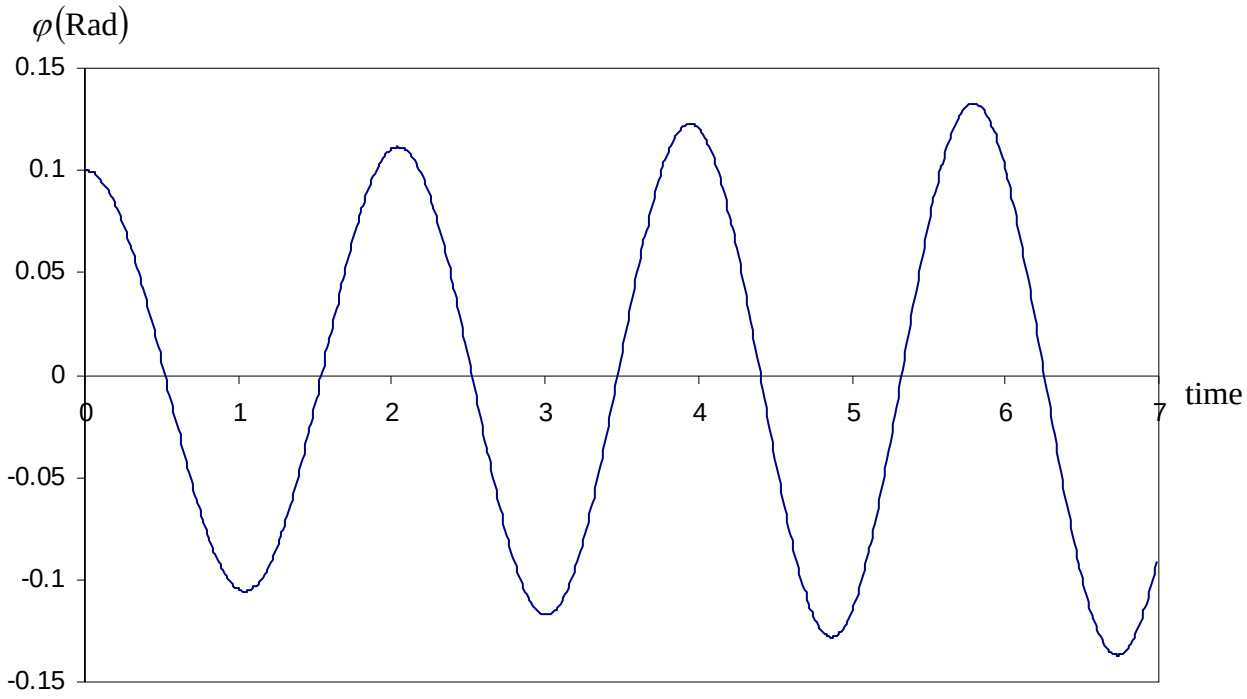

Figure 2-2 Pendulum response when the mass moves with a constant velocity of 0.2 m/s towards the pivot.

As a first example, assume that the mass moves with a constant velocity towards the pivot point with the motion given by $s(t) = 1.4 - 0.2t$. In this motion, the mass starts moving from the tip of the pendulum with a constant velocity of 0.2 toward the pivot which is reached in 7 sec. The pendulum response, described by its angle versus time, is shown in Figure 2-2. Two important conclusions can be made by carefully studying this response. First, the amplitude of

the pendulum oscillations increases with time. This is what we expect since the mass velocity is negative and, consequently, according to Eq. (2.10), the damping ratio should also be negative. The calculated damping ratio is around -1.44% based on the solution shown in Figure 2-2.

Second, it is observed that the period of pendulum oscillation decreases as the mass moves towards the pivot: the period of vibration is 2.04 *s* for the first cycle and it is 1.85 *s* for the third one. Based on Eq. (2.11), the instantaneous period should be 2.04 *s* for t=1, 1.89 for t=3 and 1.84 for t=5, which shows a decreasing trend. However, for t=6 it is 1.87 and for t=7 it is 1.94 which is an increasing rate. This shows that in general, the instantaneous frequency calculated through Eq. (2.11) cannot be used since the equation only considers the inertia of the mass supposedly fixed at location *s*. In other words, the effects from the mass movements are not included in the equation.

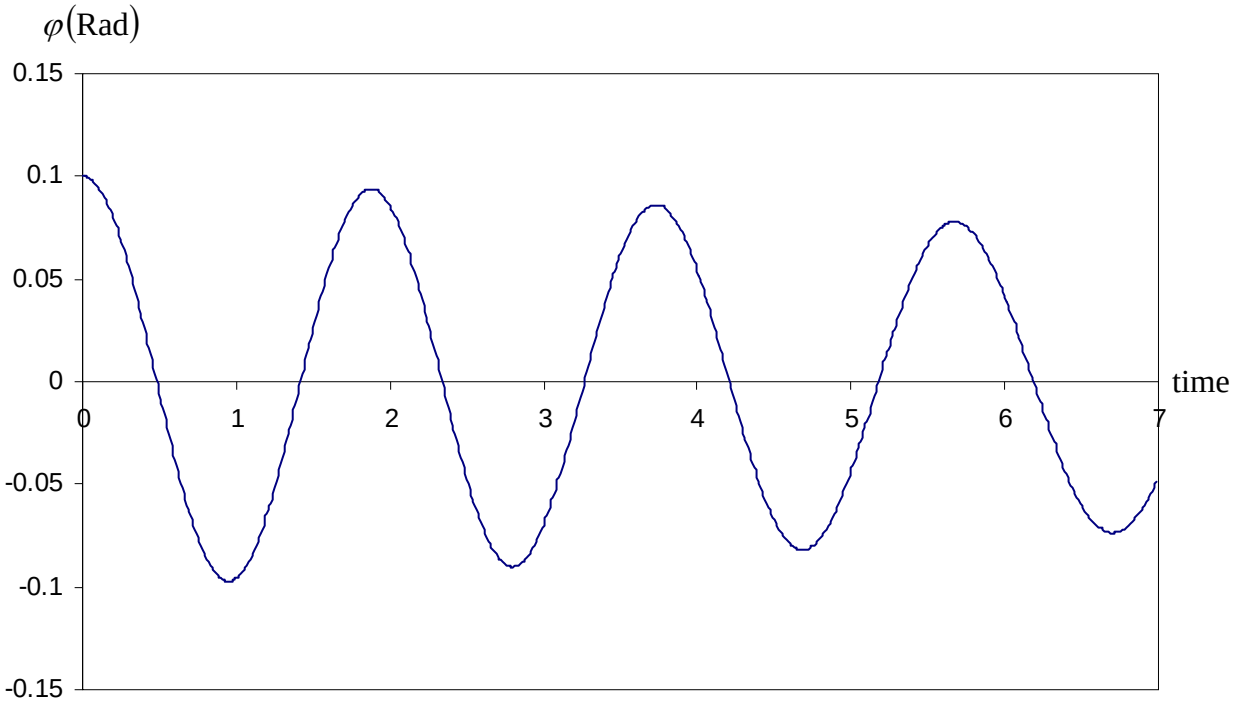

Figure 2-3 Pendulum response when the mass moves with a constant velocity of 0.2 m/s from the pivot to the pendulum's tip.

In the next example, it is assumed that the mass moves with a constant positive velocity away from the pivot point. For instance, the pendulum response when the mass motion is given by $s(t) = 0.2t$ is shown in Figure 2-3 (the mass starts its motion from the pivot point and moves all the way to the tip of the pendulum). As it is expected, this mass motion causes the pendulum vibration to attenuate since the mass velocity is positive and so should be the damping ratio (see Eq. (2.10)). From Figure 2-3 the damping ratio is estimated to be around 1.48%. Like the previous case, it is also observed that the period of vibration changes when the mass moves along the pendulum. This time, it is increasing from 1.88 *s* in the first cycle to 1.94 *s* in the third one. Based on Eq. (2.11) the instantaneous period is 1.87 for t=1 and 1.89 for t=6, which is again does not agree with the actual period since the mass velocity is not included in this equation. In other words, Eq. (2.11) only considers the fact that the mass is at some location *s* and its movement is disregarded. This effect will be discussed in more details in the following sections.

Based on the results shown in Figures 2-2 and 2-3, it is concluded that attenuation of vibration can be obtained if the mass moves away from the pivot. However, once the mass reaches the tip of the pendulum (and essentially stops at this point) attenuation effect will cease. As a result, for obtaining further attenuation, the mass has to move back to the pivot point to repeat the attenuating cycle (which is moving from the pivot to the tip). But the problem is the backward mass movement (from the tip to the pivot) will cause amplification. In fact, it can be shown that the amplification and attenuation effects caused by the mass motion to and from the pivot, are canceling out one another. This means that this periodic motion of the mass does not cause continuous attenuation (or amplification) of the pendulum's vibration. Consequently, more advanced strategies for mass motion should be developed for obtaining continuous attenuation. This was done in a previous work by Szyszkowski and Stilling (2005) where a synchronization

pattern for mass motion is proposed. In the following sections, more details on this strategy will be discussed.

2.4. Finite Element Formulation of the Problem

Consider the pendulum-moving mass structure shown in Figure 2-1. To analyze this problem, the pendulum should first be discretized into finite elements, by using the beam elements, as shown in Figure 2-4a. In such a model, all the beam elements should be treated normally except for the element currently being traversed by the mass since it interacts directly with this element. Two different approaches are generally available for modeling this interaction, as described below.

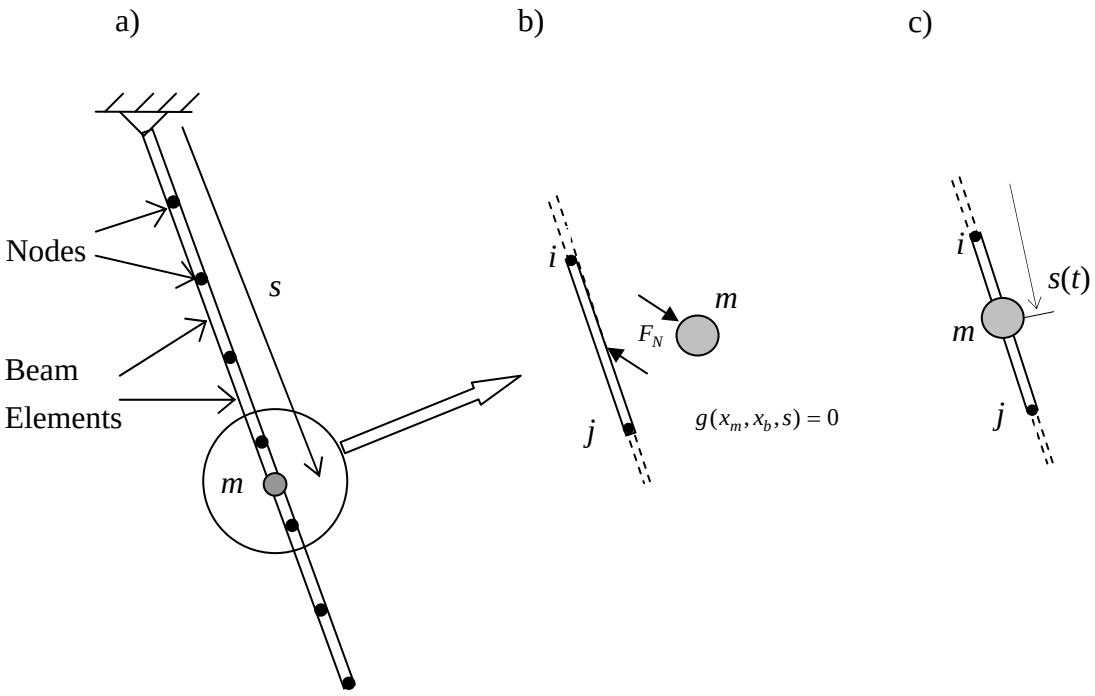

Figure 2-4 Finite element model of the pendulum and moving mass interaction.

1- In the *standard* approach, the beam and the moving mass would be treated as separate bodies, as indicated in Figure 2-4b. The mass matrix for the beam element and the mass matrix for mass *m* would be both time-independent. However, the equations of motion for these two bodies would involve the interaction forces between them (denoted symbolically by F_N in the figure). In turn, these forces could be eliminated by using the geometrical constraints in the form $g(x_m, x_b, s)=0$ representing the relationships between the mass coordinates x_m, the beam coordinates x_b, and the traveling coordinate *s*(*t*) at the contact point. Such an approach was used in some of the previous works (like Y.B. Yang and Y.S. Wu 2001, Y.B. Yang et al. 2004 and P. Lou 2004) to simulate the vehicle-bridge or vehicle-rail interactions.

2- The approach proposed in this research is to consider the moving mass *m* and the traversed beam as one 'combined' beam element with variable inertia properties. Consequently, the mass matrix of this element must be time-varying. This new approach is depicted in Figure 2-4c.

The main advantage of this proposed approach is that, in such a 'combined' element, the interaction forces F_N will formally disappear (since it is internal or self-equilibrated) and the geometrical constraints $g(x_m, x_b, s)=0$ will be met automatically. All the effects due to the relative motion in the element are completely recovered from its time-varying mass matrix, as will be shown in the next section. These effects will be represented by the forces at nodes *i* and *j* directly related to the pattern of relative motion *s*(*t*), which is convenient for simulating control aspects of the problem. Also, a significant numerical effort may potentially be saved because in this approach the properties of the system's stiffness are not affected by the relative motion and the inertia properties are affected only locally.

The inertia forces associated with the combined element depicted in Figure 2-4c will be handled differently than in the standard FEM formulation: the mass matrix of such an element,

$M_e(t)$, is time varying which means the mass matrix assembled for the system, $M(t)$, is time varying too. However, the system's total mass remains constant. This allows formulating the inertia forces as the derivatives of momentum instead of the usual product of mass and acceleration (such a formulation is also considered more convenient for various systems involving structure-fluid interaction in which the total mass is constant). Therefore, the equation of motion for the problem with the combined elements can be written in the form:

$$\frac{d}{dt}[M(t)\dot{X}] + C\dot{X} + KX = F \qquad (2.12)$$

where $M(t)$ is the mass matrix of the combined element which includes the effect of both mass relative motion and the beam. Matrices C and K are the usual damping and stiffness matrices. The nodal degrees of freedom and nodal forces are denoted by X and F, respectively. Eq. (2.12) can be rewritten as:

$$M(t)\ddot{X} + \dot{M}(t)\dot{X} + C\dot{X} + KX = F \qquad (2.13)$$

In the new approach, the extra 'mass-rate' term $\dot{M}(t)\dot{X}$ will reflect the effects of the rate of internal mass movement which takes place in the combined (traversed) element. Therefore, this term has to be determined only for this element. The remaining terms in Eq. (2.13) (i.e. $M(t)\ddot{X}$, $C\dot{X}$, $K\dot{X}$, and F) can be routinely handled by most commercial FEM software. Nevertheless, it is worth noticing that the first term in Eq. (2.13) includes only the current position of the moving mass, and the fact that the mass is moving along the beam element is not considered. As it will be demonstrated later, the mass-rate $\dot{M}(t)$ is proportional to the relative velocity of the moving mass, and vector $\dot{X}$ can be approximated by an average rotation of the traversed element. Therefore, $\dot{M}(t)\dot{X}$ can be interpreted as representing the Coriolis type effects in the system. Using the notation $f^c = \dot{M}(t)\dot{X}$ allows rewriting Eq. (2.13) in the form:

$$M(t)\ddot{X} + C\dot{X} + KX = F - f^c \tag{2.14}$$

where vector f^c will be referred to as the Coriolis force. This vector will be non-zero only for the nodes of the beam element being traversed by the mass *m* (i.e. for the remaining elements $f^c = 0$). Note that, in Eq. (2.14), the whole problem is formulated in such a way that the left-hand-side (LHS) of this equation can be handled by any standard FEM software, while the right-hand-side (RHS) contains a new additional force f^c that will represent all the effects due to the relative motion. This force vector is discussed in detail next.

2.4.1 Calculating Vector of Coriolis Forces

To determine the vector f^c, the combined element in Figure 2-4c is considered in the local coordinate $\bar{s}$, where $0 \le \bar{s} = [s(t) - s_i]/L_e \le 1$ is indicated in Figure 2-5a (L_e is the element's length, the moving mass current position is denoted by *s*, and s_i is the location of the i^{th} node). The deflection is expressed by $v = \mathbf{N}X_e$, where the shape functions vector for this element is **N**, and the vector X_e represents the corresponding degrees-of-freedom (DOF) in the local coordinate system. The mass matrix for the element can formally be determined from

$$M_e(t) = \int_{L_e} \mathbf{N}^T [A\rho + m\delta(s' - s)]\mathbf{N}ds' = M_{eo} + m\mathbf{N}^T(\bar{s})\mathbf{N}(\bar{s}) \tag{2.15}$$

where *A* and ρ are the area and material density respectively, $\delta(.)$ is the Dirac Delta function (s' is an integration variable), and $M_{eo} = \int_{L_e} \mathbf{N}^T A\rho\mathbf{N}ds'$.

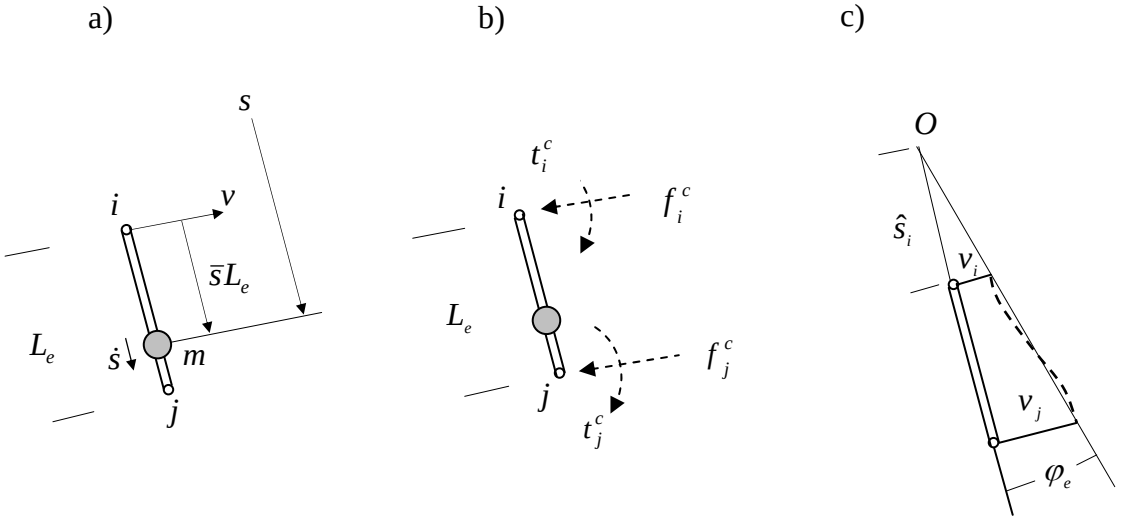

Figure 2-5 The traversed beam element and the Coriolis forces.

Matrix M_{eo} in Eq. (2.15) is a standard constant mass matrix for the beam element. The second term of Eq. (2.15) is obtained by utilizing the properties of Dirac's function. This time-dependent term assigns mass *m* at the current location $s(t)$ to particular DOFs of the element. The time dependency is hidden in vector $\mathbf{N}(\bar{s})$ in which the shape functions have to be taken at the current mass location defined by $\bar{s}(t)$. By chain-differentiating Eq. (2.15), the mass-rate matrix of the element is obtained as:

$$\dot{M}_e(t) = m\frac{\dot{s}}{L_e}\frac{\partial}{\partial \bar{s}}(\mathbf{N}^T\mathbf{N}) \qquad (2.16)$$

As can be seen, the mass-rate matrix for this particular element is proportional to $\dot{s}$, the velocity of the traveling mass. Clearly, the mass matrices are time-independent for the remaining elements of the pendulum (i.e. $M_e(t) = M_{eo}$ and $\dot{M}_e = 0$ for such elements).

As already mentioned, the standard Hermitian beam element is used in this research to model the main structure (i.e. pendulum in this example). The DOFs of this element are

$X_e^T = \begin{bmatrix} v_i & \theta_i & v_j & \theta_j \end{bmatrix}$, where v_i and θ_i are the nodal deflections and rotations, respectively. The corresponding shape functions are the cubic polynomials (i.e. $N_1 = 1 - 3\bar{s}^2 + 2\bar{s}^3$, $N_2 = L_e(\bar{s} - 2\bar{s}^2 + \bar{s}^3)$, etc.). By substituting these shape functions into Eq. (2.16) the mass-rate term $\dot{M}_e \dot{X}_e$ gives the following Coriolis-type force vector:

$$f_e^c = \dot{M}_e \dot{X}_e = \frac{m\dot{s}}{L_e} \frac{\partial}{\partial \bar{s}} \begin{bmatrix} N_1^2 & N_1 N_2 & N_1 N_3 & N_1 N_4 \\ & N_2^2 & N_2 N_3 & N_2 N_4 \\ & & N_3^2 & N_3 N_4 \\ sym & & & N_4^2 \end{bmatrix} \begin{bmatrix} \dot{v}_i \\ \dot{\theta}_i \\ \dot{v}_j \\ \dot{\theta}_j \end{bmatrix} = \begin{bmatrix} f_i^c \\ t_i^c \\ f_j^c \\ t_j^c \end{bmatrix} \tag{2.17}$$

The components of vector $f_e^c = \begin{bmatrix} f_i^c & t_i^c & f_j^c & t_j^c \end{bmatrix}^T$ are indicated in Figure 2-5b ($f_e^c = 0$ for the remaining elements). It is important to notice that, according to (2.17), these components are proportional to the relative velocity of the moving mass $\dot{s}$ and are also affected by the current mass position (via the shape functions **N**) and the rate of variation of the element's DOFs. In general, the values of $N_i(\bar{s}(t))$ and $\dot{X}_e(t)$ can be determined in the numerical procedure at any time instant. However, the features of forces f_e^c can be understood better if the 'average' rotational velocity of the element (see Figure 2-5c) defined by $\dot{\varphi}_e = (\dot{v}_j - \dot{v}_i)/L_e$ is used. The instantaneous center of rotation is positioned at point *O* at the distance $\hat{s}_i = L_e v_i / (v_j - v_i)$ from node *i*. Next, assuming that the Coriolis effects are mostly due to the element's average angular velocity, which permits approximating $\dot{\theta}_i \cong \dot{\theta}_j \cong \dot{\varphi}_e$, the nodal velocity vector becomes: $\dot{X}_e^T = \dot{\varphi}_e \begin{bmatrix} \hat{s}_i & 1 & \hat{s}_j & 1 \end{bmatrix}$, where $\hat{s}_j = \hat{s}_i + L_e$. Substituting it into (2.17) renders the ratios $f_{i,j}^c / m\dot{s}\dot{\varphi}_e$ (the normalized Coriolis forces) and $t_{i,j}^c / m\dot{s}\hat{s}_i\dot{\varphi}_e$ (the normalized Coriolis torques) dependent only on $\bar{s}$ and the ratio of $\hat{s}_i / L_e$. For the Hermitian cubic shape functions and for the

ratio of $\hat{s}_i / L_e = 5$ these dependencies are plotted in Figure 2-6. The nodal Coriolis forces defined this way will be referred to as *consistent*.

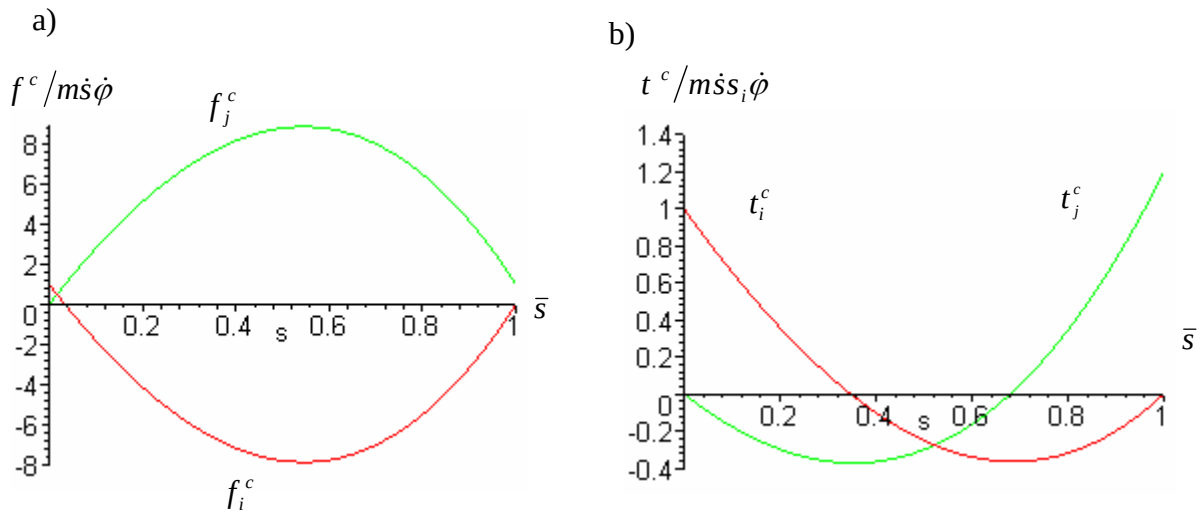

Figure 2-6 Variation of the consistent nodal forces and moments with $\bar{s}$.

For the pendulum problem case, further approximations of the Coriolis forces can be obtained by assuming that the beam is rigid and hinge-connected at the nodes, which is equivalent to assuming the combined element's deflection is defined by $v = (1-\bar{s})v_i + \bar{s}v_j$. This, in turn, allows using the following 'simplified' shape functions in Eq. (2.17): $N_1 = (1-\bar{s})$, $N_2 = 0$, $N_3 = \bar{s}$, $N_4 = 0$. The corresponding set of forces, referred to as the *lumped* nodal Coriolis forces, is calculated from

$$f_e^c = \frac{m\dot{s}\dot{\varphi}_e}{L_e}\begin{bmatrix} -2N_1 & 0 & N_1 - N_3 & 0 \\ & 0 & 0 & 0 \\ & & 2N_3 & 0 \\ symm & & & 0 \end{bmatrix}\begin{bmatrix} \hat{s}_i \\ 1 \\ \hat{s}_j \\ 1 \end{bmatrix} = \begin{bmatrix} f_i^c \\ t_i^c \\ f_j^c \\ t_j^c \end{bmatrix} \qquad (2.18)$$

The nodal moments are now automatically zero (i.e.: $t_i^c(\bar{s}) = t_j^c(\bar{s}) = 0$), and the nodal forces are $f_i^c(\bar{s}) = m\dot{s}\dot{\varphi}(N_1 - N_3 - \hat{s}_i / L_e)$ and $f_j^c(\bar{s}) = m\dot{s}\dot{\varphi}(2N_3 + \hat{s}_i / L_e)$; also, $f_i^c(\bar{s}) + f_j^c(\bar{s}) = m\dot{s}\dot{\varphi}$. Since the shape functions applied are linear, the *lumped* nodal Coriolis forces are also linear in terms of distance $\bar{s}$ and depend on the ratio of $\hat{s}_i / L_e$. For example, the normalized *lumped* forces in terms of $\bar{s}$ for $\hat{s}_i / L_e = 5$ are plotted in Figure 2-7.

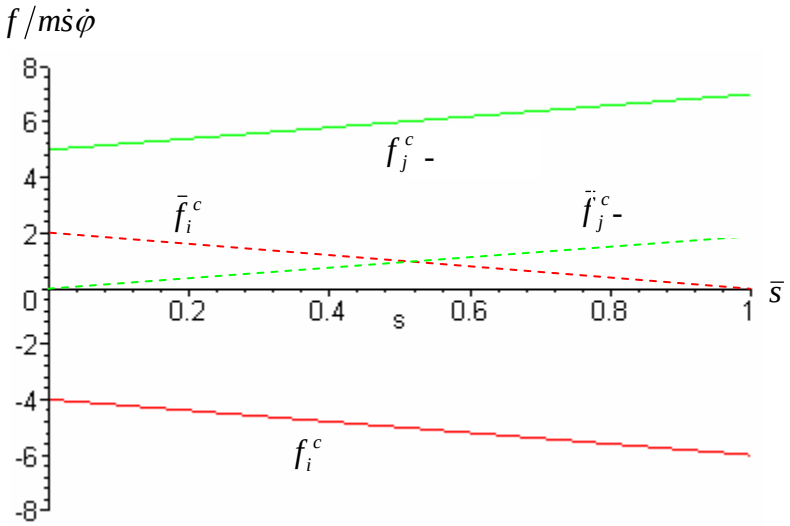

Figure 2-7 Variation of the lumped and proportional nodal forces and moments with $\bar{s}$.

Finally, the simplest version of the Coriolis forces can be obtained by noticing the following property of the *consistent* forces plotted in Figure 2-6: namely, it can directly be verified that the resultant torque of these forces about the instantaneous rotation center of the element is $T_0^c(\bar{s}) = 2m\dot{s}\dot{\varphi}_e[\hat{s}_i(1-\bar{s}) + \hat{s}_j\bar{s}]$. For example, if m is at node i then from Figure 2-6 one has $f_i^c(0) = m\dot{s}\dot{\varphi}$, $t_i^c(0) = m\dot{s}\hat{s}_i\dot{\varphi}$, and $T_o^c(0) = 2m\dot{s}\dot{\varphi}_e\hat{s}_i$. Similarly if m is at node j then $f_j^c(1) = m\dot{s}\dot{\varphi}$, $t_j^c(1) = m\dot{s}\hat{s}_j\dot{\varphi}$, and $T_0^c(1) = 2m\dot{s}\dot{\varphi}_e\hat{s}_j$.

On the other hand, the same resultant torque is generated by 'equivalent' force $F_m^c = 2m\dot{s}\dot{\varphi}_e$ acting at the current location of mass *m*. The nodal Coriolis forces referred to as *proportional* are generated by breaking F_m^c into two nodal forces $\bar{f}_i^c(\bar{s})$, $\bar{f}_j^c(\bar{s})$ proportionally to the distance of mass *m* (and force F_m^c) from particular nodes, that is

$$\bar{f}_i^c(\bar{s}) = (1-\bar{s})F_m^c \tag{2.19}$$

$$\bar{f}_j^c(\bar{s}) = \bar{s}F_m^c \tag{2.20}$$

The sequence of generating the above forces is sketched in Figure 2-8.

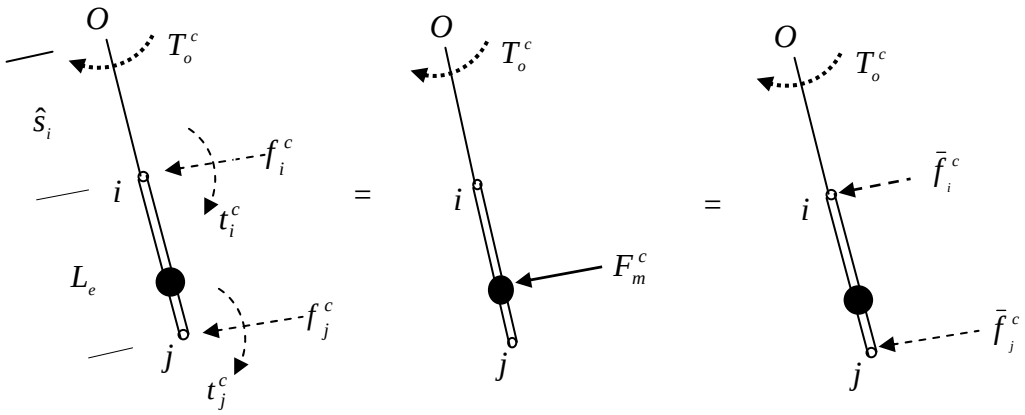

Figure 2-8 Generation of the proportional nodal Coriolis forces.

It should be noticed that the *proportional* Coriolis nodal forces vary linearly with $\bar{s}$ in the range $0 \le \bar{f}_{i,j}^c \le F_m^c = 2m\dot{s}\dot{\varphi}_e$ and are independent of the $\hat{s}_i / L_e$ ratio. These forces are also plotted in Figure 2-7.

It can be easily verified that the *lumped* nodal Coriolis forces defined by (2.18) give the resultant torque about *O* equal to $T_0^c(\bar{s}) = 2m\dot{s}\dot{\varphi}_e[\hat{s}_i(1-\bar{s}) + \hat{s}_j\bar{s}]$ as well. As a result, all the forces discussed above, which represent and replace the mass-rate term $\dot{M}_e\dot{X}_e$, are best

illustrated by the equivalent force $F_m^c = 2m\dot{s}\dot{\varphi}_e$, which is clearly defined as a classical Coriolis force due to the relative velocity $\dot{s}$ of mass *m* moving along the beam that rotates with the angular velocity $\dot{\varphi}_e$. On the other hand, one may note that the three types of the nodal Coriolis forces (i.e. *consistent, lumped*, and *proportional*) are quite different. These differences are indicated in Figure 2-9*abc* for mass *m* at node *i* ($\bar{s}$ =0) and in Figure 2-9*def* for mass *m* at the midpoint ($\bar{s}$ =0.5). All forces and torques are given in terms of $f_0 = m\dot{s}\dot{\varphi}_e$. Note that the magnitudes and directions of these forces to represent the mass *m* at a particular location are quite different. Despite that, our simulation results (to be presented in the following sections) were, somewhat surprisingly, similar for each type of the above forces applied.

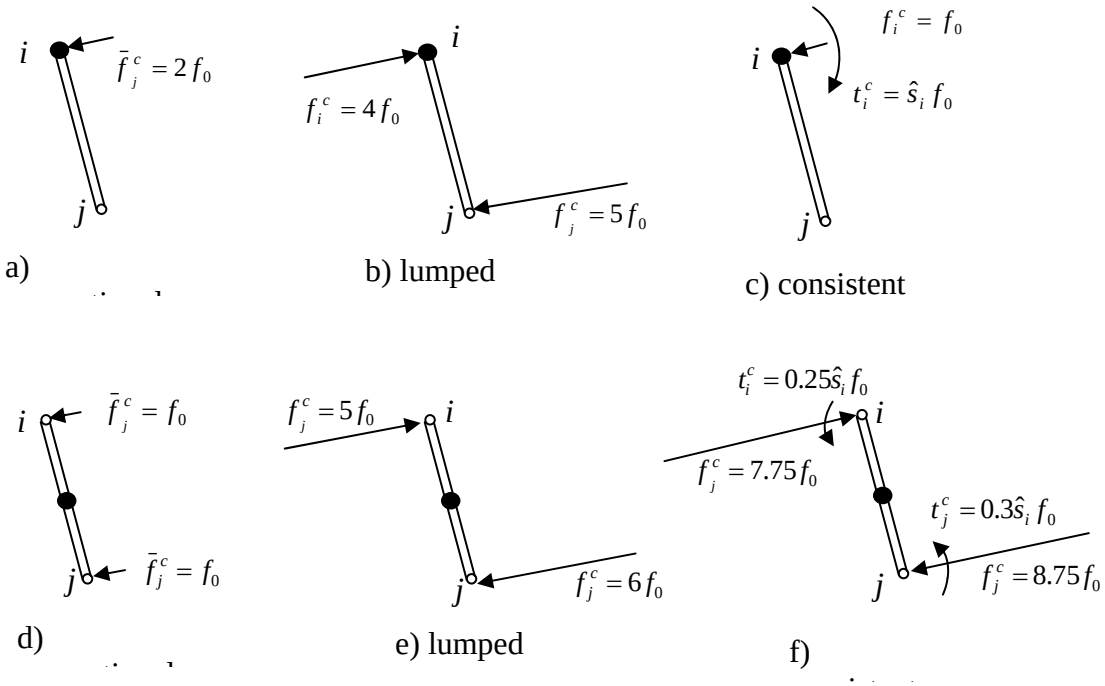

Figure 2-9 Components of Coriolis force f^c for different patterns if *m* is at node i (a, b, c), and if *m* is in the middle of element (d, e, f).

The fact that all these forces produce identical torque about the center of instantaneous rotation ($T_0^c(0) = 2m\dot{s}\dot{\varphi}_e\hat{s}_i$ for forces in cases (*abc*), and $T_0^c(0.5) = m\dot{s}\dot{\varphi}_e(\hat{s}_i + \hat{s}_j)$ for forces in cases (*def*)) seems to be the main reason for such an apparently low sensitivity of the simulation results to the type of the nodal Coriolis forces adopted.

2.4.2 The Proposed FEM Procedure

To model the pendulum problem by FEM, first the structure is discretized to finite elements as shown in Figure 2-4. As already mentioned, the standard FEM equation should be solved for all the elements except the one which is traversed by the moving mass. In this element, the generalized FEM equation, Eq. (2.14), should be solved where the Coriolis force vector is calculated from either Eq. (2.17), Eq. (2.18) or Eqs. (2.19) and (2.20). Also, it should be noted that the mass matrix in Eq. (2.14) includes both the standard (time-independent) mass matrix of a beam element and the time-varying matrix which corresponds to the moving mass (see Eq. (2.15)). As a result, for the element being traversed by the mass, not only should the Coriolis force vector be calculated and applied, but also the time-varying part of element's mass matrix should be considered. This portion of the mass matrix can be obtained from:

$$m_{ij}^e(\bar{s}_k) = mN_i(\bar{s}_k)N_j(\bar{s}_k) \qquad (2.21)$$

If Hermit's cubic polynomials are used as the shape functions, then $m_{ij}^e(\bar{s}_k)$ defines the *consistent* mass matrix. If the linear shape functions (the same as those used in Eq. (2.18) for obtaining the *lumped* Coriolis forces) are substituted into Eq. (2.21) then the diagonal *lumped* mass matrix is obtained, in which certain portions of mass *m* are assigned to particular nodes according to:

$$m_i^e(\bar{s}_k) = m(1-\bar{s}_k)(1+\bar{s}_k\,\tfrac{L_e}{s_i}) \qquad (2.22)$$

and

$$m_j^e(\bar{s}_k) = m\bar{s}_k[1-(1-\bar{s}_k)\tfrac{L_e}{s_j}] \qquad (2.23)$$

The *lumped* mass matrices can be applied in ANSYS, with the help of the '*ekill/ealive*' procedure. However, this is somewhat inconvenient (and in some cases not practical) because the masses to be used must be declared *prior* to starting the procedure (i.e. for the entire ANSYS' load step).

Finally, the masses assigned to a particular node can also be calculated as follows:

$$m_i^e(\bar{s}_k) = m \text{ if } \bar{s}_k \le 0.5 \text{ and } m_j^e(\bar{s}_k) = m \text{ if } \bar{s}_k > 0.5 \qquad (2.24)$$

According to the above formula, the mass *m* is placed at the nearest node for current time step. The mass matrix defined by Eq. (2.24) can be referred to as the *step* mass matrix. This matrix can be implemented in ANSYS by using 'ekill' and 'ealive' commands as will be discussed later. As mentioned earlier, different methods of calculating the time-varying portion of the mass matrix will affect only the accuracy of the term $M_e\ddot{X}_e$. The numerical experiments indicate, however, that using either type of the mass matrices presented above provides sufficient accuracy of the system's simulation. This is generally a consequence of the fact that the errors due to simplifications in the term $M_e\ddot{X}_e$ are much less important than the errors due to the accuracy of calculating forces f_e^c (the Coriolis force vector).

The FEM procedure can now be proposed as the following steps.

1- The pendulum is modeled by using regular hermitian beam elements in the available FEM software (which is ANSYS in this research). A procedure for solving the transient dynamics problems will be applied. In this research, the Newmark's constant-average-acceleration procedure available in ANSYS is used.

2- In the pendulum's sector to be traveled by the mass (or the whole pendulum as in some examples presented in the following sections), nodal mass elements with properties identical to the moving body are created at each node.

3- At each time step, the current position of the mass is determined. Then, the Coriolis force vector f^c is calculated for the element currently traversed using one of the equations (2.17) - (2.20) and the DOF's known from the previous time step. Only one mass element which is closest to the current position of the mass is activated and all other mass elements are deactivated. This is done by using the 'ekill' and 'ealive' commands available in ANSYS.

4- The current time step is solved and the next time step can be started, in which only step 3 is to be repeated.

Steps 2 and 3 of the above procedure are in fact modeling the interaction of the moving mass and the main structure. They include considering the inertia effect of the mass at each instance (by activating/deactivating mass elements), as well as the effect of mass relative motion (by calculating and applying Coriolis force). In this procedure, the mass motion can have any arbitrary pattern. For more basic patterns, on the other hand, the procedure can be simplified significantly. For example, if the mass moves with a constant velocity, then the time step and element length can be adjusted such that the mass is located on a node at each time step. This will eventually simplify the procedure for calculating Coriolis forces as well as the procedure for including the time-varying part of the mass matrix. Also, if the mass motion is sinusoidal, with a constant amplitude and frequency of oscillation, then a similar simplification can be applied where the time step and element size are adjusted such that the mass is located on a node at each time step.

2.4.3 The numerical integration issues

It is assumed that one of the standard integration schemes will be applied to integrate the equations of motion (2.14). In particular, the Newmark's constant-average-acceleration procedure available in the ANSYS software will be used in the numerical testing. As already mentioned, in order to handle the relative motion problems, besides the routine calculations dealing with the LHS of Eq. (2.14), the Coriolis force f_c must be additionally determined and applied in the RHS of this equation. How to perform the latter operation is the main subject of this section. In particular, the time-steps required to secure sufficient accuracy of the numerical integrations are discussed. Essentially, the integration time step may be viewed as the time interval of sampling of the continuously changing system's state. The changes to be monitored in the problem considered include the following:

- The motion of the structure. The time step at which this motion is updated, which can also be considered as the time step for integrating LHS of Eq. (2.14), will be referred to as Δt_i. At this stage the purpose of simulating the mass-structure interaction is to control the system's fundamental mode of vibration. We assume that the structure motion is characterized by the current period T_p of this mode. Normally, the time step $\Delta t_i \le T_p / 20$ would be required to recreate it accurately. In other words, this integration time step will secure accuracy of the solutions if the mass is located at a certain stationary point on the pendulum.
- The variation of the Coriolis forces. As demonstrated in the previous section, the values of these nodal forces vary when the mass is traversing a particular beam element. Then the components of f^c change locations when entering the next element. The time step at which the Coriolis force vector is updated is referred to

as Δt_l and is in fact the so-called load-step in the ANSYS' procedure. The time duration Δt_l is also used to control the variation of the mass matrix in time. As already mentioned, the changes to $M(t)$ in Eq. (2.14) can be executed in ANSYS program by applying the '*ekill*' and '*ealive*' commands, which allow removing/placing the mass m (or its fractions) at a sequence of nodes in proper times to mimic the mass movement along the structure.

In the actual ANSYS code, there are two time period parameters to control the integration: Δt_i which is the integration time step and Δt_l which is the load step time increment. As already mentioned, a value of $T_P / 20$ for Δt_i is normally sufficient for obtaining acceptable accuracy when only the integration of the LHS of Eq. (2.14) is considered. Generally, as will be shown later, the value of Δt_l has to be much smaller for obtaining acceptable accuracy in calculations of the Coriolis force vector. On the other hand, it should be noted that in the ANSYS code, the integration time step has to be smaller than or equal to the load step time increment. Consequently, if Δt_l is sufficiently small for accurate calculation of the Coriolis force vector, then Δt_i will automatically be small enough, and, the accuracy of the integration procedure will be secured.

2.4.4 Different variation of the proposed approach

The approach proposed in section 2.4.2 can be used for any mass motion pattern. However, as mentioned earlier, if the mass motion is simple, for instance if it moves with a constant velocity or has sinusoidal motion with constant frequency, the approach can be simplified considerably. In the simplified approach, to be referred to as procedure I, the nodes in the vicinity of the mass

motion are placed such that at each time step, Δt_l, the mass is exactly located on a node. This adjustment can be done by using the predefined pattern of mass motion. For instance, if the mass moves with a constant velocity v_0, then by placing nodes on equal distance of $v_0 \Delta t_l$ as shown in Figure 2-10a, it is guaranteed that the mass is exactly on a node at the beginning of each load step. As another example, if the mass motion is given by $s = s_0(1 - \varepsilon \sin(\omega_0 t))$, where s_0, ε and ω_0 are constant, the nodal points can be placed such that the mass is at a certain node at each load step (i.e. for $t = \Delta t_l$, $t = 2\Delta t_l$, etc.). However, the load step time increment for this case should be a divisor of the mass motion oscillation period (that is $\Delta t_l = T_m / n$ where $T_m = 2\pi / \omega_0$ and n is an integer). The advantage of this procedure is that instead of using Eq. (2.17), or one of its equivalences, the Coriolis force, $2m\dot{s}\dot{\varphi}$, can be directly applied on the node where the mass currently is. Also, since the mass is at a node in the beginning of the load step, the modeling of the time-varying part of the mass matrix is simplified to activating the mass element at the current mass position.

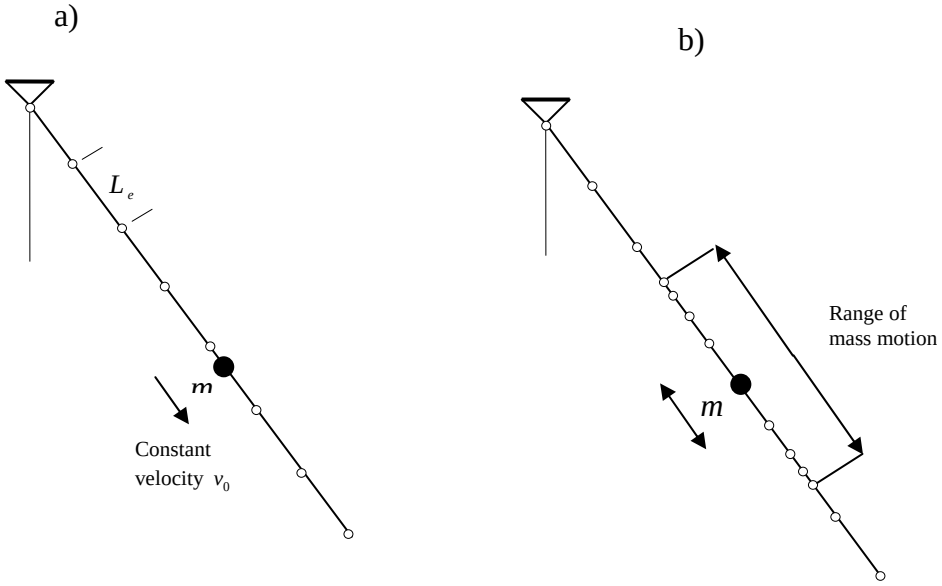

Figure 2-10 Different discretization scheme of the FEM models in procedure I.

While the FEM approach, including calculation of Coriolis force vector and mass matrix, is simpler using procedure I it has some disadvantages. First, it can only be applied if the mass motion pattern is simple and straight forward, like when the mass moves with a constant velocity. As it will be discussed later, continuous attenuation is obtained when the mass motion is sinusoidal with a varying oscillation frequency. This pattern of motion cannot be modeled by using procedure I. Also, since in this method the element size and the time step are dependent (they have to be adjusted such that the mass is exactly at a node in each load step), normally the element size has to be shortened when the time step decreases. Consequently, in some cases where a small time step should be used for obtaining sufficient accuracy, a small element size should also be used, which eventually leads to divergence of the solutions. In fact, as will be shown later, procedure I cannot produce acceptable solutions for certain patterns of the mass motion.

On the other hand, the element size and time step are independent in the regular proposed approach, which is based on the procedure mentioned in section 2.4.2. This version of the proposed approach, to be referred to as procedure II, is more general and can be applied for any pattern of mass motion. While the formulation is more complicated in this procedure, it will be shown that the procedure is capable of producing results with sufficient accuracy for any pattern of mass motion.

Procedure II can be applied in different ways depending on which formulation is used for calculating and applying the Coriolis force vector. In other words, the Coriolis force vector can be calculated and applied based on either Eq. (2.17), Eq. (2.18) or (2.19) and (2.20) which will result in three different ways of applying procedure II. The results based on these different methods will be discussed later.

The time step Δt_l in procedure II can be characterized by Δt_t, the time that is required for the mass to traverse one element. The time period Δt_t can be determined once the pattern of mass motion, $s(t)$, is given. Generally, Δt_t should be such that $s(t_i + \Delta t_t) - s(t_i) = L_e$ where L_e is the size of the beam element being traversed. Obviously, Δt_l cannot be larger than Δt_t because in this case the mass would be in one element at the beginning of the load step but end up in a different element at the end of the load step. This is in conflict with the assumption implied in formulation of the proposed approach that the mass should be in one certain element for the entire load step. On the other hand, Δt_l can be smaller than Δt_t, which means that during the time period that the mass is traversing that certain element, the Coriolis forces and time-varying mass matrix are updated more than once. As will be discussed later, the accuracy of the solution depends on both Δt_l and the element size.

2.5 Testing the Proposed Approach for Pendulum Problem

The problem considered in section 2.3 will be analyzed again in this section by using the proposed FEM approach. The pendulum and mass parameters are the same as those in section 2.3; however, different patterns of mass motion will be considered here which include:

Pattern 1: Mass *m* moving with a constant velocity (and in one direction). If $\dot{s} = v_0 = const$ then, as shown previously, the damping ratio will be always positive (attenuation) for $v_0 > 0$ and negative (amplification) if $v_0 < 0$.

Pattern 2: Periodic motion of *m*. When mass *m* is oscillating around $s = s_0$ according to $s(t) = s_0(1 - \varepsilon \sin \omega_m t)$ with an amplitude of εs_0 and a frequency of ω_m, Eq. (2.9) represents a self-exciting system. If ω_m=constant then the system response is characterized by amplification

alternating with attenuation, which generally results in a beating phenomenon. However, if the mass motion is synchronized in such a way that $\omega_m = 2\omega(t)$ then a continuous attenuation with $\xi(t) \approx$ constants (a viscous-like damping) can be achieved. Examples for the beating phenomenon and continuous attenuation will be presented in the following sections.

The parameters for the pendulum and the mass, which are the same as those considered in section 2.3, were selected in such a way that if mass *m* is at s_0=1.1 then its instantaneous frequency (see Eq. (2.11)) is $\omega(s_0) = \pi$ (in *rad*/*sec*). It would correspond to the period t_p^0 = 2.00 *sec* of the pendulum's oscillations if the mass *m* was *stationary*. This period would vary from t_p^0=1.84 *sec* for s_0=0 to t_p^0=2.13 *sec* for s_0=1.4 *m* with the same parameters.

If the mass was fixed, then the integration time-step $\Delta t_r \approx t_p / 20 \approx 0.1 sec$, would normally be recommended to analyze this case almost independently of the number of elements used. In fact, our numerical tests rendered accurate results by using only two (or more) elements. This is important to remember because for the moving mass cases much more elements will have to be used. Also, much shorter time-steps, like Δt=0.01*sec*, will be applied for the moving mass cases which reduces any 'stationary' errors of integration in the analysis to a negligible level.

Some general features of the numerical errors of integrating Eq. (2.14) and their relations to the relative motion of mass are briefly discussed first. Assume that the mass' path is given by $s(t) = 1.4 - 0.2t$ (the exact solution for this case has been shown in Figure 2-2). The pendulum's oscillations should be amplified because *m* is moving towards the rotation center with velocity $v_0 = -0.2\ m/sec$ resulting in $c(t) < 0$.

Based on the exact solution the initial amplitude φ_0=0.1 increases in the 3rd cycle to φ_3=0.133, as expected. Then, the FEM model with 28 elements of the length $L_e = 0.05m$ is

integrated by applying Procedure I with the *proportional* nodal Coriolis forces applied. For this case the duration of the load-step Δt_l is equal to 0.05/0.2=0.25 *sec* and $\Delta t_i = 0.01 sec$. This means that every transfer from one node to the next is integrated using 25 time-steps. The results are shown as the '*FEM*' curve in Figure 2-11 (the exact solution is also shown in the figure). The 3rd amplitude increases to φ_3=0.117 (which is about 13% *less* than the exact value). Also, the time to reach this amplitude is *longer* than the exact time, which indicates some period elongation. Generating the negative amplitude error and positive period error appears to be a general feature of the numerical integration of the FEM model for any $v_0 < 0$. The opposite is true for $v_0 > 0$, i.e. the amplitude error becomes positive, and the period error becomes negative (no such case is shown in Figure (2.11), for the sake of brevity).

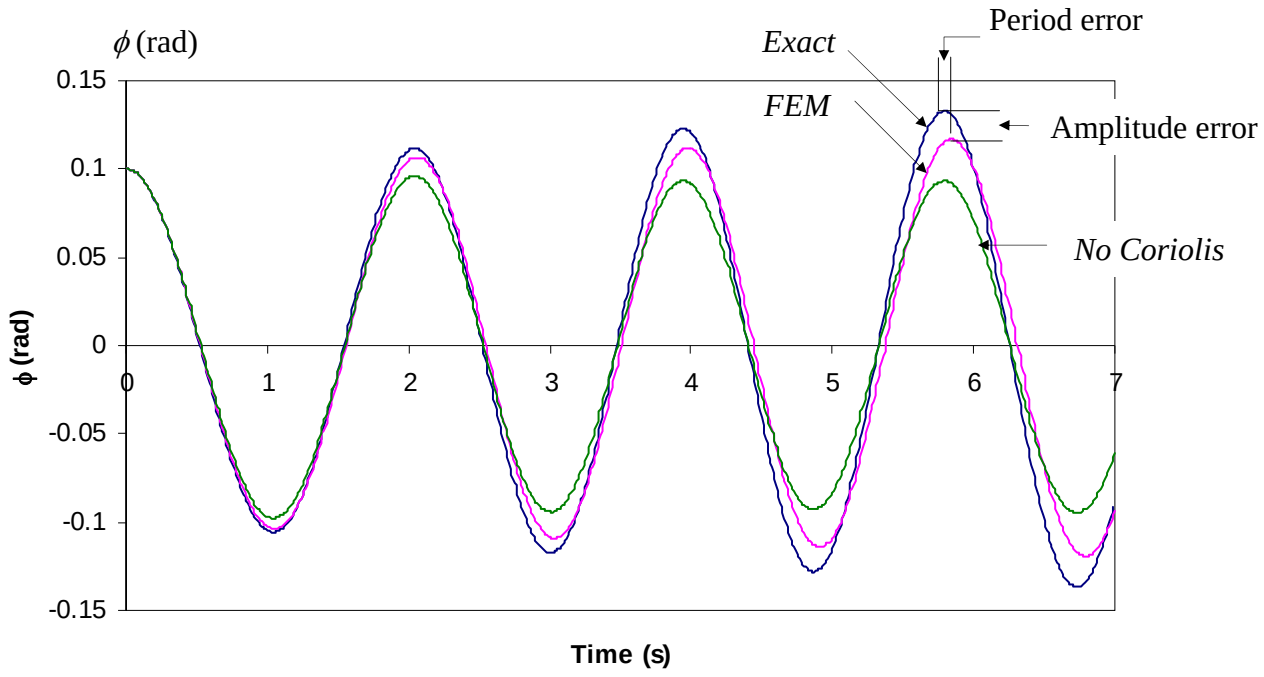

Figure 2-11 The pendulum's responses to mass motion with $v_0 = -0.2$ according to different analysis methods.

Next, some consequences of modeling the mass *m* traveling along the pendulum by applying the ANSYS standard procedure with '*ekill*' and '*ealive*' steps (which places/removes the mass in a sequence of nodes at proper times) are presented. One should realize that such an operation affects only the term $M(t)\ddot{X}$ in the equation of motion (2.13) by changing the system's mass matrix from $M(t_i)$ into $M(t_{i+1})$ when *m* is first assigned to node *i* at t_i and next reassigned to node *i*+1 at $t_{i+1} = t_i + \Delta t_t$. However, the fact that mass *m* is moving with velocity $\dot{s}_i$, while in node *i* at t_i, is completely omitted (similarly as velocity $\dot{s}_{i+1}$ at node *i*+1 for t_{i+1} is omitted). This in turn means that $\dot{M}(t)\dot{X}$ =0, or that all the Coriolis effects discussed in the previous section are omitted as well. Using such an approach, the curve denoted as '*No Coriolis*' in Figure 2-11 was obtained. Note that, according to this curve, the system is actually attenuated, with the 3rd amplitude reduced to φ_3=0.092 (this amplitude increased to 0.133 for the exact solution), indicating that such a simulation misinterprets completely the effects of the mass motion on the structure's behavior.

It is also interesting to mention that omitting the term $\dot{M}(t)\dot{X}$ is equivalent to neglecting the term $2m\dot{s}s\dot{\varphi}$ in Eq. (2.6) (or assuming $\zeta(t) = 0$ in Eq. (2.9)). Consequently, the standard FEM results obtained by applying only the '*ekill/ealive*' commands will approximate, no matter whether $\dot{s}$ =0 or $\dot{s} \neq 0$, the solution to the pendulum-mass system's equation in the form:

$$(I_o + ms^2)\ddot{\varphi} + g(m_p l_c + ms)\sin\varphi = 0 \qquad (2.25)$$

The solution to this equation, which can be obtained by integrating it using Runge-Kutta method for example, is almost indistinguishable from the '*No Coriolis*' curve obtained from Newmark's integration of the FEM model (see Figure 2-11). This only indicates that the procedure

combining Newmark's integration with the '*ekill*/*ealive*' commands is accurate; however, the Coriolis effects are being completely overlooked.

2.5.1 Testing procedure I

Procedure I is well suited for constant velocity cases. For an assumed load step time interval Δt_l, all elements of the beam should be of the same length $L_e = |\Delta t_l v_0|$, as indicated in Figure 2-10. This procedure was already applied to obtain the 'FEM' curve in Figure 2-11 for the case of $v_0 = -0.2\ m/sec$ by using 28 elements of equal length. The amplitude error after three oscillations was about 13%, or about 4.3% per oscillation. The load-step duration $\Delta t_l = 0.25 sec$ and the time-step $\Delta t_i = 0.01 sec$ were applied (for this time-step the amplitude error per oscillation for a 'stationary' mass is around 0.05%). The relatively large error of integration for the moving mass' case can be attributed to a poor representation of the variation of the Coriolis forces in time (i.e. load-step time is too long). For this case, the load applied is sampled every $\Delta t_l = 0.25 sec$, while if the mass was 'stationary' then the time-step $\Delta t_r \approx 0.1 sec$ would be required to integrate the equations of motion for such a system accurately. This will give the ratio $\Delta t_l / \Delta t_r$ =2.5 which is apparently too big and produces the relatively large error of 13%. To reduce the error the load step time interval should be shortened. On the other hand, for a given mass velocity in Procedure I, the length of the element should also be reduced when the load step time increment decreases.

The effects of different Δt_l (Δt_r for the system is assumed to be 0.1*sec*) on the amplitude error for constant mass velocity cases are shown in Figure 2-12. These results were obtained using the *proportional* nodal Coriolis forces. As expected, the amplitude error decreases with the decreasing of the load step time interval. It is also observed that the error is slightly less for

positive velocities. For $\Delta t_l / \Delta t_r = 1$ the amplitude error is around 0.5%. Incidentally, for a 'stationary' mass, if $\Delta t_i = 0.1 sec$ is used, then the amplitude error is also around 0.5% (if $\Delta t_i = 0.02 sec$ that error decreases to 0.1%, and to 0.05% for $\Delta t_i = 0.01 sec$).

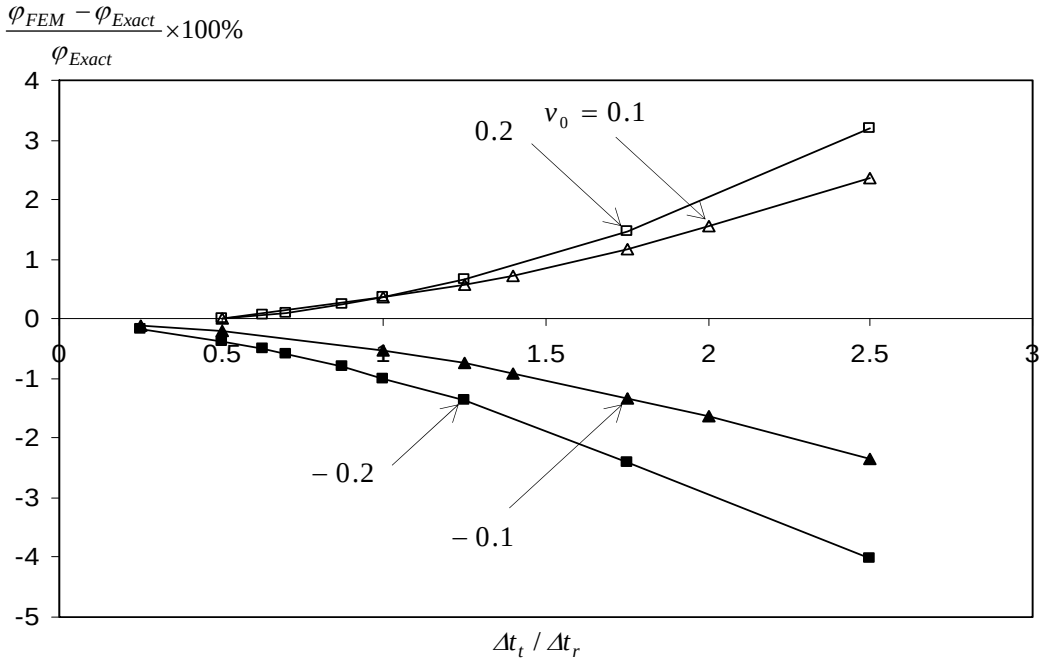

Figure 2-12 Effect of the load step time increment on the amplitude error for $\dot{s}$ =const.

Therefore, one may conclude that the amplitude error for this moving mass case is affected by the load step time Δt_l somewhat similarly as the amplitude errors for 'stationary' case are affected by the integration time step Δt_i. The difference is that any stationary case for the tube could be run with two or three elements, while the moving mass case requires, depending on the mass velocity, a much larger number of elements.

For example, if v_0=0.1*m/s* then L_e=10 *mm*, which means that 140 elements for 1.4 *m* long pendulum are needed to have Δt_l=0.1*s* (the case v_0=0.1*m/s* and Δt_l = 0.025*s* shown in Figure 2-12 was simulated using L_e=2.5 *mm* or 560 elements).

The effect of Δt_l on the period error is depicted in Figure 2-13. The irregularities of the curves are mostly due to inabilities to determine the period precisely from the ANSYS' output (the results, including the pendulum angle, are only available in instances which are multiplier of the integration time-step). Note that the percentage values for this error are about one order smaller than for the amplitude error. In conclusion, by considering the results in Figures 2-12 and 2-13, it is observed that sufficient accuracy can be obtained if $\Delta t_t / \Delta t_r \leq 1$.

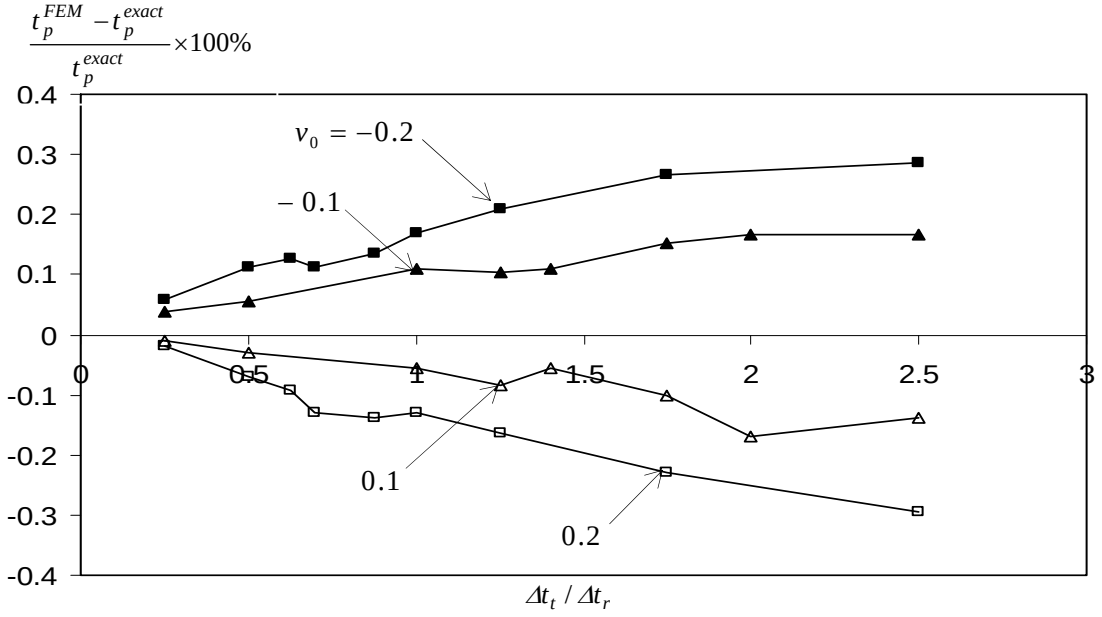

Figure 2-13 Effect of the load step time increment on the period error for $\dot{s}$ =const.

If the mass velocity varies, then fixing the time interval Δt_l leads to an irregular meshing of the beam, as shown in Figure 2-10b. In particular, the required L_e may become very small for the sectors of slow motion of the mass (such as at the vicinity of the turning points of any periodic motion). The numerical difficulties and the corresponding integration errors are illustrated on the example of a path given by $s(t) = s_0\left[1 - \varepsilon \sin\left(\omega_m^0 t\right)\right]$. If s_0 =1.1 *m* and ε =0.2 then the mass *m* oscillates between 0.88m and 1.32m. Recall that $\omega(s_0) = \pi$ *rad*/*sec* corresponds to the period t_p^0 = 2.00 *sec* of the pendulum's oscillations with the mass *m stationary* at s_0. If the frequency of the mass motion is constant and such that $\omega_m^0 = 2\omega(s_0) = 2\pi$ (or that the period of the mass motion is t_m^0 =1.00*sec*) then, according to Szyszkowski and Stilling 2005, such a motion should attenuate several cycles of the pendulum's oscillations followed by amplification of the subsequent cycles. The system's response for up to 20 *sec* (or about 10 pendulum's cycles) is presented in Figure 2-14.

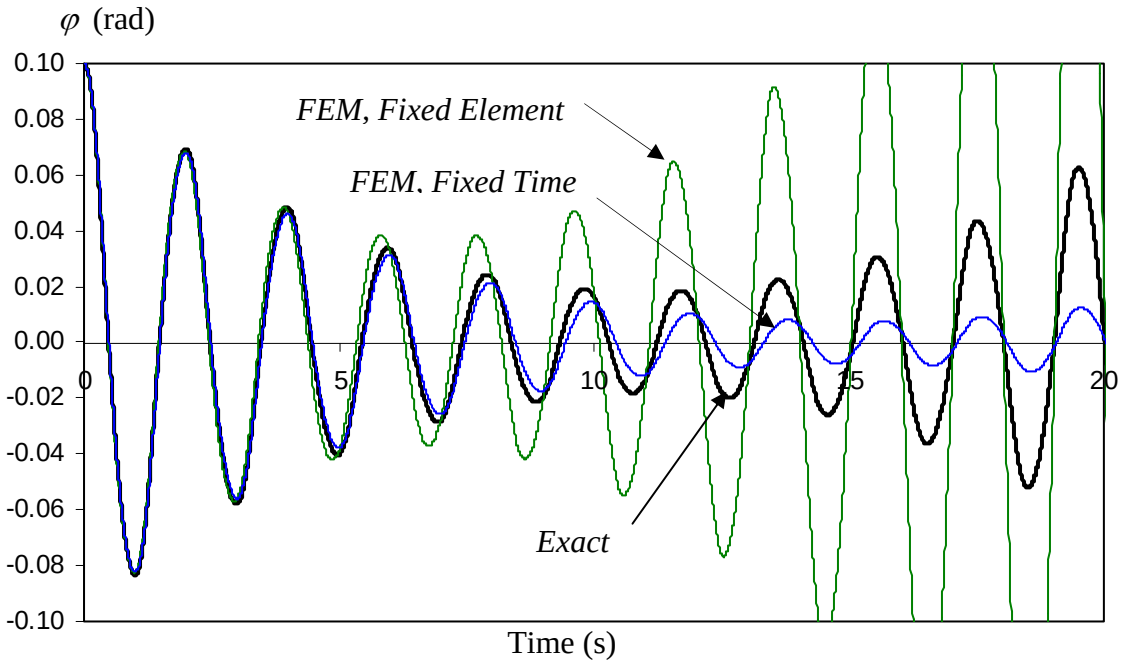

Figure 2-14 The pendulum's response to $s(t) = 1.1\left(1 - 0.2\sin 2\pi t\right)$ by Procedure I.

The results denoted as '*Exact*' were obtained by integrating Eq. (2.6) with the help of the Runge-Kutta procedure. Only the first cycle is properly synchronized to cause attenuation (according to Szyszkowski and Stilling 2005 the damping ratio for this cycle should be ξ=0.058). Due to slight variations in the period of the pendulum oscillations (and T_m remaining the same), the synchronization is gradually lost resulting in amplification after about five cycles. This will be explained in more details in the following sections.

The 'FEM Fixed Time' results in Figure 2-14 was obtained by using Procedure I with the load step time $\Delta t_l = t_m^0 / 28$=0.0357*sec* (which gives the ratio $\Delta t_l / \Delta t_r$=0.357) and the element length varying from L_e=49 *mm* at the center of the mass motion range to L_e=5.5 *mm* at the turning points (the element sizes were determined from $L_e = \Delta t_t \left| \dot{s}_{avg} \right|$). For consistency with the results presented in previous section, the integration time step was again $\Delta t_i = 0.01 sec$. As it is observed in Figure 2-14, the results diverge quite severely from the exact results despite of a relatively low $\Delta t_l / \Delta t_r$ ratio. The amplitude of the 10th cycle, φ_{10}^{FEM}, is only about 20% of the exact one (or $\varphi_{10}^{exact} / \varphi_{10}^{FEM}$=5).

The way to improve this accuracy would be to reduce Δt_l further, which in turn requires increasing the number of elements covering the motion range. For instance, when $\Delta t_l = 0.0078 s$ (it gives $\Delta t_l / \Delta t_r$=0.078 which is 4.6 times smaller than before) the amplitude of the 10th cycle is still 1.33 times less than the exact one. It is also important to note that the FEM solution does not converge for Δt_l smaller than 0.0078*s* since the elements near the turning points become too small to render meaningful results.

Procedure I was also used with a *fixed* element size and *varying* load step interval (this method is less convenient to program). The motion range was divided into 16 elements of equal length L_e=27.5mm, then the load step intervals were adjusted by using $\Delta t_l = L_e / \left|\dot{s}_{avg}\right|$, as before. The results are indicated by the curve denoted as '*FEM, fixed element*'. Interestingly, this approach produces the positive amplitude errors (for example, the amplitude of the 10th cycle is about four times greater than the exact one, or $\varphi_{10}^{FEM} / \varphi_{10}^{exact}$=4), which is opposite to the negative amplitude error generated by the fixed load step time approach. Thus, as shown in Figure 2-14, for a periodic motion neither of the methods estimates the exact solution with sufficient accuracy despite using relatively small traverse periods.

Finally, it is important to note that Procedure I appears to be insensitive to the patterns of applying the Coriolis forces. The differences between the amplitude and period errors obtained by using either *proportional*, *lumped*, or *consistent* forces were insignificant.

2.5.2 Testing procedure II

In Procedure II the duration of the load step Δt_l can be a fraction of the traverse interval Δt_t, which allows the use of a longer element size L_e. Any discrete time t_k, with the mass between the nodes, can be considered to calculate and apply the Coriolis forces (either *proportional*, *lumped*, or *consistent* forces located at $\bar{s}_k = \bar{s}(t_k)$ where $0 \le \bar{s}_k \le 1$) and the mass matrix of the traversed element $M_e(t_k)$. The time-varying mass matrix is calculated and applied based on the approximation of Eq. (2.24). As shown previously in this section, and also will be shown later, the error for calculation of the time-varying mass matrix is much smaller than that of the Coriolis

force vector. Consequently, even the approximation of Eq. (2.24) was proven to be effective in modeling the time-varying mass matrix.

In order to compare the performance of Procedure I (presented in Figures 2-12 and 2-13) with Procedure II, the constant velocity **Pattern 1** was tested first. The accuracy of both procedures appeared to be almost identical if the same load-step duration Δt_l was used, although with different sizes of the elements. For instance, in Procedure I for the case of $v_0 = 0.1 m/sec$, the amplitude error of about 0.3% was obtained assuming $\Delta t_l = 0.1 sec$, which required the element length L_e = 10 *mm* (recall that $L_e = \Delta t_t v_0$). In Procedure II, the same accuracy was obtained if $\Delta t_l = \Delta t_t / 2.5 = 0.1 sec$ with the element length of L_e = 25 *mm* was used. Thus, accuracy of Procedure II for **Pattern1** can be characterized by the plots in Figures 2-12 and 2-13 but with much less elements applied. For the 1.4*m* long tube, for example, in order to achieve the 3% accuracy mentioned above, Procedure I required 140 beam elements, while Procedure II only 56 elements.

The difference between the two procedures is even more pronounced for the sinusoidal mass motion of **Pattern2**. If applying Procedure I, then the lowest obtained error of the 10th cycle amplitude was about 25% (see Figure 2-14). The accuracy of this procedure could not be increased due the limitations on the size of elements, as mentioned before. These limitations disappear in Procedure II because much larger elements are permitted. To illustrate that difference, the problem presented in Figure 2-14 was analyzed again by applying Procedure II with *lumped* nodal Coriolis forces. The results are plotted in Figure 2-15. The mass motion's range was divided into 16 elements of $L_e = 27.5 mm$ long (the same size as before for the '*FEM, fixed element*' case). Load-step durations of Δt_l equal to 0.05sec, 0.02*sec*, 0.01*sec*, and 0.005*sec*

were used. The results for Δt_l=0.05*sec* are comparable to those shown as the '*FEM, fixed time*' curve in Figure 2-14 (obtained by Procedure I, an error characterized by $\varphi_{10}^{exact}/\varphi_{10}^{FEM}$=5). However, the error of Procedure II drops to $\varphi_{10}^{exact}/\varphi_{10}^{FEM} \cong 2.1$ for Δt_l=0.02*sec* and to $\varphi_{10}^{exact}/\varphi_{10}^{FEM} \cong 1.3$ for Δt_l=0.01*sec*. If Δt_l=0.005*sec* (not shown in the figure) then $\varphi_{10}^{exact}/\varphi_{10}^{FEM} \cong 1.00$ and the FEM curve is indistinguishable from the exact solution curve in the graph's scale.

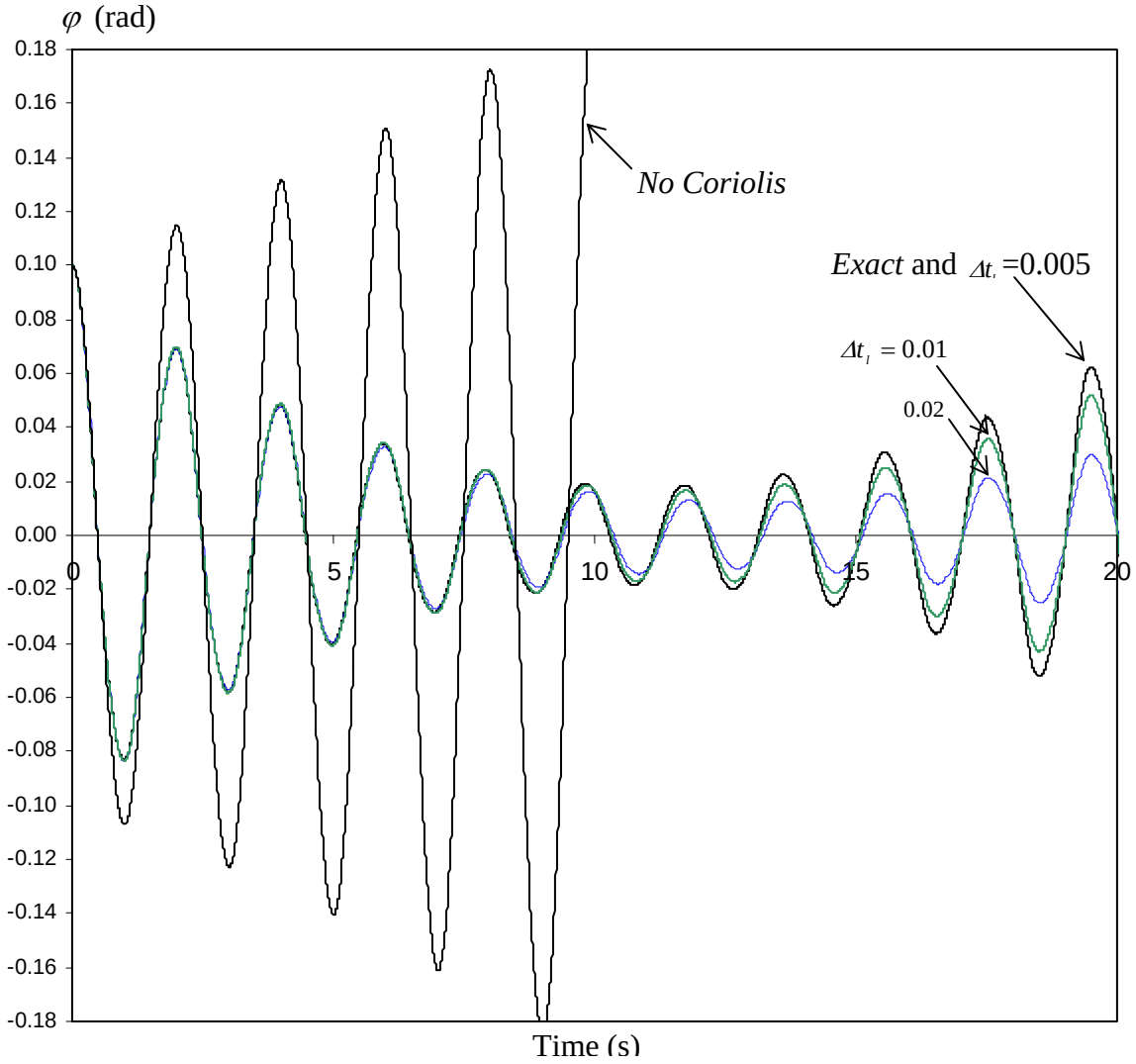

Figure 2-15 The pendulum's response to $s(t) = 1.1(1 - 0.2\sin 2\pi t)$ by Procedure II.

The consequences of using the standard FEM approach with the '*ekill/ealive*' commands (i.e. without applying the Coriolis forces defined in section 2.4.1) to model the periodic mass movement were also examined. Such results are labeled in Figure 2-15 as '*No Coriolis*' (similarly as in Figure 2-11 for the constant velocity case). The FEM solution shown was obtained for $\Delta t_l = 0.03$ *sec* and $L_e = 27.5mm$.

The amplitude error of this solution, which is determined by comparing the FEM results with the 'exact' results obtained from Eq.(2.25), was less than 0.5%. This error, which is due to Newmark's integration of the FEM model as well as modeling the time-varying mass matrix by using Eq. (2.24), is considerably smaller than that caused by calculation of Coriolis force (which was more than 50% for $\Delta t_l = 0.02$). According to Szyszkowski and Stilling 2005, Eq. (2.25) for the case considered can be simplified to $\ddot{\varphi} + \omega_p^2(1 + 0.3397\varepsilon \sin 2\omega_p t)\varphi = 0$, which is a Mathieu's type equation to represent self-exited oscillations with the solution diverging (amplification) with the rate of about 2.2% (the harmonic terms are multiplied by $e^{0.022t}$). Recall that in the exact solution obtained by including the Coriolis forces the first cycle is actually attenuated with the rate of 5.8% (ξ=0.058).

The '*No Coriolis*' curves in Figures 2-15 and 2-11 indicate that modeling the mass movement by only the '*ekill/ealive*' type of commands does not mimic the mass-structure interaction. The inclusion of the Coriolis forces appears to be essential for obtaining any meaningful results.

Recall that in **Pattern 1** (of constant velocity of mass), Procedure I generated positive or negative amplitude errors for positive (causing attenuation) or negative (causing amplification) mass velocities, respectively (see Figure 2-12). The errors were essentially independent of the type of Coriolis forces applied, and the magnitude of an accumulative error always increased with the number of cycles of the pendulum's oscillations. However, for **Pattern 2** with the mass

moving periodically, the positive and negative errors should alternate; therefore, the accumulative amplitude error does not necessarily increase with each cycle. Such an accumulative amplitude error for the first five cycles and for Δt_l=0.005*sec* is depicted in Figure 2-16. Only the results obtained by using Procedure II are presented.

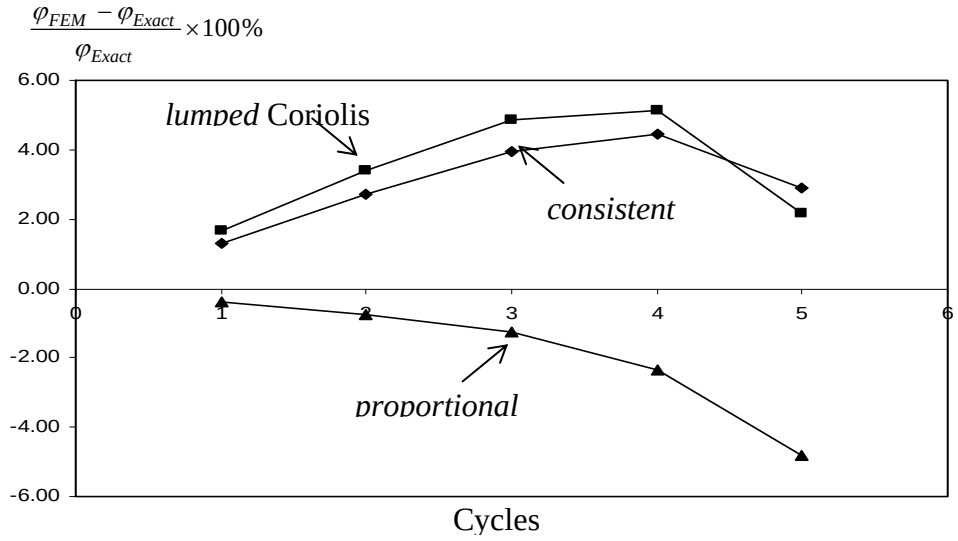

Figure 2-16 Accumulative amplitude error for first five cycles.

These errors were affected by the patterns of applying the Coriolis forces. The *lumped* and *consistent* forces yield somewhat similar positive errors with the magnitudes first increasing then decreasing, while the *proportional* forces yield negative errors with their magnitudes always increasing. Note that, in this phase of motion (attenuation), all these accumulated errors are less than 5%.

The accumulative errors after five cycles, and then after 10 and 15 cycles are shown in Figure 2-17. For these cycles, the pendulum's oscillations were amplified (see Figure 2-15).

Interestingly, the error almost vanishes for the *lumped* Coriolis forces after 10 cycles and for the *consistent* forces after 15 cycles. The error continuously increases for the *proportional* forces.

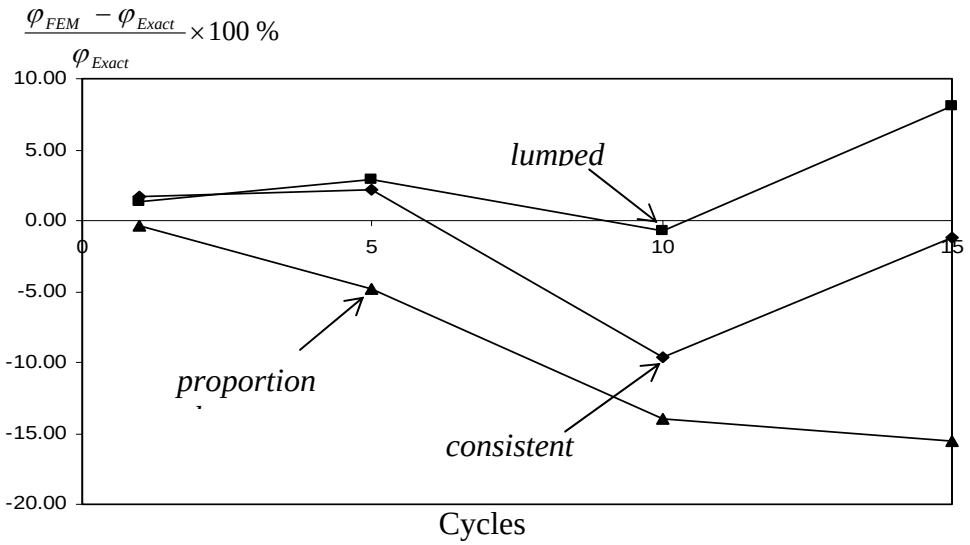

Figure 2-17 Accumulative amplitude error after different number of cycles.

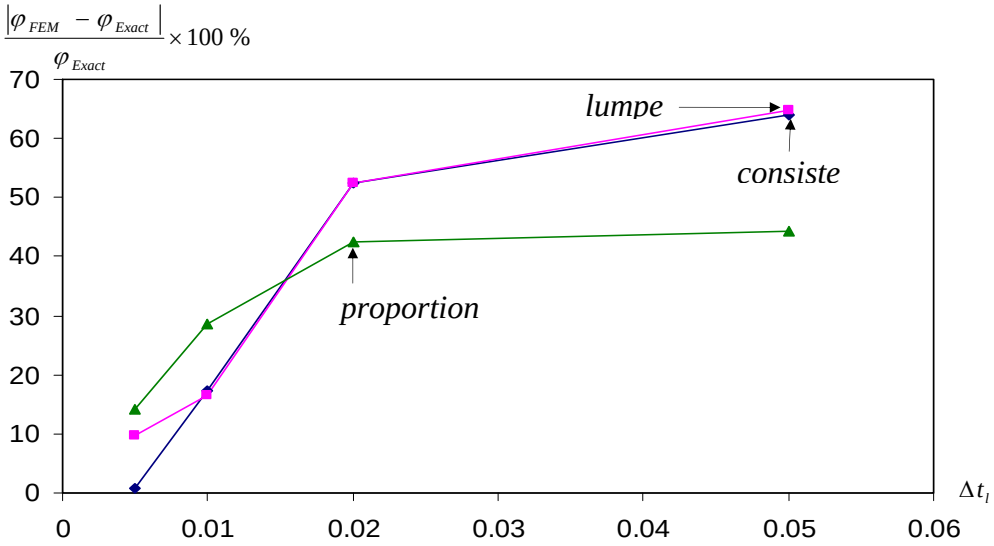

Figure 2-18 Effect of Δt_l on the accumulative amplitude error after 10 cycles for different patterns of the Coriolis forces.

The effects of Δt_l on the accumulative amplitude errors after 10 pendulum's oscillation cycles obtained by applying either the *proportional*, or *lumped*, or *consistent* Coriolis forces are presented in Figure 2-18. The accuracy is generally poor for $\Delta t_l > 0.02 sec$. It should be emphasized, however, that the above results obtained by applying Procedure II are still much better than those of Procedure I with comparable durations of the load-step Δt_l.

2.6 Simulating a Continuous Attenuation Case

As mentioned earlier, the advantage of the proposed FEM approach is its ability to simulate problems with arbitrary movement of the mass acting as a controller. To illustrate this point, **Pattern 2** of periodic motion of the mass, similar to those presented in Figures 2-14 and 2-15, is analyzed again. In this pattern, the mass motion is such that its frequency is almost twice the frequency of the pendulum. As shown in the figures, the pendulum vibration is attenuated for the first few cycles. Prior to discussing how continuous attenuation can be obtained, it is very important to explain why this pattern of mass motion causes attenuation for the first few cycles and, also, why the attenuation-effects of the moving mass gradually changes into amplification-effects.

As it has been noted previously, regardless of the sign of $\dot{\varphi}$, the mass motion will attenuate the system vibration for $\dot{s} > 0$ and will amplify the system vibration for $\dot{s} < 0$. Also, since the damping-like effect of the relative mass motion comes from the mass Coriolis acceleration (which is equal to $2m\dot{s}\dot{\varphi}$), the damping like effect is proportional to both mass relative velocity, $\dot{s}$, and pendulum's angular velocity, $\dot{\varphi}$. Consequently, the synchronization for obtaining attenuation should be such that when $\dot{s}$ is positive $|\dot{\varphi}|$ is maximum (which results in maximizing

the attenuation effect). Also, when $\dot{s}$ is negative, $|\dot{\varphi}|$ should be minimum (resulting in minimization of amplification effect). Figure 2-19 shows a typical synchronization of the mass motion and pendulum oscillation for obtaining attenuation. The main feature of this mass motion, s, is that its frequency is twice the frequency of φ. Also, the phase for s, which is denoted by ψ, should be zero when φ is zero, as shown in the figure.

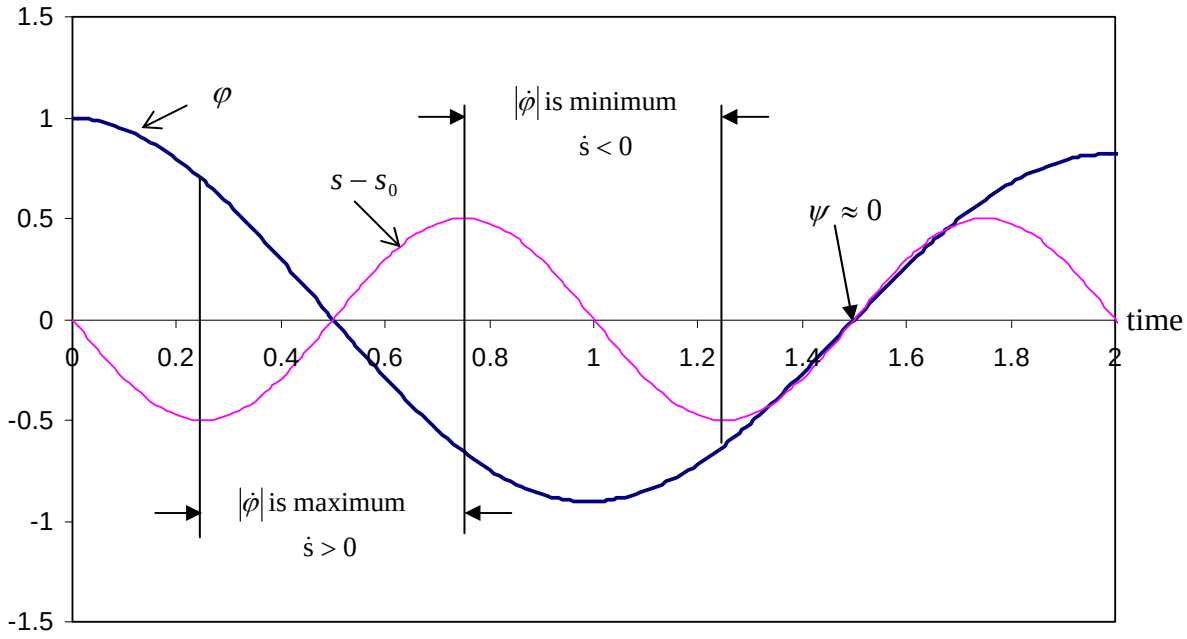

Figure 2-19 A typical cycle of motion for the angle φ and mass position s to obtain attenuation.

The condition $\psi = 0$ is a very important feature of the mass motion for obtaining attenuation. In fact, it can be shown that if the mass motion is such that $\psi = 0$ when φ is zero (the mass motion is in phase with pendulum oscillation) then the attenuation effect is maximum. If $\psi = \pi/2$ when φ is zero (neutral phase) then the amplification and attenuation effects cancel out and finally if $\psi = \pi$ when φ is zero (out of phase) then the amplification effect is maximum.

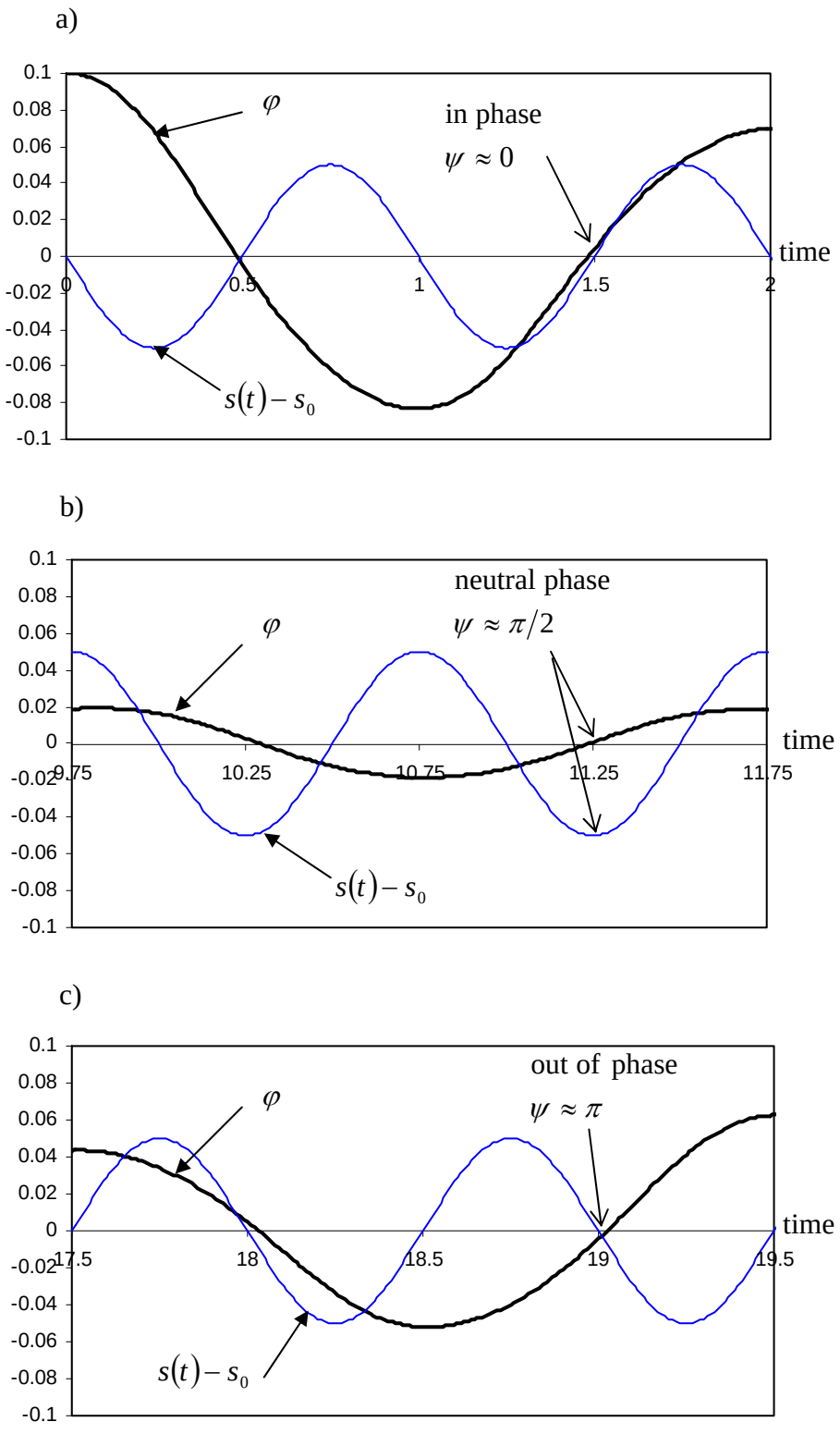

Figure 2-20 The mass motion and the pendulum oscillation for different cycles (a) attenuation cycle (b) neutral cycle (c) amplification cycle.

By considering the role of ψ in the pendulum's response, which was just discussed, the beating phenomenon (amplification followed by attenuation) shown in Figure 2-15 can now be explained. To this end, three different cycles of motion from the exact solution presented in Figure 2-15 are redrawn in Figure 2-20 a, b and c. The mass motion oscillation (in terms of $s(t)-s_0$) is also shown in these figures. In Figure 2-20a, which is for the first cycle of pendulum's vibration, the mass motion and pendulum's vibration are almost perfectly in phase, $\psi \approx 0$, which, according to the previous discussion, maximizes the attenuation effects and eventually the pendulum's amplitude of oscillation, φ, decreases. A detailed study of the pendulum's vibration shows that its frequency of vibration, which is almost equal to π in the first cycle, changes slightly in the second and the following cycles. For instance the period of first cycle is 1.99 sec while it is 1.98 for the second one. The reason for this slight change is the disturbance caused by the relative motion of the mass. For the case shown in Figure 2-15, the period of pendulum vibration decreases in the attenuation phase (the first 5 or 6 cycles) while it increases in the amplification phase (the following cycles).

Due to this change in the period of the pendulum's vibration, the synchronization of the mass and the pendulum is gradually lost. As shown in Figure 2-20b, which renders the sixth cycle, the mass motion phase is almost neutral, $\psi \approx \pi/2$, and consequently, no attenuation or amplification is caused by the mass motion. In the cycles followed by this neutral one, the mass motion gradually gets out of phase, $\psi \approx \pi$, resulting in amplification of vibration as illustrated in Figure 2-20c.

The approach to be used for obtaining continuous attenuation is to keep the mass motion and the pendulum oscillation in phase. To this end, the frequency of pendulum oscillation, which can be expressed in terms of pendulum rotation angle φ, should be monitored continually. Then,

whenever there is a change in this frequency, the mass motion frequency should be updated to twice this frequency. The mass motion is then given by:

$$s = s_0\left(1-\varepsilon\sin\left(2\omega_p t\right)\right) \tag{2.26}$$

where ω_p is the current pendulum vibration frequency. It is noted that in more complicated structures, like beams and frames, this synchronization process is more complicated and involves more details which will be discussed in the following chapters.

Figure 2-21 shows the pendulum's vibration over time when this approach is used to synchronize the mass motion pattern. This case was simulated using Procedure II and the results are obtained for $\Delta t_l = 0.01 sec$. It is noted that, in the plot, these results are indistinguishable from the exact solution reported in Szyszkowski and Stilling (2005).

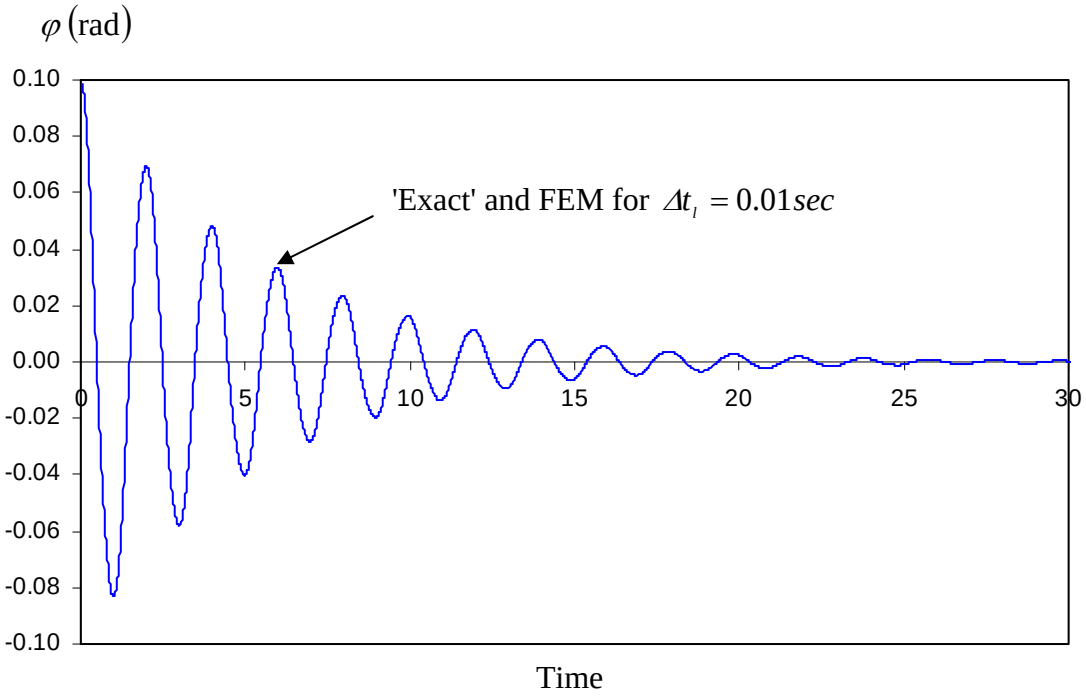

Figure 2-21 Pendulum response when the mass motion is synchronized.

If we plot similar curves to those of Figure 2-20, where no synchronization was done, it is observed that the mass motion and the pendulum oscillation are always in phase. This is shown in Figure 2-22 where the mass motion and the pendulum angle are illustrated for the first and tenth cycles. Note that ψ stays close to zero for different cycles which means the pendulum's vibration is attenuating in each cycle.

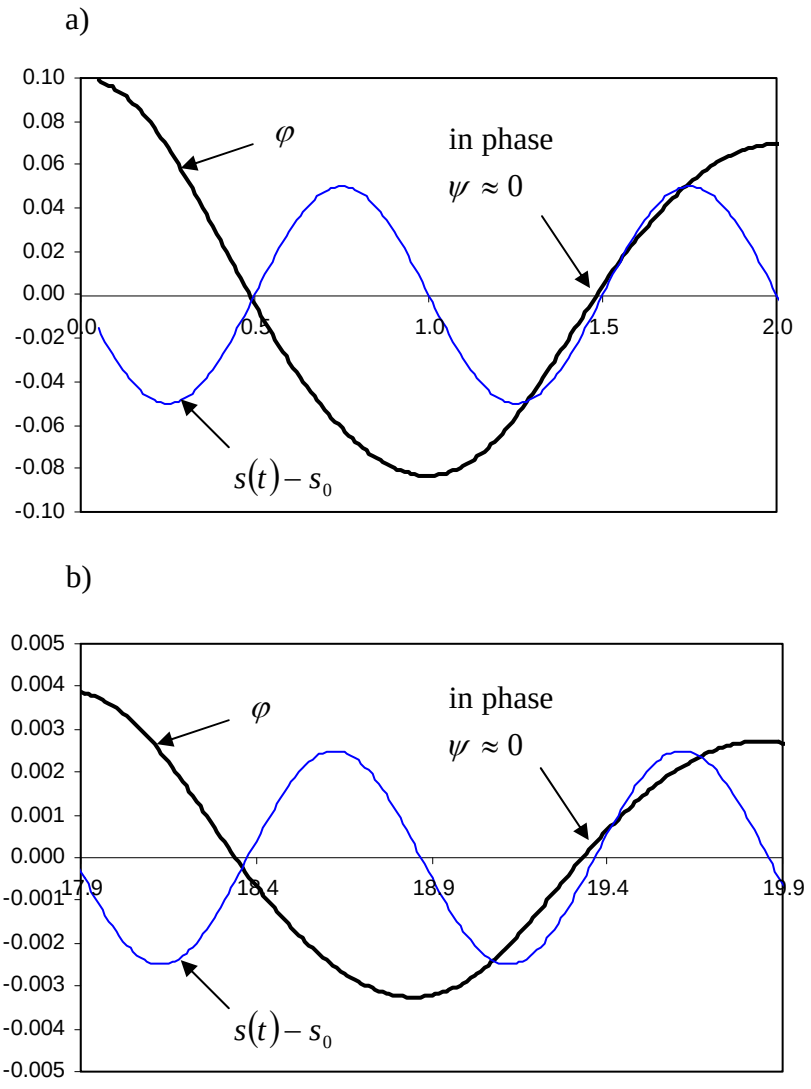

Figure 2-22 The mass motion and the pendulum oscillation for first and tenth cycles.

Recall that previously for $\Delta t_1 = 0.01 sec$ procedure II yielded more accurate results in the attenuated phase of the pendulum's oscillations than in the amplified phase, as shown in Figure 2-15. Because the pendulum's oscillations in Figure 2-21 are always attenuated, the accuracy of Procedure II for the synchronized mass motion appears to have improved somewhat (differences between the FEM and exact results can be visually detected only if $\Delta t_1 > 0.02 sec$).

If the pendulum vibration shown in Figure 2-21 is approximated as a damped sinusoidal motion, i.e. $\varphi = \varphi_0 e^{-\zeta \omega_p t} \cos(\omega_p t)$, then the corresponding equivalent damping ratio for this case will be 5.7 %. From the control point of view, it is desirable to increase this active damping ratio which can be done by changing the mass motion pattern. As a result, it is interesting to investigate how changing the mass motion parameters, including s_0 and ε, will affect the pendulum response and the corresponding active damping ratio. To this end, several analyses with different mass motion parameters have been done and the results are summarized in Figures 2-23 and 2-24. The parameters that are investigated are mass's oscillation amplitude, $s_0 \varepsilon$, and the average location of mass, s_0, which are both non-dimensionalized with respect to the pendulum's length, L.

Figure 2-23 shows the effect of mass motion amplitude on active damping ratio. As shown previously, the resisting Coriolis force is proportional to $m\dot{s}\dot{\varphi}$. On the other hand, based on Eq. (2.26), the mass relative velocity, $\dot{s}$, is proportional to $s_0 \varepsilon$. This means that the damping ratio is expected to increase with the amplitude $s_0 \varepsilon$ which agrees with the results shown in Figure 2-23, where the damping ratio increases almost linearly with the amplitude $s_0 \varepsilon$. The results shown in Figure 2-23 also compares the damping ratio obtained for two different values of s_0. This

comparison shows that s_0 has a slight impact on the equivalent damping ratio; however, it is not as significant as the effect of amplitude $s_0\varepsilon$.

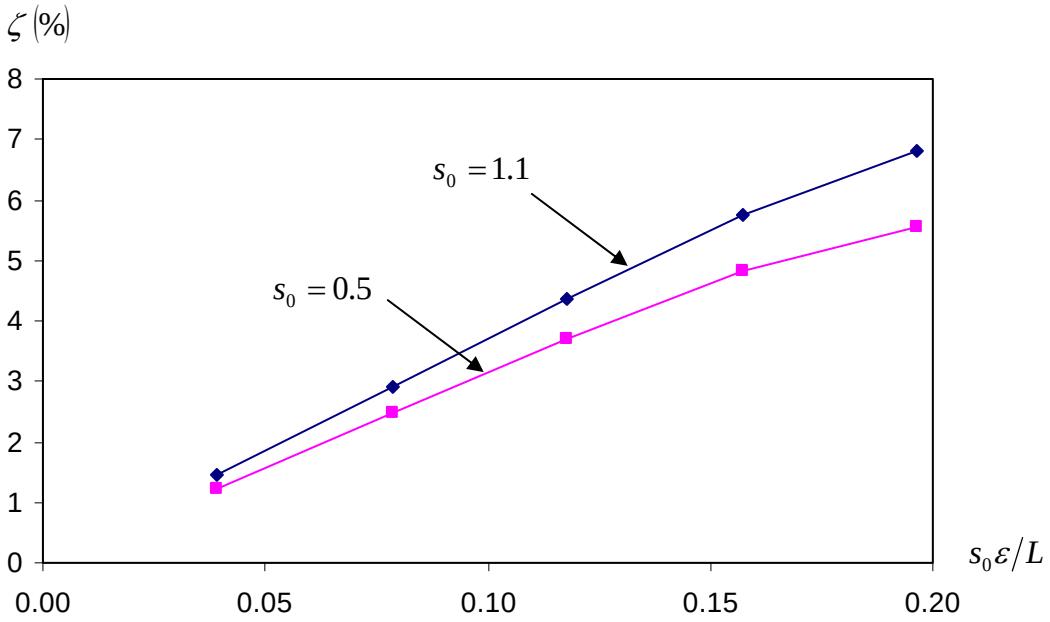

Figure 2-23 Effect of mass oscillation's amplitude on the equivalent active damping ratio.

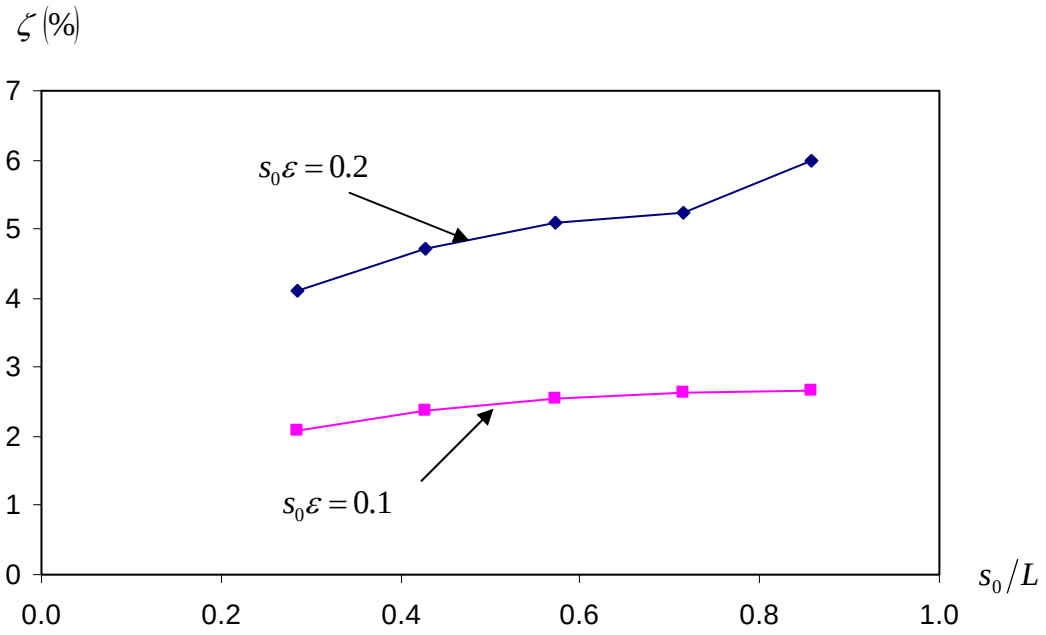

Figure 2-24 Effect of mass averaged location on the equivalent active damping ratio.

The effect of mass average location on the damping ratio is better shown in Figure 2-24 where damping ratio is plotted versus non-dimensional averaged location for two different mass motion amplitudes, $s_0\varepsilon$. Based on these results, it is observed that the damping ratio increases when s_0 increases which is expected since the torque (about the pivot) caused by the Coriolis force gets larger as the average distance, s_0, increases. Also, according to Eq. (2.10), it can be shown that for the case considered here, the instantaneous damping ratio increases with s, but the increase is not proportional (term $s(t)$ is present in both the numerator and denominator of the expression). This is why the effect of s_0 on the damping ratio is not as large as the effect of $s_0\varepsilon$.

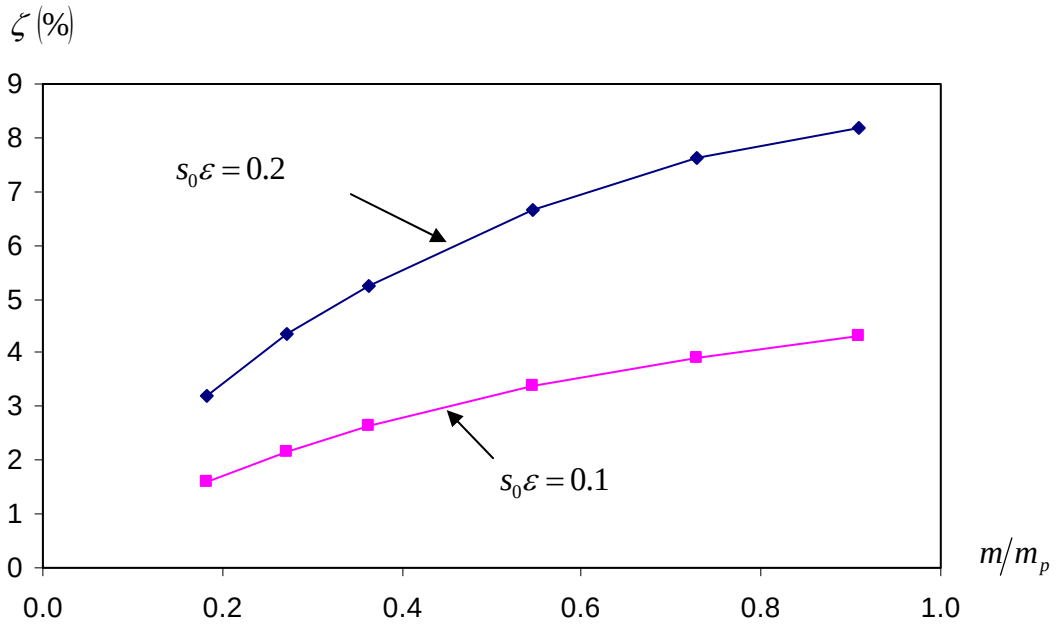

Figure 2-25 Effect of mass, m, on the equivalent active damping ratios.

All the results in Figures 2-23 and 2-24 are obtained by using a mass of 1 kg for the moving body, $m=1$. Since the Coriolis force is also proportional to this mass, it is expected that the damping ratio increases with m. Figure 2-25 shows how the damping ratio is changing with m for two different values of mass motion amplitude, $s_0\varepsilon$, and $s_0=1$. The mass m is non-

dimensionalized with respect to the mass of the pendulum, m_p. As expected, damping ratio increases with m; however, it appears that there is a maximum obtainable damping ratio since the curves in the figure tend to asymptotically go to a maximum value. In fact, as the mass m gets larger, and thus the damping ratio increases, the synchronization process gets harder to do. For the case shown in Figure 2-25 the maximum damping ratio that can be obtained for $s_0 = 1$ and $\varepsilon = 0.2$ occurs at $m = 2.5$ kg and is about 8.16%.

CHAPTER 3

CONTROLING FLEXURAL VIBRATION OF A DISTUBED BEAM

3.1 Introduction

In this chapter, the vibration control approach discussed in the previous chapter will be applied for controlling flexural vibration of a beam. Figure 3-1 shows a typical vibrating beam. The mass m slides back and forth along the beam and to attenuate its vibration, which can be achieved by synchronizing the relative motion of the mass m with the motion of the beam.

Unlike for the pendulum problem, the mass motion-beam interaction should be modeled by the Finite Element Method, because any analytical approach becomes too complicated, especially when the control aspect (attenuation) of the problem is included.

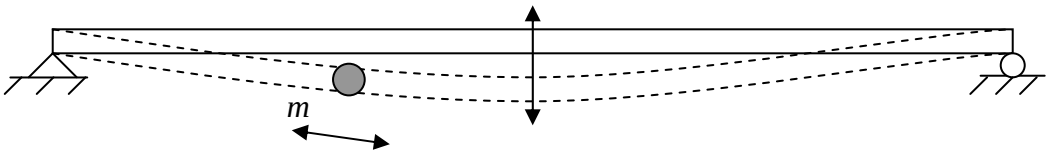

Figure 3-1 Scheme of a vibrating beam along which a mass is moving.

A time-varying beam element, formulated for the pendulum case, is capable of modeling the problem considered in this section; however, the motion of the beam is now more complicated, which results in more complicated mass motion (it has a centripetal acceleration in addition to Coriolis acceleration). This means that the formulations have to be extended very carefully to model the mass-beam interaction correctly.

The dynamic modeling of the pendulum problem was relatively simple. An analytical solution could be obtained by numerically integrating the dynamic equations; thus, the FEM results could

be verified by comparing them with this ‘exact’ solution. For the beam problem, however, as will be shown later, the dynamic formulation is more complicated, which makes it harder to obtain any analytical solution and evaluate its accuracy. Consequently, verifying the results obtained by the proposed FEM approach is more challenging for this case.

Furthermore, since the beam is modeled as a continuum, it basically has an infinite number of vibration modes while, for the pendulum case, only one mode of vibration was present. As a result, the beam’s vibration response is affected by more than one mode of vibration which makes the moving mass synchronization process more complex.

In this chapter, the FEM model for the moving mass-beam structure is first established by extending the formulation already presented in the previous chapter. Then, the results obtained based on this approach will be verified by comparing them to the (limited) results available in the literature. In the next step, the mass synchronization method presented in the previous chapter is explained and extended in more details. Finally, the proposed synchronization methods will be applied to different beam problems and the results will be discussed and compared to one another.

3.2 Modeling the Moving Mass-Beam Interaction by FEM

Understanding the dynamic response of a beam to masses moving along its axis in a predefined patterns is important for a wide range of engineering problems, from modeling a bridge with a traveling vehicle (usually at a constant velocity) to controlling vibration of an elastic system by appropriately relocating its components, which is the purpose of this research. The problem has been formulated and analyzed in numerous works with the complexity levels varying in quite a wide range. An important aspect differentiating these works is the treatment of interaction between the mass and the beam. In particular, significant Coriolis and centripetal

types of interaction forces may be generated that are not easy to include into the analysis (other aspects, such as the rotational inertia of a moving mass, adding an elastic bed for the beam, etc. can be considered as more routine ones). As will be discussed later, in some cases the Coriolis and centripetal accelerations caused by the relative mass motion can be ignored without losing the accuracy of the model. However, it will be shown that in some other cases, these effects are important and neglecting them may lead to completely incorrect solutions. In general, the methods used to formulate and solve the problem could be classified into four categories, from the simplest to the most complex, as follows:

a) The moving mass is modeled by its weight. In this approach, the beam is actually traversed by a moving force equal to the body's weight. Any changes in the transversal position of the moving mass are completely ignored. Consequently, all inertia effects of the mass are ignored too. Such moving-force models are relatively simple and were used in the early works (for example A.N. Kryloff 1905 and S.P. Timoshenko 1911). This approach was used also in more recent works where there were more than one moving forces on a multi-span beam (K. Henchi and M. Fafard 1997 and D.Y. Zheng et al 1997), a sinusoidal motion for the mass (K. Watanabe et al 1997), nonlinear effects in beam's equation (V.H. Nguyen and D. Duhamel 2006), or applying a time-varying traveling force (A. Garinei and G. Risitano 2008) were considered.

b) The moving mass' acceleration in the transversal direction is considered in addition to the model in (a). This generally creates a time-variable coefficient at the inertia term, which complicates the solution technique. While the vertical motion of the mass due to beam's flexural vibration is accounted for, any effects related to the relative motion of the mass with respect to the beam (the Coriolis and centripetal effects) are omitted. This approach was applied in most of the previous works on the moving mass- beam interaction problems. Somewhat different

solution procedures and methods (finite difference approach in X. Xu et al. (1997), infinite series in R.J. Jiang et al. (2003) and Y.B. Yang and C.W. Lin (2005), Green functions in M.A. Foda and Z. Abduljabbar 1998), or different assumption about the moving mass (moving a mass-spring system along the beam in .B. Yang and C.W. Lin (2005) and assuming the mass to be partially distributed in E. Esmailzadeh and M. Ghorashi (1995) and J. R. Rieker and M. W. Trethewey 1999), or different levels of complexity (including nonlinear effects in X. Xu et al. 1997 and moving the mass along multi-span beam in M. Ichikawa et al. 2000) were used in these papers.

c) The Coriolis effects are considered in addition to the model in (**b**). Such an approach has been used in G.T. Michaltsos and A.N. Kounadism 2001, S.A.Q. Siddiqui et al. (2003) and A. Nikkhoo et al. (2007) to obtain analytical solutions by applying an infinite series, and in H.J. Schneider et al. (1983) by the finite element method.

d) A 'complete' model of the mass-beam interaction. Within the linear dynamics (small deflections/rotations of the beam) this approach includes all the possible effects, in particular, the Coriolis and centripetal types of forces.

In this section the dynamic equations are formulated based on the most general form (d). Then, the FEM formulation is derived by generalizing the combined beam element proposed in the previous section. It is noted that the proposed method allows running the model (d), or models (a-c), if some of the effects mentioned above are excluded. This means that the results obtained by including/excluding different mass acceleration terms can be studied.

3.2.1 Deriving the Exact Dynamic Equations

The interaction between the beam and the moving mass *m* can be determined by analyzing the equations governing the motions of these two bodies separately. The beam of stiffness *EI* and

unit mass ρA is loaded by the interface forces F_N and F_t, as well as the forces due to gravity and possibly by some forces F_k of fixed locations (all these forces are indicated in Figure 3-2). Also, the axial forces denoted by $n(x)$ may be present.

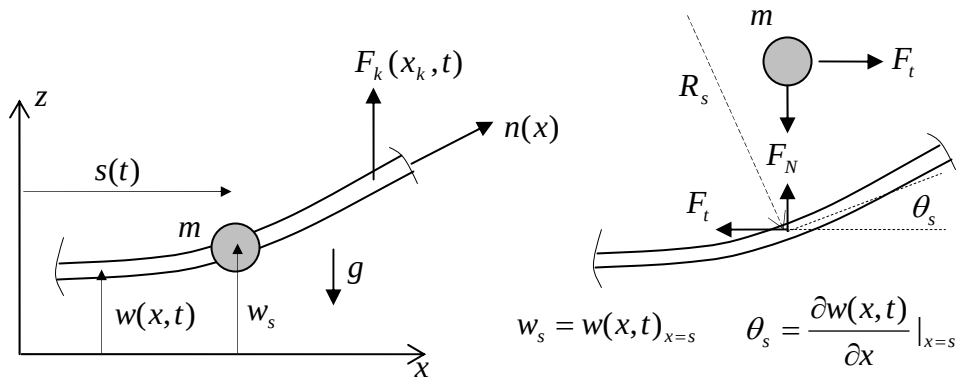

Figure 3-2 The beam with the moving mass.

The motion of mass *m* obeys the equations:

$$m\ddot{s} = F_t \tag{3.1}$$

$$m\ddot{w}_s = -mg - F_N \tag{3.2}$$

Based on the Euler beam theory, the vertical motion of the beam is given by:

$$\rho A\frac{\partial^2 w}{\partial t^2} - n\frac{\partial^2 w}{\partial x^2} + EI\frac{\partial^4 w}{\partial x^4} = -\rho Ag + (F_N + F_t\theta_s)\delta(x-s) + \sum_1^n F_k(x,t)\delta(x-x_k) \tag{3.3}$$

where $\delta(.)$ denotes the Dirac's delta function, and a dot means the time derivative.

Applying the chain rule of differentiation, the vertical acceleration of mass *m* is:

$$\ddot{w}_s = \frac{d^2}{dt^2}w(x,t)_{x=s} = \frac{d}{dt}(\frac{\partial w}{\partial t} + \frac{\partial w}{\partial x}\dot{s})_{x=s} = \frac{\partial^2 w}{\partial t^2}|_{x=s} + 2\dot{s}\frac{\partial^2 w}{\partial x \partial t}|_{x=s} + \dot{s}^2\frac{\partial^2 w}{\partial x^2}|_{x=s} + \ddot{s}\frac{\partial w}{\partial x}|_{x=s} \tag{3.4}$$

Making use of Eq. (3.1), (3.2), and (3.4), the interaction term in Eq. (3.3) becomes:

$$\begin{aligned} F_N + F_t\theta_s &= -m(g + \frac{\partial^2 w}{\partial t^2}|_{x=s} + 2\dot{s}\frac{\partial^2 w}{\partial x \partial t}|_{x=s} + \dot{s}^2\frac{\partial^2 w}{\partial x^2}|_{x=s}) \\ &= -mg - m\frac{\partial^2 w_s}{\partial t^2} - 2m\dot{s}\dot{\theta}_s - m\frac{\dot{s}^2}{R_s} = -F_g - F_{in} - F_{Cr} - F_{cp} \end{aligned} \tag{3.5}$$

where $\dot{s}$ is the relative velocity of the mass with respect to the beam, $\dot{\theta}_s = \frac{\partial}{\partial t}\frac{\partial w}{\partial x}|_{x=s}$ is the angular velocity of the beam, and $R_s = 1\Big/\frac{\partial^2 w}{\partial x^2}|_{x=s}$ is its radius of curvature at the contact.

Only force $F_g = mg$, which represents the weight of *m*, would be included in method (**a**) mentioned in the previous section. Method (**b**) would add force $F_{in} = m\frac{\partial^2 w_s}{\partial t^2}$ representing the conventional vertical inertia force. The Coriolis force $F_{Cr} = 2m\dot{s}\dot{\theta}_s$ would be included in method (**c**), and finally the centripetal force $F_{cp} = m\frac{\dot{s}^2}{R_s}$ would be added in method (**d**). All these forces should be applied at the current location of mass *m*.

Substituting Eq. (3.5) into Eq. (3.3) one obtains:

$$(\rho A\ddot{w})_{eq} - n_{eq}\frac{\partial^2 w}{\partial x^2} + EI\frac{\partial^4 w}{\partial x^4} = -(\rho A)_{eq}\, g + \sum_1^n F_k(x,t)\delta(x - x_k) \tag{3.6}$$

where

$$(\rho A\ddot{w})_{eq} = \rho A\frac{\partial^2 w}{\partial t^2} + m(\frac{\partial^2 w}{\partial t^2} + 2\dot{s}\frac{\partial^2 w}{\partial t \partial x})\delta(x - s) \tag{3.6a}$$

$$n_{eq} = n - m\dot{s}^2\delta(x - s) \tag{3.6b}$$

$$(\rho A)_{eq} = \rho A + m\delta(x - s) \tag{3.6c}$$

It should be noted that the interaction forces (F_N and F_t in Figure 3-2) are not present in the above equations, and that the Dirac function in Eq. (3.6a)-(3.6c) make them difficult to solve, analytically or numerically. The notation used in Eq. (3.6) allows identifying the correspondence between some terms in these equations and the forces specified in Eq. (3.5) and also correlates to the approaches (**a**) to (**d**) listed in the previous section.

Namely, if $F_{in} = F_{Cr} = F_{cp} = 0$, then the terms defining the equivalent inertia force and the axial force are $(\rho A\ddot{w})_{eq} = \rho A\dfrac{\partial^2 w}{\partial t^2}$ and $n_{eq} = n$, respectively, as in method (**a**). If one assumes that $F_{Cr} = F_{cp} = 0$ (i.e. F_{in} is considered) then the inertia term is $(\rho A\ddot{w})_{eq} = \rho A\dfrac{\partial^2 w}{\partial t^2} + m\dfrac{\partial^2 w}{\partial t^2}\delta(x-s)$, which corresponds to method (**b**). In turn, if only $F_{cp} = 0$ is assumed, then $n_{eq} = n$ and $(\rho A\ddot{w})_{eq}$ is as defined by Eq. (3.6a), which represents method (**c**). Finally, using the full definitions, Eq. (3.6a) to (3.6c), for the inertia, axial and gravity forces corresponds to method (**d**).

3.2.2 The FEM Formulation of the Combined Beam Element

Like the pendulum case, it is obvious that only the beam element currently being traversed by the mass needs special consideration. The motion of the beam in this element must be governed by Eq. (3.6) which is more general than the pendulum motion (Eq. (2.6)). The remaining elements can be modeled by any standard beam elements with the deflection approximated by $w = \mathbf{N}X_e$, where **N** and X_e represent the shape functions and the corresponding degrees-of-freedom (DOF), respectively. The mass, stress stiffening, and bending stiffness matrices for such

standard elements are defined by $M_{eo} = \int_{L_e} \mathbf{N}^T A\rho \mathbf{N} dx'$, $K^g_{eo} = \int_{L_e} \mathbf{N}^T_{,x} n \mathbf{N}_{,x} dx'$, and $K_{eo} = \int_{L_e} \mathbf{N}^T_{,xx} EI \mathbf{N}_{,xx} dx'$, where $0 \le x' \le L_e$ and L_e is the element length.

The element equation for such elements is usually written in a standard form as:

$$M_{eo}\ddot{X}_e + C_{eo}\dot{X}_e + (K_{eo} + K^g_{eo})X = F_e \qquad (3.7)$$

The term $C_{eo}\dot{X}_e$ is added to represent any natural damping effect, and F_e is the vector of usual 'internal' forces acting on the element at nodes.

However, the element currently being traversed by the mass (to be referred to as the combined element) is governed by the 'full' Eq. (3.6) and therefore needs special considerations. Note that, formally, the presence of mass *m* should only affect the mass and stress stiffening matrices of this element. Further, one may conclude that, in order to recreate the effects due to forces F_{in}, F_{Cr} (see Eq. (3.5)), the mass matrix should be modified, while the effects due to F_{cp} would require modifications of the stress stiffening matrix.

The mass matrix for such elements becomes time-dependent and can be written, similar to Eq. (2.15), in the form:

$$M_e(t) = \int_{L_e} \mathbf{N}^T [A\rho + m\delta(s' - s)]\mathbf{N} ds' = M_{eo} + m\mathbf{N}^T(\bar{s})\mathbf{N}(\bar{s}) = M_{eo} + M_{em}(t) \qquad (3.8)$$

where $0 \le \bar{s} = \bar{s}(t) = [s(t) - s_i]/L_e \le 1$.

Matrix M_{eo} in Eq. (3.8) is the same as in Eq. (3.7), and matrix $M_{em}(t)$ assigns mass *m* at the current location $s(t)$ to particular DOFs of the element. The time dependency is hidden in vector $\mathrm{N}(\bar{s})$ in which the shape functions have to be taken at the current mass location defined by $\bar{s}$ that is changing with time. In particular, for a 'lumped' mass approach (which is discussed later

in detail) this term allows splitting mass *m* into two masses $m_i(t)$ and $m_j(t)$ assigned to the end nodes of the traversed element.

Normally, one may be tempted to identify the inertia term for the combined element similarly as in Eq (3.7), that is by just replacing the constant matrix M_{eo} by the time dependent mass matrix $M_e(t)$ determined by Eq. (3.8) to obtain $M_e(t)\ddot{X}_e$. However, as it was proven analytically for the pendulum problem in chapter 2 and will be demonstrated later in this chapter, such an approach is equivalent to including only force F_{in} into considerations, while the Coriolis force F_{Cr} that reflects the presence of relative motion of the mass along the beam (and appears to be essential in the control aspect of the mass-beam interaction) is completely neglected.

It turns out that the effects due to both forces, F_{in} and F_{Cr}, are included if, instead of the usual product of mass and acceleration as in Eq. (3.7), the inertia term is defined as the derivative of momentum (for the composite element both definitions are formally equivalent, because its combined mass remains constant) in the form:

$$\textit{Inertia term} \rightarrow \frac{d}{dt}[M_e(t)\dot{X}_e] = M_e(t)\ddot{X}_e + \dot{M}_e(t)\dot{X}_e = M_e(t)\ddot{X}_e + f_e^c \qquad (3.9)$$

The term $M_e(t)\ddot{X}_e$ above can now be interpreted as representing the element in which the position of mass *m* may be considered 'frozen' at a particular time *t*, while effects of the relative velocity of *m* with respect to the beam will be represented by the mass rate matrix $\dot{M}_e(t)$, or by vector $f_e^c = \dot{M}_e(t)\dot{X}_e$. If, as already mentioned, the term $M_e(t)\ddot{X}_e$ is related to force F_{in} (or to the inertia effects due to vertical motion of *m*), then the mass rate matrix or vector f_e^c should be related to the Coriolis force F_{Cr}.

Since normally just the mass matrix (constant or time-variable) is calculated in most commercial FEM software, the approach using only $M_e(t)$ will be referred here as 'standard', while the approach that includes also $\dot{M}_e(t)$ or f_e^c as a 'new' one. Note that in both formulations one has to make sure that matrix $M_e(t)$ is updated frequently enough to secure a sufficient accuracy of calculations. Some challenges related to the new formulations are discussed next. Differentiating Eq. (3.8) and using the chain rule, the mass-rate matrix of the element, similar to Eq. (2.16), is obtained as:

$$\dot{M}_e(t) = \dot{M}_{em}(t) = m\frac{\dot{s}}{L_e}\frac{\partial}{\partial \bar{s}}(\mathbf{N}^T\mathbf{N}) \tag{3.10}$$

One should note that this matrix is explicitly proportional to $\dot{s}$, the velocity of the traveling mass, and independent of the beam's mass.

In chapter 2 vector $\dot{X}_e$ was proportional to $\dot{\theta}_e$, the angular velocity (which was the same throughout the structure) of rigid elements used to model the pendulum. For flexible elements used here $\dot{X}_e$ is also proportional to $\dot{\theta}_e$, which is interpreted as an average angular velocity of the element and varies from element to element. Since vector f_e^c is proportional to the product of $\dot{s}$ and $\dot{\theta}_e$, it will in fact be representing the Coriolis effects, or the effects due to force F_{Cr}. As mentioned, this force appears to play a dominant role in analyzing vibrations to accompany the mass-beam interaction; in particular, in generating apparent attenuation or amplification effects for control purposes.

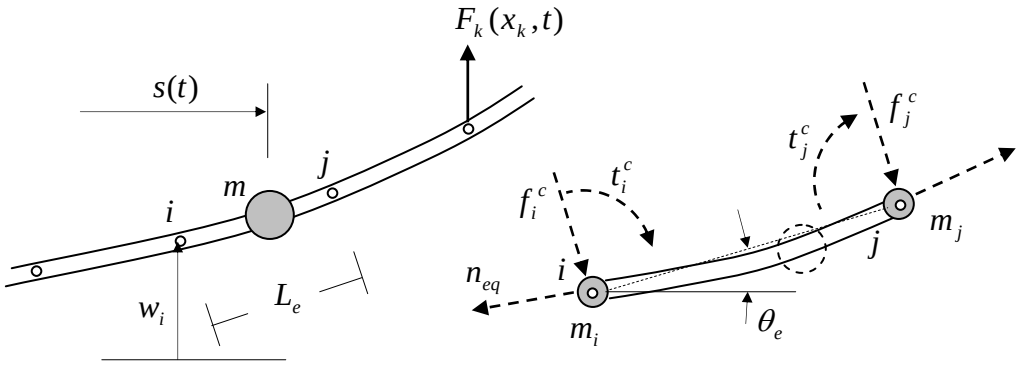

Figure 3-3 The FEM model and the composite beam elemen.

The 4-DOF hermitian beam element from the ANSYS software is used (i.e. $X_e^T = \begin{bmatrix} w_i & \theta_i & w_j & \theta_j \end{bmatrix}$, where v_i and θ_i are the nodal deflections and rotations, respectively) with the Hermit's cubic shape functions (i.e. $N_1 = 1 - 3\bar{s}^2 + 2\bar{s}^3$, $N_2 = L_e(\bar{s} - 2\bar{s}^2 + \bar{s}^3)$, etc.). By making use of Eq. (3.10) the components of vector f_e^c associated with the DOFs for such an element are determined, same as Eq. (2.17), as:

$$f_e^c = \dot{M}_e(t)\dot{X}_e = \frac{m\dot{s}}{L_e}\frac{\partial}{\partial \bar{s}} \begin{bmatrix} N_1^2 & N_1N_2 & N_1N_3 & N_1N_4 \\ & N_2^2 & N_2N_3 & N_2N_4 \\ & & N_3^2 & N_3N_4 \\ sym & & & N_4^2 \end{bmatrix} \begin{bmatrix} \dot{v}_i \\ \dot{\theta}_i \\ \dot{v}_j \\ \dot{\theta}_j \end{bmatrix} = \begin{bmatrix} f_i^c \\ t_i^c \\ f_j^c \\ t_j^c \end{bmatrix} \qquad (3.11)$$

Hence, vector $f_e^c = \begin{bmatrix} f_i^c & t_i^c & f_j^c & t_j^c \end{bmatrix}^T$, as indicated in Figure 3-3 (note that $f_e^c = 0$ for the remaining elements), represents the set of time-varying forces and moments applied to the nodes. Several ways of handling f_e^c numerically are discussed later in this section.

The centripetal effects, or the effects due to force F_{cp} in the analytical model, can be determined numerically for the composite element by substituting the equivalent axial force defined by Eq. (3.6b) to the stress stiffening matrix to obtain:

$$K_e^g = \int_{L_e} \mathbf{N}_{,x}^T n_{eq} \mathbf{N}_{,x} dx = K_{eo}^g - m\dot{s}^2 \mathbf{N}(\bar{s})_{,x}^T \mathbf{N}(\bar{s})_{,x} = K_{eo}^g + K_{em}^g(t) \qquad (3.12)$$

It might be noted that the second matrix can be approximated as $K_{em}^g(t) \cong \int_{L_e} \mathbf{N}_{,x}^T n_m \mathbf{N}_{,x} dx$, where $n_m = -m\dot{s}^2 / L_e$ is an 'averaged' portion of the equivalent axial force (always negative) due to the mass velocity (which in turn may vary in time). This approximation allows applying the standard stress stiffening matrix with the axial force in the element being traversed modified to:

$$n_{\text{mod}} = n + n_m = n - m\dot{s}^2 / L_e \qquad (3.13)$$

Finally, the bending stiffness matrix of the composite element is simply K_{eo} (i.e. it is not affected by the moving mass).

Thus, including all the effects discussed above, the equation for the combined (traversed) element can be written in the form:

$$M_e(t)\ddot{X}_e + (\dot{M}_e(t) + C_{eo})\dot{X}_e + (K_{eo} + K_e^g)X = F_e \qquad (3.14)$$

or:

$$M_e(t)\ddot{X}_e + C_{eo}\dot{X}_e + (K_{eo} + K_e^g)X = F_e - f_e^c \qquad (3.15)$$

Eq. (3.14) indicates that matrices $\dot{M}_e(t)$ and C_{eo} play similar roles, meaning that the former matrix can contribute to damping vibrations in a way similar to the natural damping matrix. In order to simulate this phenomenon numerically a time-variable damping matrix $C_e(t) = \dot{M}_e(t) + C_{eo}$ should be formulated and used in the calculations.

In Eq. (3.15) the relative motion effects are represented by vector f_e^c that is treated and calculated as a regular external force applied to the element. Such an approach has been found much more convenient numerically. It allows converting the problem back into the 'standard' FEM form in which only some additional forces have to be calculated. By applying this approach, the mass-beam interaction for any pattern of the mass motion can be recreated with high precision, as will be tested in the following sections.

The form of Eq. (3.15) is such that the composite element can be routinely assembled with the remaining elements (each governed by Eq. (3.7)) into the system's equation in the form:

$$M(t)\ddot{X} + C\dot{X} + KX = F - f^c \tag{3.16}$$

All terms in the above equation appear to be 'standard' and therefore most commercially available FEM software can be applied to solve the problem. It should be noted that the interaction forces between the mass and the beam (F_N and F_t in Figure 3-2) do not appear at all in this equation, which is consistent with the absence of such forces in Eq. (3.6).

As already mentioned, vector f_e^c plays a crucial role in modeling the dynamics of the mass-beam interaction. Eq. (3.11) indicates that the components of f_e^c are proportional to the relative velocity of the moving mass $\dot{s}$ and the rate of variation of the element's DOFs, but are independent of the beam's stiffness (the current mass position also affects this vector via shape functions **N**). Vector f_e^c defined by Eq. (3.11) was referred to as the *consistent* Coriolis force vector in chapter 2 and analyzed in detail for the elements applied to simulate a pendulum-like oscillations. It was shown there that a good approximation of Coriolis forces can also be obtained by considering only an 'average' rotation of the traversed element defined as $\theta_e = (w_j - w_i)/L_e$ (see Figure 3-3). On the other hand, such a rotation corresponds to the element's deflection

assumed as $w = (1-\bar{s})w_i + \bar{s}w_j$, which in turn can be defined using the following 'simplified' shape functions: $N_1 = (1-\bar{s})$, $N_2 = 0$, $N_3 = \bar{s}$, $N_4 = 0$. Substituting these functions into formula (3.11) the set of forces, referred to as the *lumped* nodal Coriolis forces, is calculated as:

$$f_e^c = \frac{m\dot{s}\dot{\theta}_e}{L_e}\begin{bmatrix} -2N_1 & 0 & N_1 - N_3 & 0 \\ & 0 & 0 & 0 \\ & & 2N_3 & 0 \\ symm & & & 0 \end{bmatrix}\begin{bmatrix} \hat{s}_i \\ 1 \\ \hat{s}_j \\ 1 \end{bmatrix} = \begin{bmatrix} f_i^c \\ t_i^c \\ f_j^c \\ t_j^c \end{bmatrix} \qquad (3.17)$$

where $\hat{s}_k = w_k / \theta_e$ represents the distance from a particular node (k=i,j) to the element's instantaneous center of rotation. Note that in this approximation the nodal moments are automatically zero (i.e.: $t_i^c(\bar{s}) = t_j^c(\bar{s}) = 0$). It can be shown that the nodal forces, f_i^c and f_j^c, generate a moment about the element's rotation center that is equivalent to force $F'_{Cr} = 2m\dot{s}\dot{\theta}_e$ applied at the current location of mass m. This in turn allows specifying the nodal Coriolis forces, to be referred as *proportional*, in the form:

$$\bar{f}_i^c = F'_{Cr}(1-\bar{s}) \text{ and } \bar{f}_j^c = F'_{Cr}\bar{s} \qquad (3.18)$$

Numerical experimentations in chapter 2 showed that each of the above three approximations of the Coriolis force vector, despite of differences in numerical values of particular components, was capable of recreating very closely the Coriolis effects in the pendulum-like beam with no bending effects. Here, it will be demonstrated that the same approximations works well also for the beams with dominating bending effects.

The procedure for updating the time-varying part of the mass matrix, $M_{em}(t)$ in Eq. (3.8)) is similar to the pendulum where instead of using the exact form from Eq. (3.8), following approximation is used:

$$m_i^e(\bar{s}_k) = m \text{ if } \bar{s}_k \le 0.5 \text{ and } m_j^e(\bar{s}_k) = m \text{ if } \bar{s}_k > 0.5 \qquad (3.19)$$

According to the above formula, the mass *m* is simply placed at the nearest node for the entire period of traversing the element. The mass matrix defined by (3.19) can be referred to as the *step* mass matrix. This matrix can easily be implemented in ANSYS with the '*ekill/ealive*' commands. Numerical experimentations in chapter 2 showed that using either type of the mass matrices presented above provides sufficient accuracy of the system's simulation. This generally indicates that the errors due to simplifications in the term $M_{em}\ddot{X}_e$ are much less significant than the error of calculating the term $\dot{M}_{em}\dot{X}_e$ (which is represented by the vector of forces f_e^c).

The proposed FEM approach in the form of Eq. (3.16) can be integrated in time by applying any standard procedure (we used Newmark's method). Since the elements (hermitian beam elements) and the integration procedure are standard, the formulation can be incorporated into most commercial software. We made use of ANSYS, and our procedure consists of the following phases:

1- The beam is modeled by using regular hermitian beam elements in the available FEM software. A procedure solving the transient dynamics problems will be applied.

2- In the beam's sector to be traveled by the mass (or the whole beam as in some examples presented in the next section):

   a. Nodal mass elements with properties identical to the moving body are created at each node.

   b. Axial fictitious forces n_m are determined for each element.

3- For the element being currently traversed:

   a. At each time step, the current position of the mass is determined. Then, the Coriolis force vector f^c is calculated for the element currently traversed

using one of the equations (3.11), (3.17) or (3.18) and the DOF's known from the previous time step.

b. Only one mass element which is closest to the current position of the mass is activated (all other mass elements are deactivated).

c. To include the centripetal effects, only the axial force n_m for this element is added to the existing axial forces (in the remaining elements n_m are omitted).

4- Current time step is solved and the next time step can be started in which only steps 3 is to be repeated.

Note that only Phase 1 is needed for handling the moving mass problem by method (**a**) mentioned in the introduction of section 3.2. Method (**b**) requires additionally Phases 2a and 3b. Phase 3a must be added for method (**c**). Finally all the phases (in particular, Phases 2b and 3c are required to determine the centripetal effects) are to be executed in method (**d**). Effects of applying different methods on the results can be studied by simply omitting or/and including particular phases of the formulation.

3.2.3 Verification of the Proposed FEM Approach

The procedures proposed in the previous section is suitable for simulating the beam's response to motion of the mass given by any arbitrary $s(t)$. Unlike the pendulum problem discussed in Chapter 2, where an 'exact' solution was available, there is no such solution possible for the beam problem (i.e. Eq. (3.6) requires infinite series to obtain any analytical solution). However, for constant velocity cases, several solutions to such problems which have been presented in the literature can be compared to those obtained from the proposed FEM approach. Furthermore, a new solution based on infinite series for solving Eq. (3.6) numerically is used for further verification of the FEM results and for convergence analysis. It is noted that the guidelines for

the time steps of integration, mesh density, etc. established in the previous chapter for the pendulum problems will be partly reused in this chapter for the beam problems.

3.2.3.1 A mass traveling along a simply supported beam with constant velocity

The following problem was selected for testing because it was considered numerically in Schneider et al. (1983) and analytically/experimentally in Schallenkamp (1937). In these works gravity was omitted, instead, a force F was assumed to travel with the mass at a constant velocity v (see Figure 3-4).

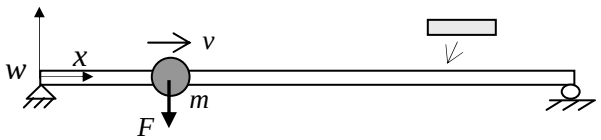

Figure 3-4 A simply supported beam with a mass and a force traveling with a constant velocity.

In the first example, the beam's length, height, and width were assumed 1 m, 0.001 m, and 0.02 m, respectively. The density was $7{,}850\,kg/m^3$ and Young's modulus was 204 GPa. The case of mass m = 0.135 kg traveling from the left to right with constant velocity $\dot{s} = v$ = 2.32 m/s is considered first. In order to be comparable with Schneider et al (1983) and Schallenkamp (1937), a force F=0.147 N, which is not related to gravity, is moving with the mass.

Figure 3-5 compares the beam's displacements at the current mass location obtained by the procedure described in section 3.2.2 with those in Schneider et al. (1983). In the figure, only the cases with the Coriolis effects excluded, which corresponds to the proposed method (**b**), or included as in method (**c**) are presented. The results calculated by method (**b**) agree very well, while some small differences are observed for method (**c**). The significance of the Coriolis

effects should be also noticed. For example, if these effects are neglected then the maximum deflection is about 50% greater.

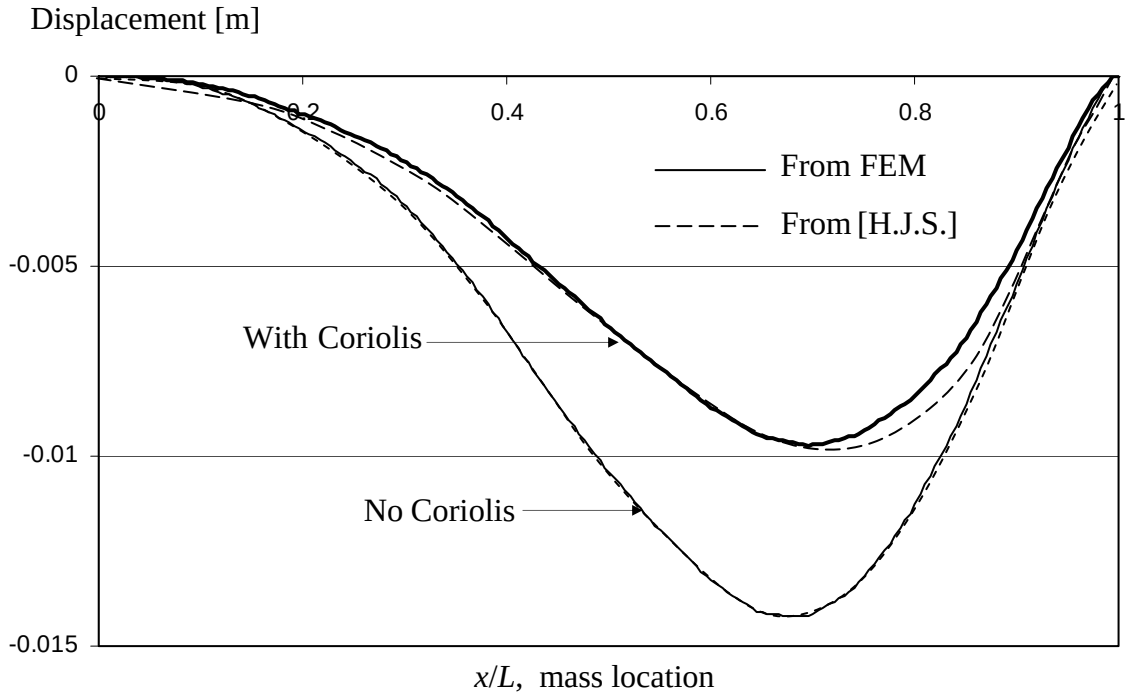

Figure 3-5 Comparison with the solutions presented in Schneider et al. (1983), [H.J.S.] on the plot.

For more comparisons different values of mass for the moving body as well as different values of the mass velocity were examined. Figure 3-6 shows the results obtained for $m = 0$ and $m = 0.0675$ with Coriolis effect included (note that the *m*=0 curves in the figure correspond to the moving force case or method (**a**)). In general, it is concluded that the solutions obtained in the two works are in good agreement.

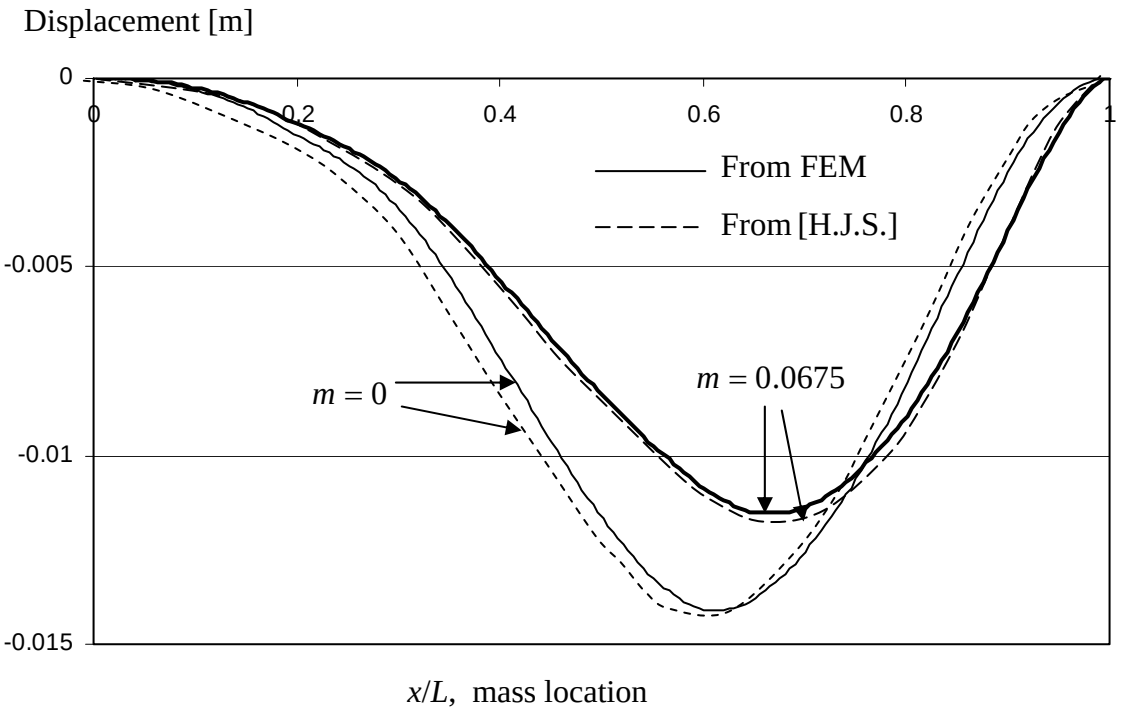

Figure 3-6 Comparison with the solutions presented in H.J. Schneider et al (1983), [H.J.S.] on the plot, for two different values of m .

3.2.3.2 Two masses traveling along a simply supported beam

In order to compare with more results reported in Schneider et al. (1983) and Schallenkamp (1937) the case of the beam in Figure 3-7 with two masses m_1 and m_2 traveling apart (a is the distance between them) at a constant velocity is considered. Also, two forces F_1 and F_2 moved along with the masses (not necessarily related to their weights).

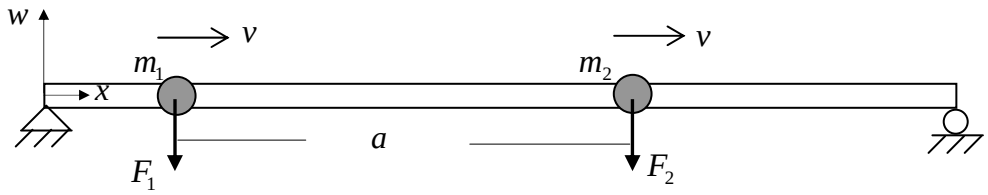

Figure 3-7 A simply supported beam with two masses moving at constant velocity.

In this numerical example, $m_1 = m_2 = 0.03\ kg$, $F_1 = F_2 = 0.147\ N$, and $v = 2.320\ m/s$. At time t=0, the first mass enters the beam from the left end. When this mass is at the distance a (a=L/2 was considered) the second mass enters the beam (from the left end). Clearly, when the second mass is at the distance a from the right end, the first mass is leaving the beam. Figure 3-8 shows the displacements of the two masses (which are the same as the beam's deflections at the locations of the two masses) as they are moving along the beam (the x-axis in the figure represents the current location of the masses). In the figure, the results taken from Schneider et al (1983) were obtained by including the masses' inertia and the Coriolis effects, which should correspond to our FEM approach by method (**c**). As can be seen, the solutions appear to be in good agreement.

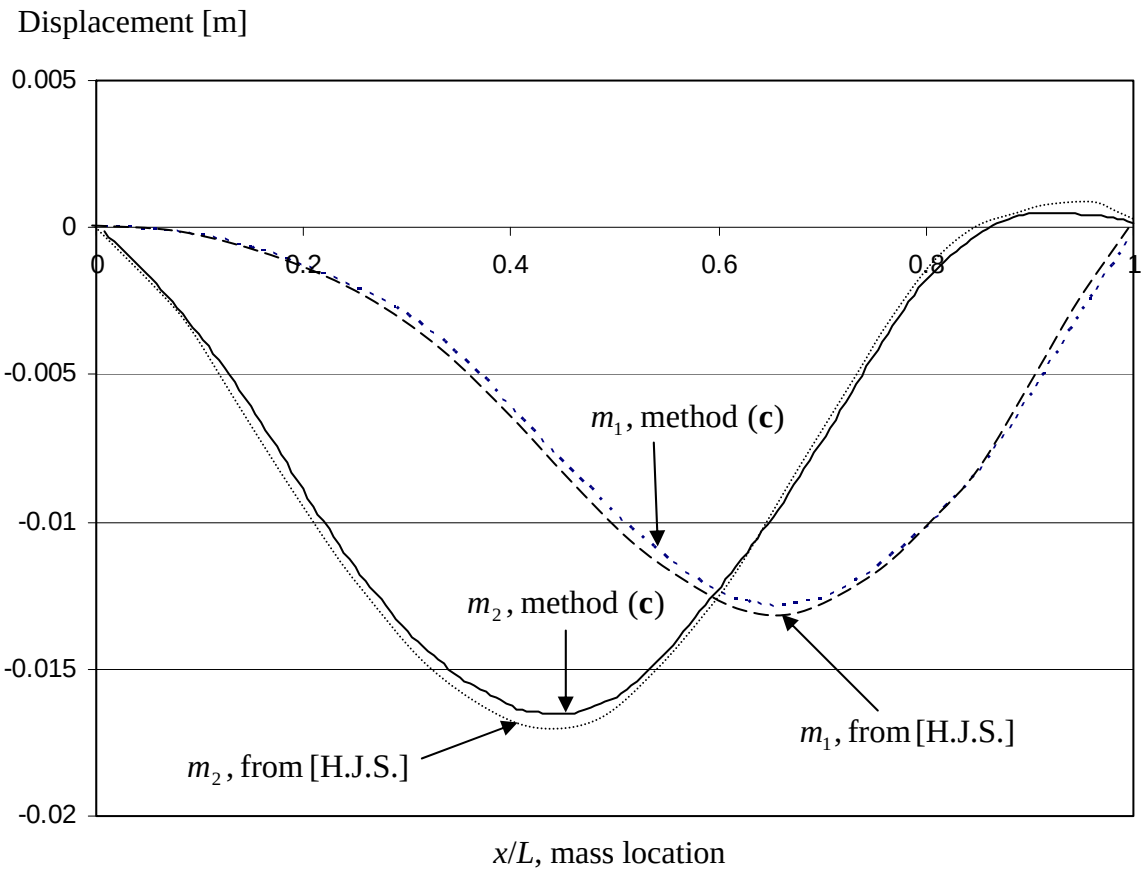

Figure 3-8 Movement of the two masses traversing the beam. Comparison with H.J. Schneider et al (1983), [H.J.S.] on the plot.

Next, in Figure 3-9 the FEM solutions obtained by method (c) are compared with those reported in A. Schallenkamp (1937). About 10% maximum differences between them are observed. Recall that the results in the paper mentioned are at least partially experimental. If in the proposed FEM simulations method (**d**) is used, i.e. if the centripetal effects are included, then the results shown in Figure 3-10 are obtained. Interestingly, the displacement obtained for the first mass, m_1, is now closer to the results of Schallenkamp (1937); however, the displacement of the second mass, m_2, deviates much more. The reason might be the experimental error of measuring the beam's deflection when two masses are moving on the beam simultaneously.

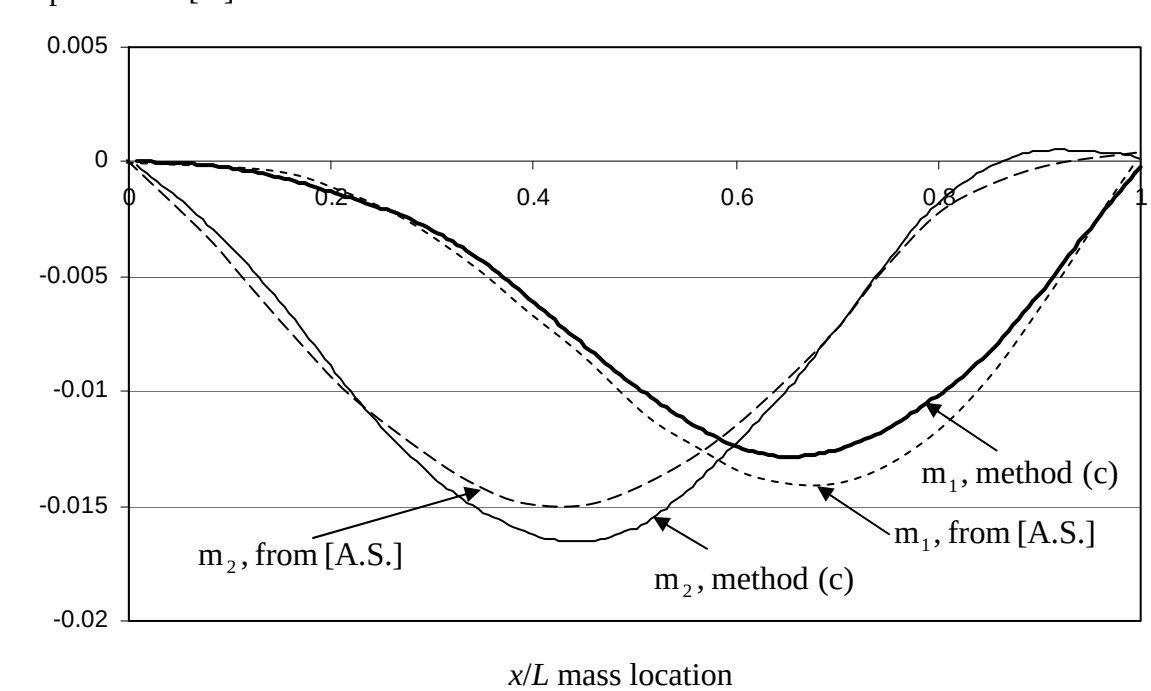

Figure 3-9 Movement of the two masses traversing the beam. Comparison with A. Schallenkamp (1937), [A.S.] on the plot.

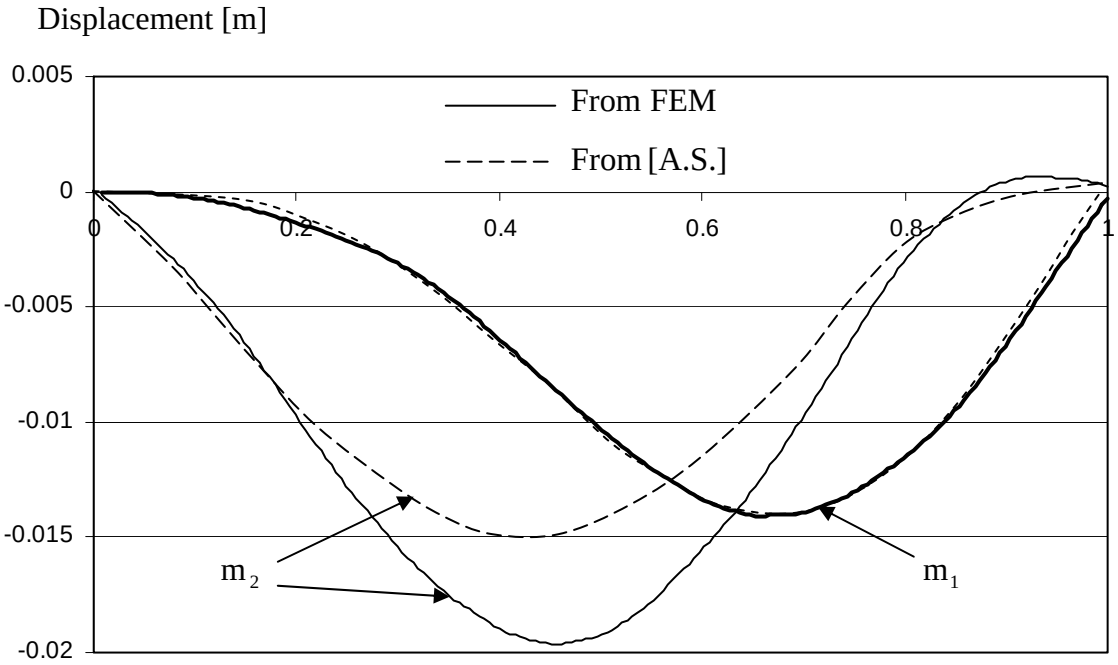

Figure 3-10 Movement of the two x/L, mass location e beam. Centripetal acceleration is included.

3.2.3.3 Using infinite series to solve the beam's dynamic equations

As already mentioned in the introduction, the dynamic equations for the beam problem, Eq. (3.6), are complicated and no direct numerical integration of the equations is possible. In fact, the presence of the Dirac Delta function in the equation on one hand, and the equation of motion being a partial differential equation on the other hand, makes the direct numerical integration extensively complicated. For the pendulum problem, however, the equation of motion is an ordinary differential equation with only one degree of freedom which is why it could be directly integrated to obtain an analytical solution.

The only possible numerical solution to Eq. (3.6) appears to be in form of an infinite series. To obtain this solution, first consider the dynamic equations of (3.6) in the absence of external forces (i.e. $F_k = 0$) and the axial force (i.e. $n(x) = 0$) as:

$$EI\frac{\partial^4 w}{\partial x^4} + \rho A\frac{\partial^2 w}{\partial t^2} = -\rho Ag - m(g + \frac{\partial^2 w}{\partial t^2} + 2\dot{s}\frac{\partial^2 w}{\partial t \partial x} + \dot{s}^2\frac{\partial^2 w}{\partial x^2})\delta(x-s) \qquad (3.20)$$

It is then assumed that a solution is possible to this equation in the form of infinite series as:

$$w = \sum_n \mathrm{X}_n(x)\Theta_n(t) \qquad (3.21)$$

in which $\mathrm{X}_n(x)$ is the n^{th} modal shape of the beam's free vibration. From the method of separation of variables, $\mathrm{X}_n(x)$ should satisfy the boundary conditions and the equation:

$$E\mathrm{X}_n'''(x) - \rho A\omega_n^2 \mathrm{X}_n(x) = 0 \qquad (3.22)$$

in which ω_n is the n^{th} natural frequency of the beam. By substituting Eq. (3.21) into Eq. (3.20) and making use of Eq. (3.22), the equation of motion in the series form is obtained as:

$$\begin{aligned}\rho A\sum_n \omega_n^2 \mathrm{X}_n(x)\Theta_n(t) + \rho A\sum_n \mathrm{X}_n(x)\ddot{\Theta}_n(t) = -\rho Ag - m\Big(& g + \sum_n \mathrm{X}_n(x)\ddot{\Theta}_n(t) \\ & + 2\dot{s}\sum_n \mathrm{X}_n'(x)\dot{\Theta}_n(t) + \dot{s}^2\sum_n \mathrm{X}_n''(x)\Theta_n(t)\Big)\delta(x-s)\end{aligned} \qquad (3.23)$$

Multiplying the two sides of this equation by $\mathrm{X}_k(x)$, integrating from 0 to L, and using the orthogonality of the modal shapes as well as Dirac's function properties will eventually lead to:

$$\ddot{\Theta}_k(t) + \omega_k^2\Theta_k(t) = -g\frac{\beta_k}{\alpha_k} - \frac{m\mathrm{X}_k(s)}{\rho A\alpha_k}\begin{pmatrix} g + \sum_n \mathrm{X}_n(s)\ddot{\Theta}_n(t) + 2\dot{s}\sum_n \mathrm{X}_n'(s)\dot{\Theta}_n(t) \\ + \dot{s}^2\sum_n \mathrm{X}_n''(s)\Theta_n(t)\end{pmatrix} \qquad (3.24)$$

where α_k and β_k are:

$$\alpha_k = \int_0^L \mathrm{X}_k^2(x')dx', \qquad \beta_k = \int_0^L \mathrm{X}_k(x')dx' \qquad (3.25)$$

Equations (3.25) are a set of simultaneous (coupled) second order differential equations in which the unknown functions are $\Theta_k(t)$. Note that $\mathrm{X}_n(s)$, $\mathrm{X}'_n(s)$ and $\mathrm{X}''_n(s)$ are known functions of time which are obtained by substituting $x = s(t)$ into the modal shape functions and their derivatives. Also, the initial conditions for functions $\Theta_k(t)$ can be determined based on the (known) initial deflection and velocity of the beam (namely $w(x,0)$ and $\dot{w}(x,0)$) together with using the orthogonality of modes. Clearly, an analytical closed form solution for the above equations is not possible. However, by considering a limited number of the modes, for instance the first three modes, a numerical solution to Eq. (3.24) may be obtained by using a numerical integration procedure like the Runge-Kutta method. In the following, this numerical solution will be compared to those obtained by FEM. It is also noted that by removing the appropriate terms in the right hand side of Eq. (3.24) (or Eq. (3.25)), the beam's response without including the effect of mass inertia, Coriolis or centripetal accelerations can be obtained.

Prior to presenting the numerical results, it is useful to rewrite Eq. (3.20) in a non-dimensional form as:

$$\frac{\partial^2 \overline{w}}{\partial \bar{t}^2} + \frac{\partial^4 \overline{w}}{\partial \bar{t}^4} = -\overline{g} - \overline{m}\left(\overline{g} + \frac{\partial^2 \overline{w}}{\partial \bar{t}^2} + 2\overline{v}\,\frac{\partial^2 \overline{w}}{\partial \bar{x}\partial \bar{t}} + \overline{v}^2\,\frac{\partial^2 \overline{w}}{\partial \bar{x}^2} \right)\delta(\bar{x} - \bar{s}) \qquad (3.26)$$

where

$$\overline{w} = \frac{w}{L}, \quad \bar{x} = \frac{x}{L}, \quad \overline{m} = \frac{m}{\rho A L}, \quad \bar{t} = \frac{t}{T_r},$$
$$T_r = \sqrt{\frac{\rho A}{EI}}L^2, \quad \overline{g} = \frac{g T_r^2}{L}, \quad \overline{v} = \frac{\dot{s} T_r}{L}, \quad \bar{s} = \frac{s}{L} \qquad (3.27)$$

If the mass velocity is constant, which is the case for most of the examples in this chapter, it is concluded that based on Eq (3.26), the system's response depends on the dimensionless mass $\overline{m}$

and velocity $\bar{v} = \text{constant}$. These dimensionless forms will be used in the following to present the numerical results.

As a first example, consider a simply supported beam with parameters: $L = 50$ m, $\rho Ag = 15 \times 10^3$ N/m, and $EI = 75 \times 10^9$ Nm^2 along which a body is moving with constant velocity of v_0 and mass of m. This can represent a bridge which is traversed by a large mass, a locomotive for instance. It is assumed that beam is initially un-deformed (i.e. $w(x,0)$) and at rest (i.e. $\dot{w}(x,0)$). Solutions obtained by the FEM and modal series methods are compared for different values of m and v_0. Also, the comparisons are made considering whether the effect of different mass accelerations is included or excluded.

Figure 3-11 shows a sample solution for $\overline{m} = 0.3$ and $\bar{v}_0 = 0.75$. The FEM solution in the figure is obtained by dividing the beam into 100 equal elements and using time step of 3.75e-4 sec. The modal solution was obtained using the fourth order Runge-Kutta method with the same time step and considering the first three modal shapes. According to the figure, the solutions, which are the deflections of the middle point of the beam versus time, are very close. In these analyses, the effect of all mass accelerations is included. If some of these accelerations are excluded both in FEM and modal solution procedures, then the simulations show that the corresponding results are still very close (they change when the effect of any mass acceleration is excluded). This means that the FEM solution agrees with the modal solution procedures including the effect of each of these accelerations. Finally, it is important to note that the modal solution does not change much if the second and third modes are ignored. In other words, for the parameters selected, the solution is dominated by the first mode only, which means the convergence of the series solution is secured (including more modal function does not change the solution).

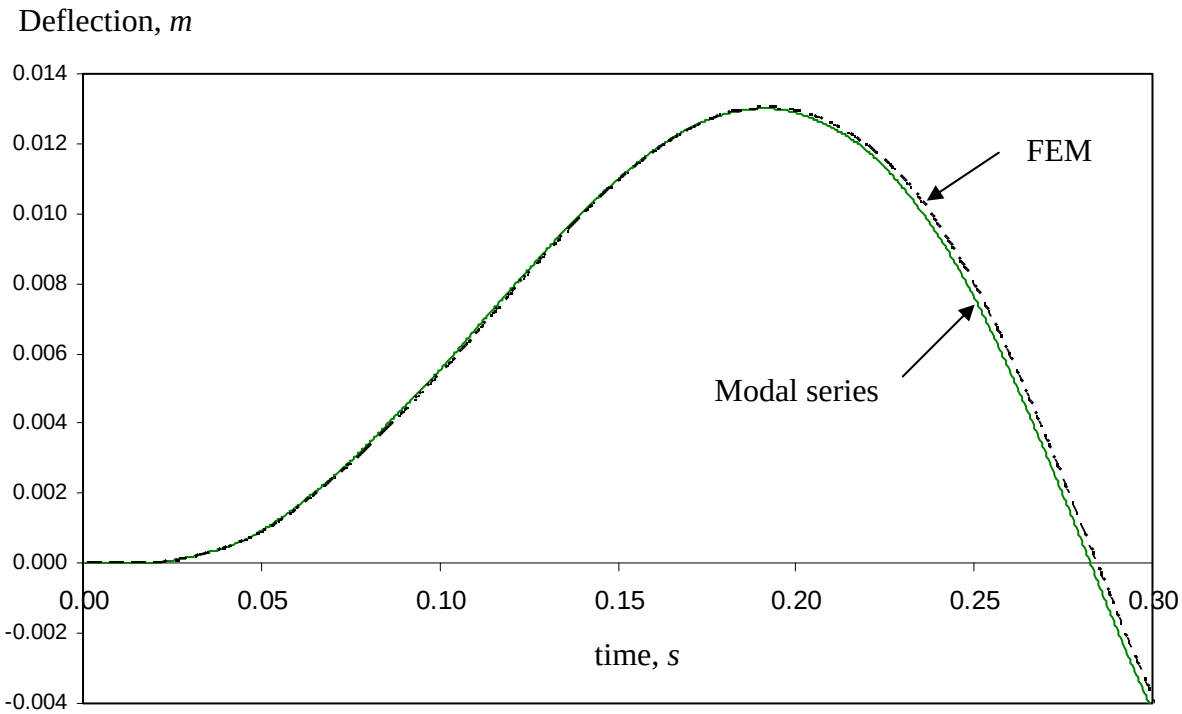

Figure 3-11 Deflection of the middle point of the beam versus time obtained by FEM and modal series for $\overline{m} = 0.3$ and $\overline{v}_0 = 0.75$.

In order to compare the solutions obtained by the two methods further, different values of $\overline{m}$ and $\overline{v}_0$ have been used and the results have been compared. These analyses show that the solutions are very close no matter what parameters are used. For instance, the case for $\overline{m} = 0.3$ and $\overline{v}_0 = 0.25$ when the centripetal acceleration is ignored is shown in Figure 3-12. As can be seen, the two solutions are almost indistinguishable.

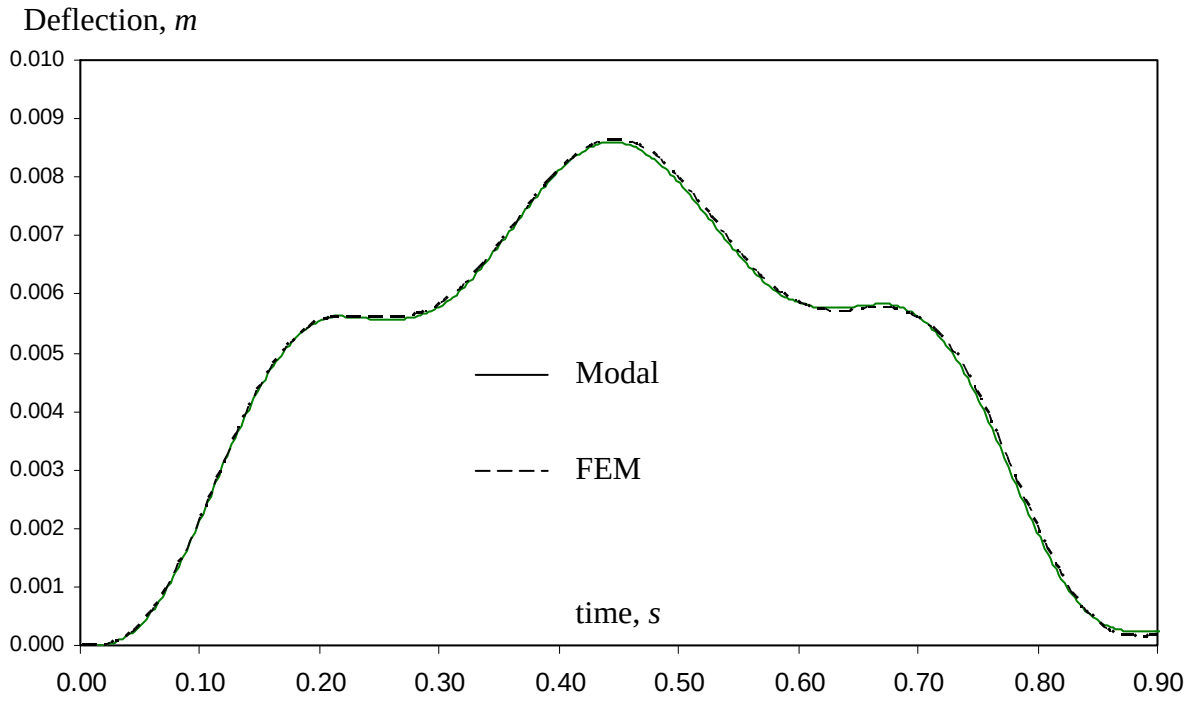

Figure 3-12 Deflection of the middle point of the beam versus time obtained by FEM and modal series for $\overline{m} = 0.3$ and $\overline{v}_0 = 0.25$.

In addition to $\overline{m}$ and $\overline{v}$, the solution of Eq. (3.26) is also dependent on the boundary conditions and initial conditions. In order to investigate a different boundary condition of the beam, next a cantilever beam along which the mass is moving with a constant velocity from the free end of the beam towards the clamped end will be considered. Figure 3-13 shows the tip deflection versus time for $\overline{m} = 0.3$ and $\overline{v}_0 = 0.2$ obtained by the two methods. Again, it is observed the solutions are very close. The results of this figure were obtained by including all the mass acceleration effects. Analyses with different values of $\overline{m}$ and $\overline{v}_0$ as well as different level of complexity (in terms of including different mass accelerations) have been done and the comparison of the solutions shows that the results of the two methods are very close.

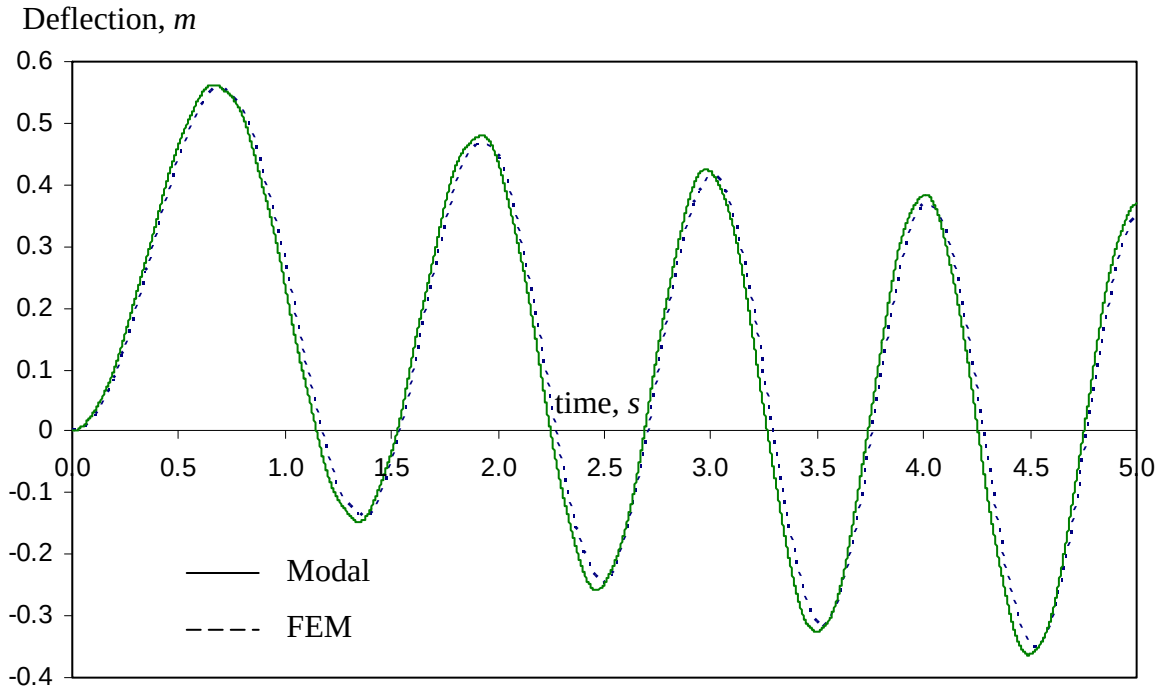

Figure 3-13 Deflection of the tip of the beam versus time obtained by FEM and modal series for $\overline{m} = 0.3$ and $\overline{v}_0 = 0.2$. All mass accelerations are included.

If the solution obtained by the modal infinite series is considered as the exact solution, then the error of FEM solution compared to this exact solution can be calculated for different values of time step and element size used in the FEM model. Consequently, one can investigate the required time step and element size for obtaining accurate results (with smaller error) by FEM. To this end, the problem of a simply supported beam, with the first natural period of 0.257 *s*, along which a body of mass $\overline{m} = 0.3$ is moving with constant velocity of $\overline{v}_0 = 0.1$, is considered. The solution obtained by modal analyses, which was obtained by including the first five modes and using a time step of 0.001 *s* is shown in Figure 3-14. It is noted that this solution almost does not change when a smaller time step was used. Also, the effects of the fourth and higher modes

are almost negligible which means this modal solution has converged. Figure 3-14 also depicts a sample solution obtained by FEM which corresponds to time step of 0.0225 *s* and the number of elements equals to 50 (the entire beam is discretized by 50 equal elements). As shown in the figure, there is a difference between the amplitude as well as the period obtained by the two methods. These two differences can be called the amplitude and the period errors (similar to the errors defined for the pendulum problem) and will be used as a criterion of how accurate the FEM solutions are.

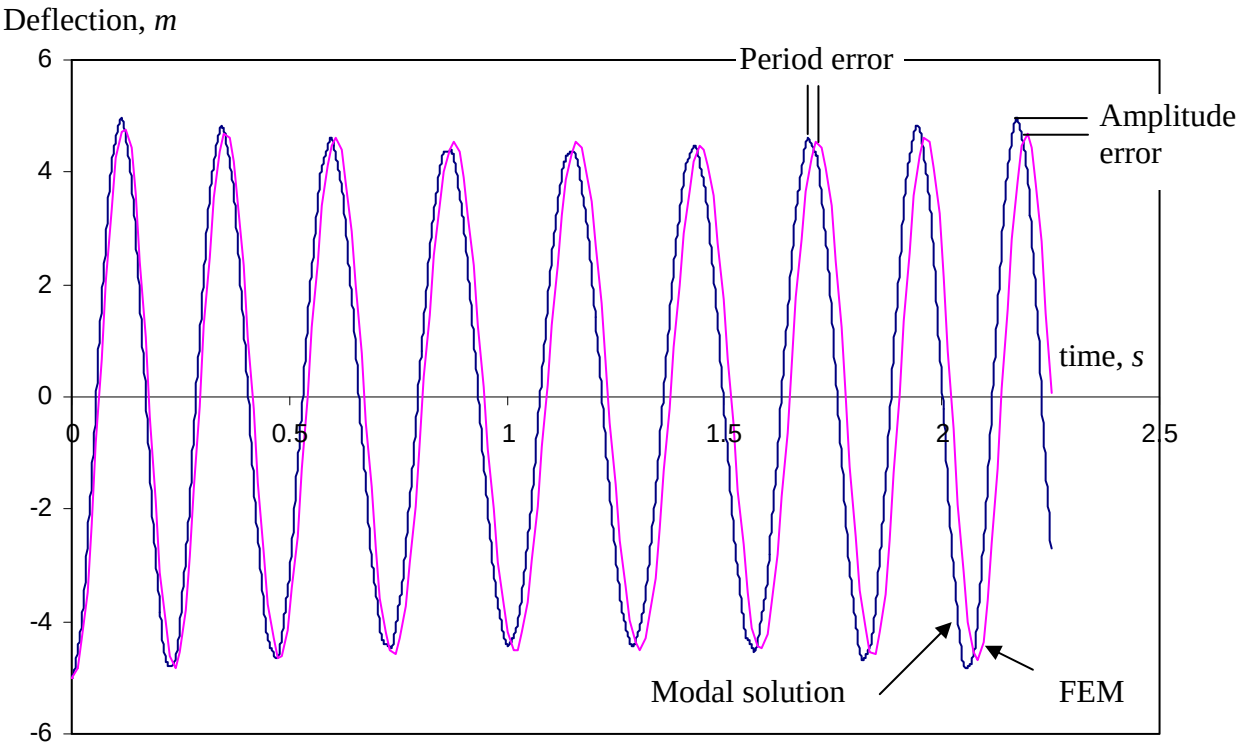

Figure 3-14 Deflection of the middle point of the beam obtained by modal analysis and FEM.

Figure 3-15 and 3-16 show how the two errors change with time step as well as the number of elements used to discretize the beam. It is noted that the time step presented in the figures has been non-dimensionalized with respect to Δt_r, which is the required time step for obtaining

accurate solution for a stationary (with no mass motion) case. As mentioned in chapter 2, this time step is usually approximated as $T_p/20$ where T_p is the first period of vibration. For the beam considered here, Δt_r is about 0.0128 sec. As it is observed in Figures 3-15 and 3-16, the error generally decreases when the time step decreases. However, the amplitude error changes in an apparently random manner with time step when the number of elements was 25. This means that using 25 elements is not sufficient for obtaining accurate results. Also, it is observed that the period error increases slightly when the dimensionless time step decreases from 0.0028 to 0.0014. This might be due to the fact the FEM solutions are only available at time instances which are multipliers of the time step. As a result, it is relatively hard to determine the period error precisely, particularly for the smaller errors, which eventually can lead to some irregularities in the calculation of this error.

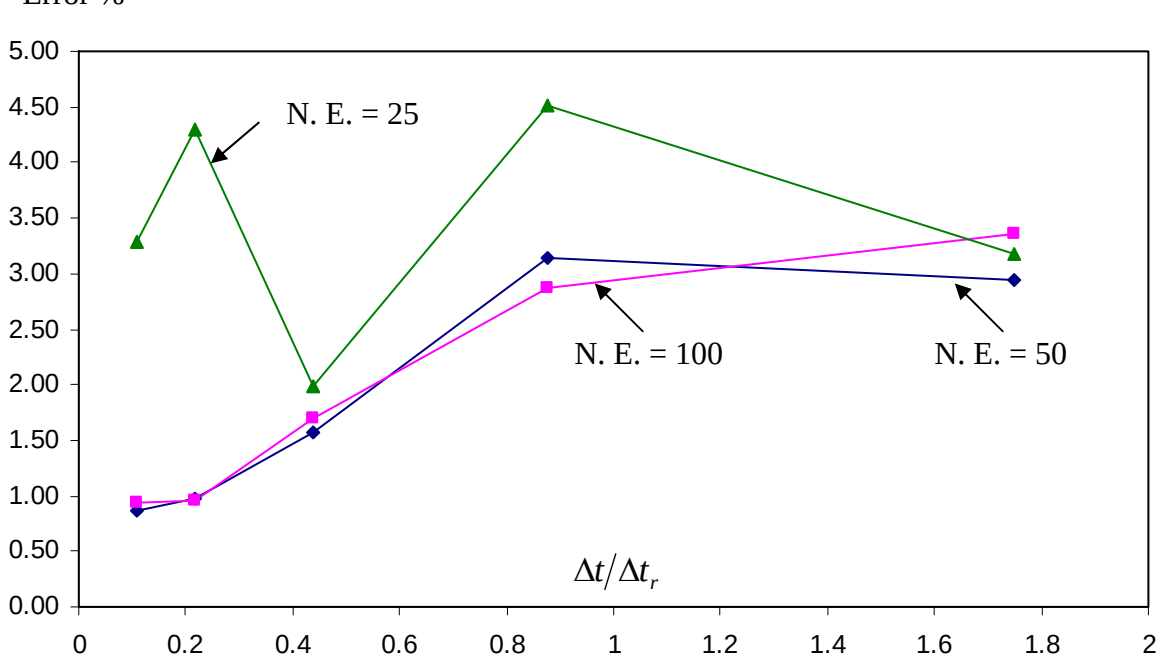

Figure 3-15 Average amplitude error versus dimensionless time step for different number of elements.

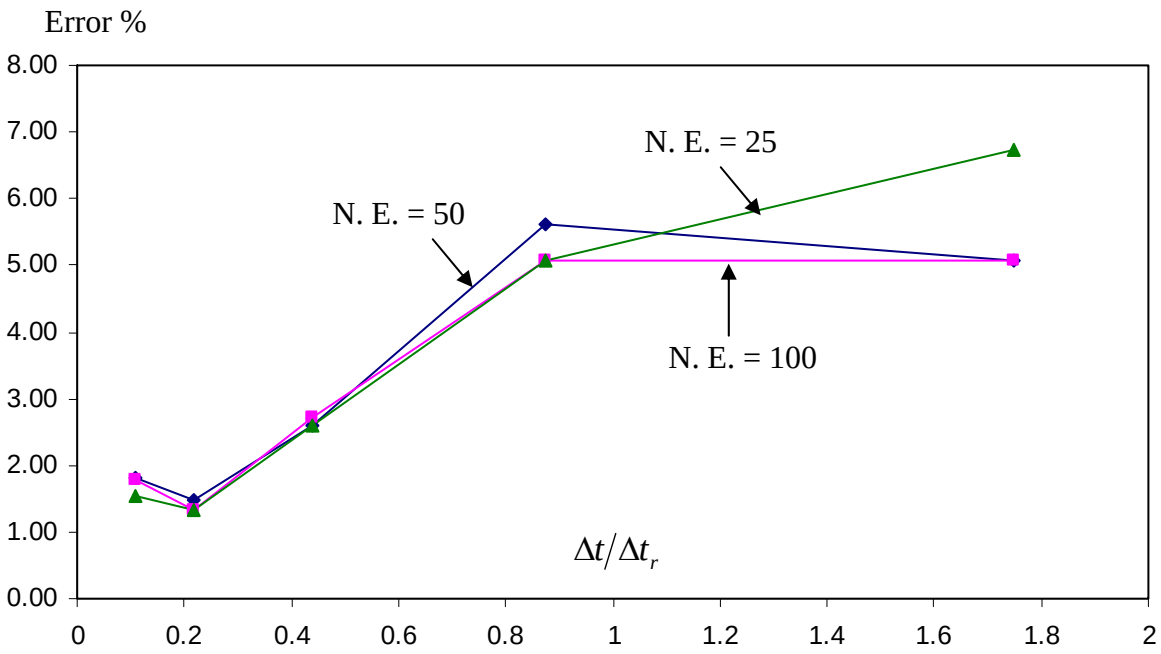

Figure 3-16 Average period error versus dimensionless time step for different number of elements.

3.2.4 Effect of including the mass Coriolis and centripetal accelerations on the solution

Once the FEM model is verified through different numerical examples, it is interesting to investigate how including each mass acceleration term (Coriolis and centripetal accelerations in particular) affects the system response. To illustrate the importance of these effects, the case that was solved in section 3.2.3.1 (see Figure 3-5) is solved again this time by using each of the four methods (**a**) to (**d**) mentioned in the introduction. From the results, which are shown in Figure 3-17, it can be concluded that the solution can change considerably when different mass acceleration terms are included/excluded.

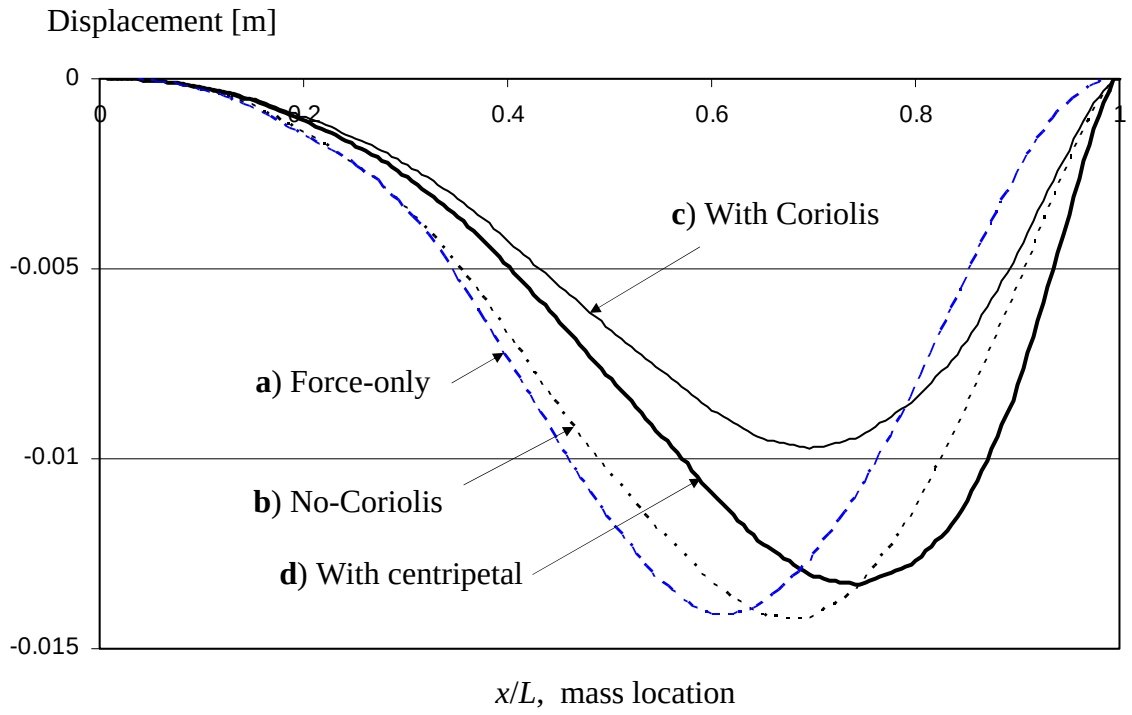

Figure 3-17 Comparison of the solutions obtained by applying methods (**a**), (**b**), (**c**) and (**d**).

It should be noted that for the case shown in Figure 3-17, the mass of the moving body is almost equal to that of the beam itself (which is 0.157 *kg*) and also, the velocity of the body can be considered relatively high (the mass passes the beam's span in 0.431 *s*, the time that is almost equal to the first period of natural frequency of 0.433 *s*). Consequently, when analyzing how various parameters of the system affect the differences presented in Figure 3-17, it is more appropriate to use the non-dimensional parameters of Eq. (3.27). The dimensionless velocity in this equation can be rewritten as $\bar{v} = T_r \big/ {}^{L}\!\!\diagup\!\!{}_{v}$ which is the ratio of the reference time T_r to the time it takes for the mass to traverse the entire beam. In general, the reference time T_r is proportional to the period T_p of natural vibrations of the beam ($T_r = \frac{\pi}{2} T_p$ for the beam in Figure 3-4). The results in Figure 3-17 were obtained for $\bar{m}$ =0.860 and $\bar{v}$ =1.576 (T_r =0.680*s*).

To investigate the effect of the mass acceleration terms, the following example was studied: an initially resting simply-supported beam was deflected by a force statically applied at the center of the beam to cause deflection of the center equal to $0.1L = 0.1m$. The force is then instantaneously removed and at the same time a mass starts to move from left end of the beam to the right with constant velocity v. Different masses and velocities were used to investigate their effects. The reason for choosing such initially-disturbed beam problems is that similar problems will be discussed in the next section where the beam's vibration will be controlled by the moving mass.

First, Figure 3-18 shows the percentage difference (the vertical axis) between the mid-span deflections obtained with and without the centripetal effects averaged over the traverse time. It is observed that the difference (to represent the difference between applying methods (**c**) and (**d**)) is small for low values of $\overline{m}$ and $\bar{v}$ but increases sharply for $\bar{v} > 1.5$, which might be attributed to quadratic relationship between the velocity and the centripetal acceleration.

Next, the numerical experiment was executed excluding both the centripetal and Coriolis effects (method (**b**)). This in turn allowed comparing methods (**b**) and (**c**), which is the effect of including and excluding the Coriolis effects (without the centripetal acceleration present). The results are summarized in Figure 3-19. This time, the maximum difference occurs at $\bar{v} \approx 1$, and increases almost linearly with $\overline{m}$. It is also noted that the differences observed in Figure 3-19 are generally greater than those of Figure 3-18 for low velocities (roughly if $\bar{v} < 1$), and smaller for high velocities (e.g. if roughly $\bar{v} > 1$). This indicates that the effect of Coriolis acceleration is more important than the centripetal acceleration especially for lower velocities.

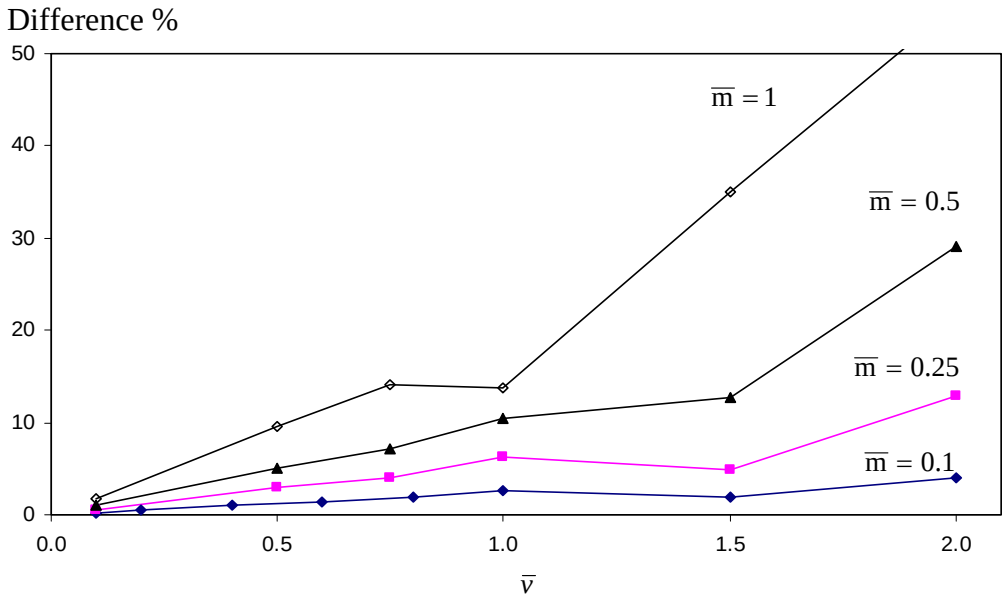

Figure 3-18 Comparison of the solutions obtained with and without the effect of centripetal acceleration.

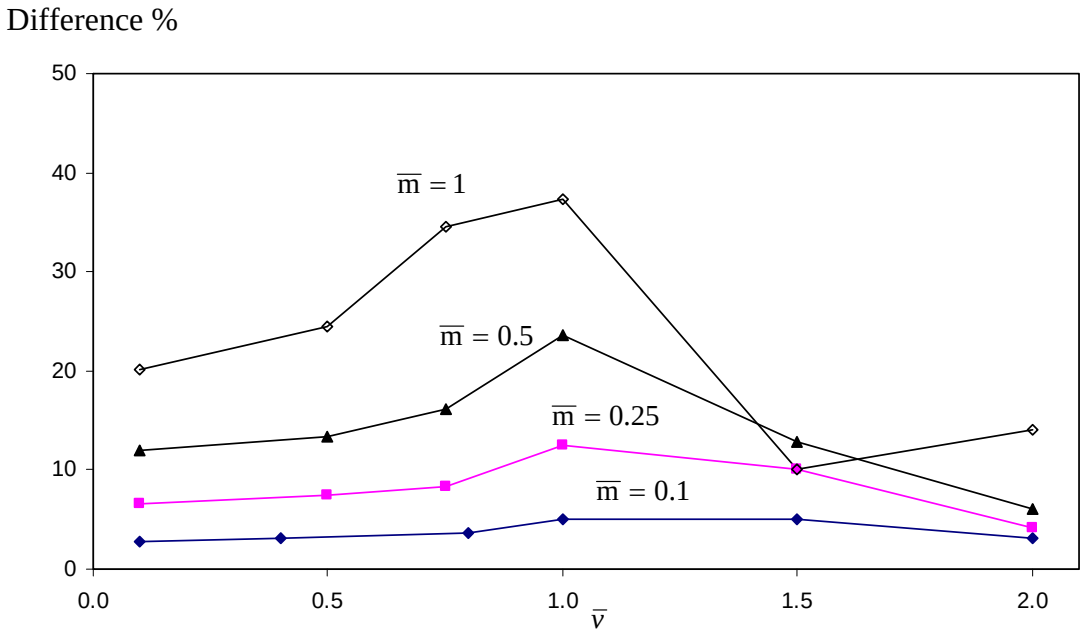

Figure 3-19 Comparison of the solutions obtained with and without the effect of Coriolis acceleration.

Based on the above results, it can be concluded that the centripetal effect is small for relatively small velocities even when the moving mass is relatively large. According to Figure 3-

18, the difference between the solutions that include or exclude this effect is less than 5% if $\bar{v}$ <0.25 for any $\overline{m} \le 1$. On the other hand, the Coriolis effect (see Figure 3-19) is only negligible for relatively small masses, if $\overline{m} \le 0.1$, while almost regardless of the velocity, it becomes quite significant for larger masses for which $\overline{m} \ge 0.5$. Similar conclusions could be drawn for beams with different initial conditions (or different patterns of disturbances).

3.3 Controlling the Beam's Vibration by Using a Moving Mass

As already mentioned in chapter 2, when the mass moves away from the structure's rotation center, its relative motion (in particular, the inertia force caused by the mass Coriolis acceleration) will attenuate the structure's vibration and vice versa (when it moves toward the rotation center it causes amplification of vibration). This amplification/attenuation effect is also observed in the beam problem. For instance, consider a cantilevered beam along which a mass is moving as shown in Figure 3-20. The beam is initially deflected by force F which is then removed and the mass starts to move along the beam. The instantaneous rotation center, which is illustrated in the figure, is moving as the mass moves along the beam. However, for the initial deflection considered in Figure 3-20, the rotation center is always to the left of the mass. This means that if the mass moves from the clamped end to the free end, it is moving away from the rotation center at all instants. Consequently, it is expected that such motion of the mass attenuates beam's vibration. On the other hand, if the mass moves from the free end to the clamped end, it is moving toward the rotation center and thus its motion should amplify the beam's vibration.

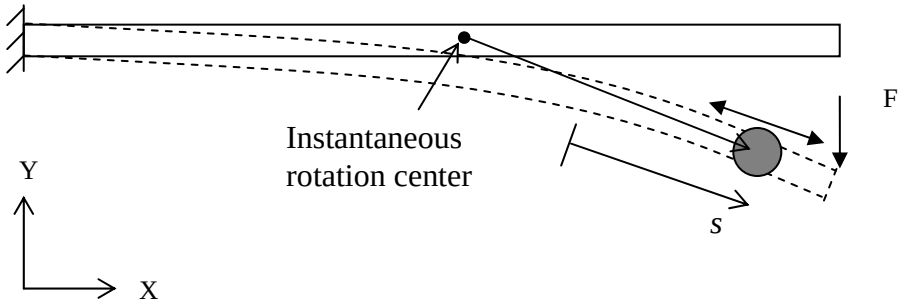

Figure 3-20 A cantilevered beam, which is initially deflected by a force, with a mass sliding along its length.

This attenuation/amplification effect can be shown through an example. Assume that the beam's parameters, shown in Figure 3-20, are: $L = 3m$, $\rho = 2800\ kg/m^3$ and $E = 200\ GPa$ and its cross sections is a rectangle of width 58*mm* and height of 5.6 *mm*. Figure 3-21 shows the beam's response, in terms of tip's displacement versus time, when a mass with $m = 2\ kg$ moves with constant velocity of $v = 0.2\ m/s$ from the clamped end all the way to the free end. As can be seen in the figure, the beam's vibration is attenuated gradually over time, as expected. In fact, the initial deflection of 0.3 *m* reduces to 0.22 *m* in the sixth cycle. It is noted that the opposite effect (amplification of beam's vibration) is observed when the mass is moving from the free end to the clamped end (the corresponding results are not shown for the sake of brevity).

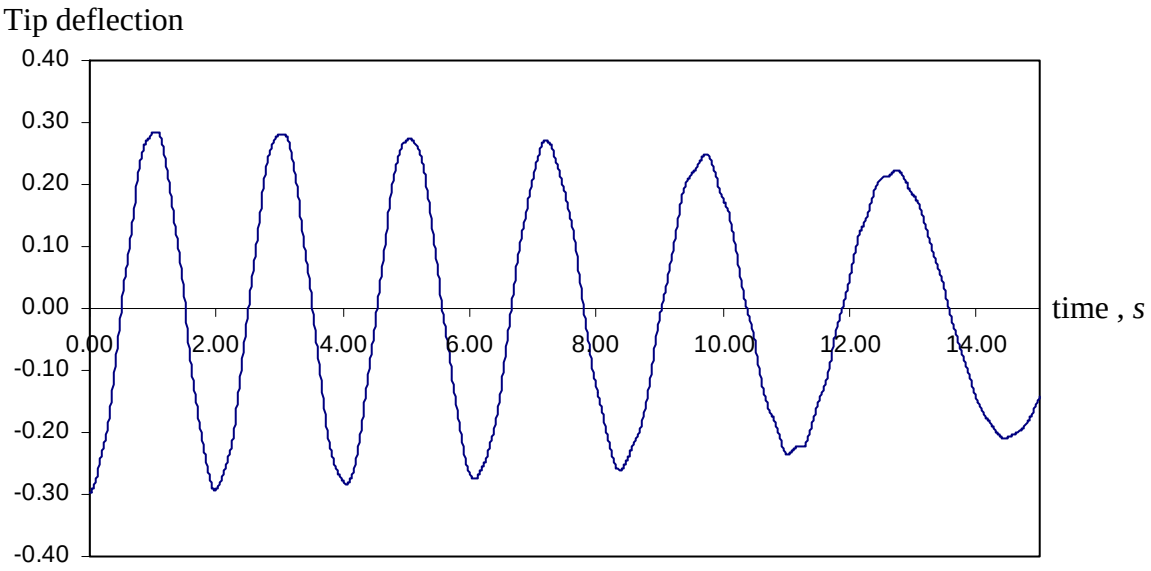

Figure 3-21 A cantilevered beam's response when a mass moves with a constant velocity from the clamped end to the free end.

Following the same technique presented in Chapter 2, a sinusoidal pattern of mass motion is proposed for obtaining continuous attenuation (or amplification):

$$s(t) = s_0\left(1 - \varepsilon \sin\left(2\omega_0 t\right)\right) \tag{3.28}$$

where ω_0 is the initial frequency of vibration for the beam, s_0 is the average location of the mass and ε is the dimensionless amplitude of mass oscillation.

Assume that the simply-supported beam in Figure 3-22 is initially deflected by a force F applied at its center. Then, at t = 0, the force is removed and a mass starts moving according to Eq. (3.28). The beam's response, in terms of mid-span deflection versus time, is shown in Figure 3-23. In this simulation, ω_0 is the first frequency of beam's vibration if the mass is at s_0, $\overline{m} = 0.3$, $s_0 = L/3$, $\varepsilon = 0.2$ (the mass motion range is $0.267L \le s \le 0.4L$) and ω_0=23.1 rad/s (the initial natural period is T_0=0.272 s). The entire beam was divided into 200 equal elements

and a time step of $\Delta t = 0.0005$ (which is about $0.002\,T_0$) was used to obtain sufficient accuracy. The dimensionless deflection used in the figure is defined as $\hat{w} = w_{L/2} / 0.05L$ (the initial deformation of the beam is such that $w_{L/2}(0) = -0.05L$).

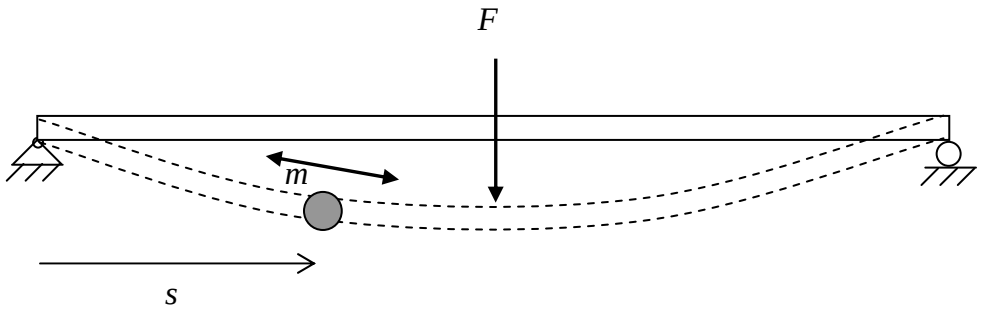

Figure 3-22 A simply supported deflected by the force *F*. Mass *m* is moving to control vibration of the beam.

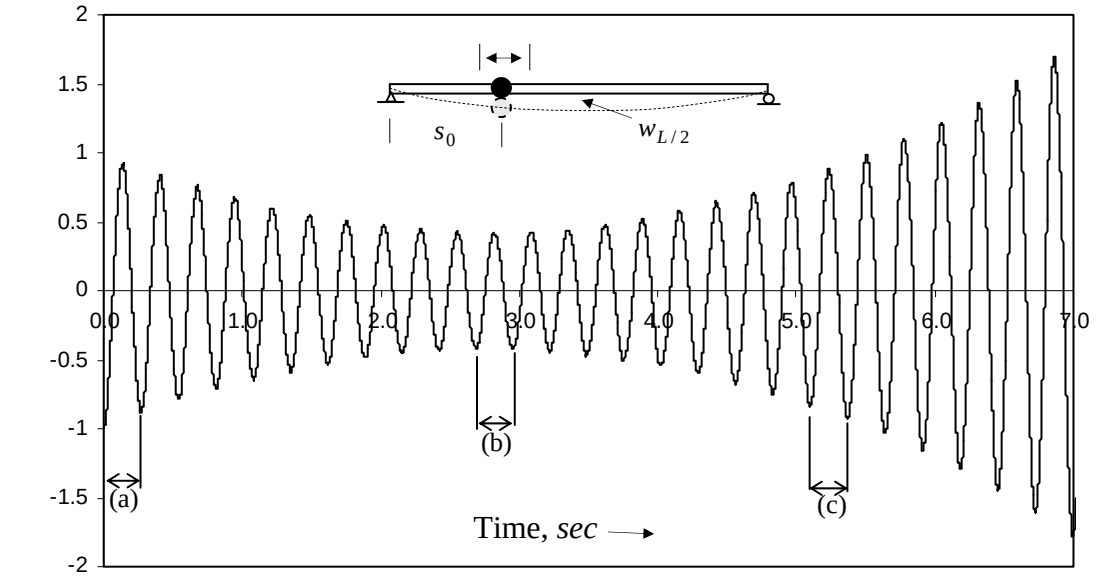

Figure 3-23 Response of a simply-supported beam to the mass motion given by $s = s_0\left(1 - \varepsilon \sin\left(2\omega_0 t\right)\right)$.

As can be observed, the first 10 cycles of the beam's vibrations are attenuated, followed by the cycles that are amplified. This beating phenomenon was also observed in the pendulum problem discussed in Chapter 2. As mentioned there, the reason for such a behavior is that due to the mass movement, the beam's vibrations are not exactly harmonic, with its frequency varying slightly. This in turn causes the initially in-phase mass motion (with its frequency kept the same) to gradually become neutral, and then out-of-phase. Like the pendulum problem, the phase of the mass' motion, ψ, can be examined at the beginning of each cycle of the beam's vibrations, when the beam is moving upward from the un-deformed configuration.

For illustration, the phases of attenuated (a), neutral (b), and amplified (c) cycles are presented in Figure 3-24. For the attenuated cycle, the mass is moving in-phase (with maximum forward velocity) as can be seen in Figure 3-24a. As explained in Chapter 2, the Coriolis forces associated with this type of relative motion should maximize the attenuation effects. In Figure 3-24b the mass is not moving at the beginning of the beam's vibration cycle generating the Coriolis forces that balance the attenuation and amplification effect. Consequently, such a cycle is neutral. Finally in Figure 3-24c, the mass is moving out-of-phase (with maximum backward velocity) generating the Coriolis forces that maximize the amplification effects.

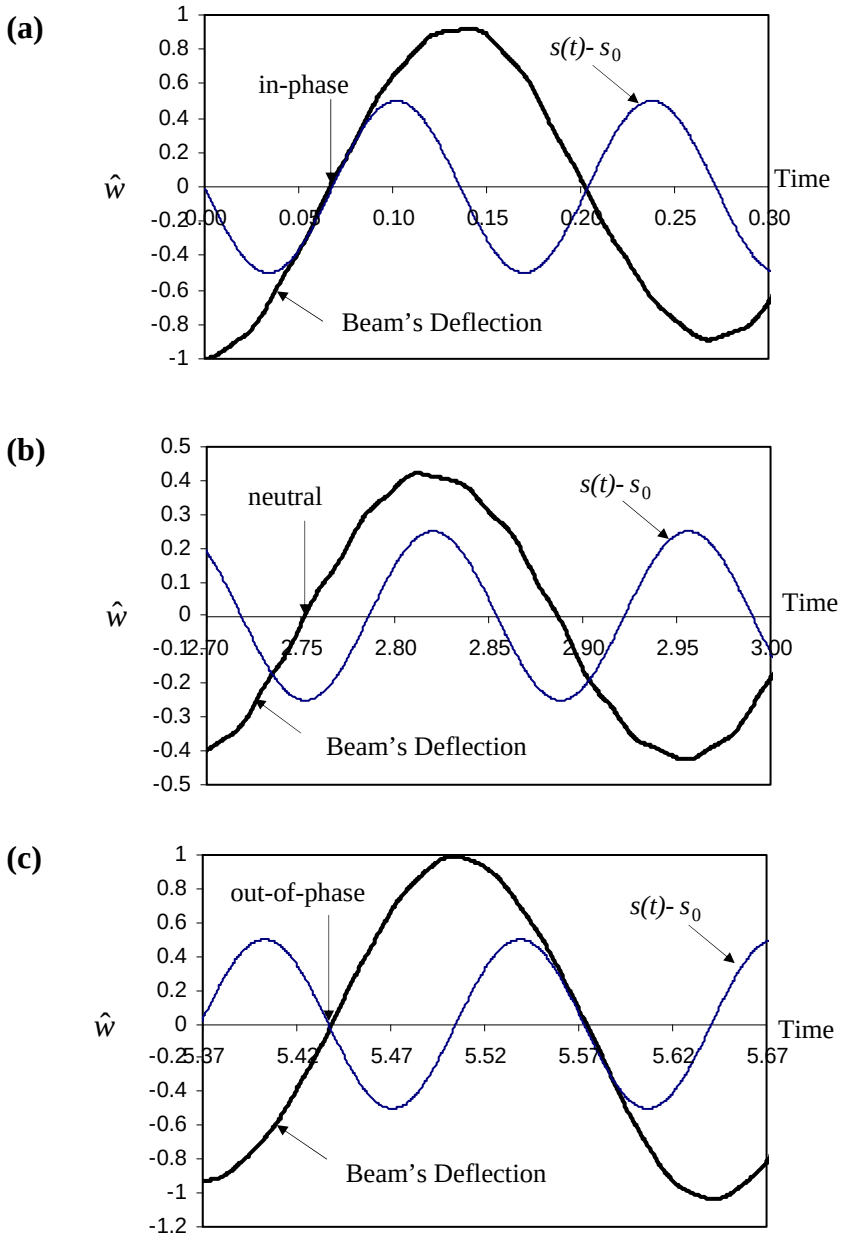

Figure 3-24 The mass' motion and the beam's deflection for attenuation (a), neutral (b), and amplification (c) cycles.

As discussed in Chapter 2, in order to obtain continuous attenuation, the mass motion should be synchronized such that its motion is always in correct phase with the main structure's vibration (as shown in Figure 3-24a). The procedure proposed in Chapter 2 will be reused here;

however, it should be generalized for the beam problem. A proper synchronization process should follow these steps:

1- Monitor the main structure's motion, in this case the beam's flexural vibration. This can include monitoring the slope of the beam at the current location of mass, slope at a certain point or displacement of a certain point.

2- Set the frequency of mass motion to twice the frequency of the main structure whenever it changes.

3- Adjust the phase and/or the frequency of mass motion if it's not in the correct phase with the beam's vibration.

Based on these steps, different schemes for synchronization may be implemented. Also, the mass motion should be expressed as:

$$s = s_0\left(1 - \varepsilon \sin\left(\omega_m t + \Delta\psi\right)\right) \tag{3.29}$$

Then, the mass motion parameters, ω_m and $\Delta\psi$, need to be updated when the frequency of the beam's vibration changes. At such instances of motion, the following schemes seem possible for updating ω_m and $\Delta\psi$:

1- ω_m is set to twice the frequency of main structure vibration, and $\Delta\psi$ is changed such that the mass motion, given by Eq. (3.29), is continuous.

2- ω_m is set to twice the frequency of main structure vibration, and $\Delta\psi$ is changed such that the mass is in the correct phase (i.e. $\omega_m t + \Delta\psi = \pi$). In this scheme, the mass motion will not be continuous.

3- According to Figure 3-24a, if the mass motion is perfectly synchronized, then it is expected that $\omega_m t + \Delta\psi = \pi$ at the instance when the sign of φ changes. If the mass

phase, $\omega_m t + \Delta\psi$, is smaller (or bigger) than π, then this delay (or being ahead) should be made up for in the next cycle by speeding up (or slowing down) the mass motion. In this scheme, the deviation of the mass phase from π is calculated and used to decrease (or increase) ω_m. Then, the value of $\Delta\psi$ can be updated such that the mass motion is continuous.

On the other hand, the synchronization can be done based on either the slope (angle) or the displacement at the current mass location or at a particular point of the beam. Combined with the three schemes mentioned above, different strategies seem possible for the synchronization process. In the following sections, the results obtained by using these strategies are presented and compared.

3.3.1 Controlling Vibration of a Cantilevered Beam

As will be shown later, the results as well as vibration control strategies that need to be used, varies for different beam types (i.e. beams with different boundary conditions). Consequently, the results obtained for each beam is presented in one separate section.

Consider the cantilever beam in Figure 3-20 which is excited by first applying a force at the free end to deflect the beam and then removing the force. The free vibration of the beam should then be controlled by moving a mass along its length as shown in the figure. The mass motion, which can be expressed by Eq. (3.29), should be synchronized based on one of the strategies mentioned previously. The length of the beam is L = 3 *m* and its parameters are such that its first natural period (without the mass) is about 2 *s*.

Figure 3-25 shows how the beam's tip deflection is changing with time when the mass motion parameters are: $\bar{s}_0 = s_0/L = 0.83$, $\varepsilon = 0.1$ and mass of the moving body is about one third of the

beam's mass. The synchronization used is based on the first scheme and the tip displacement (deflection) is used for the process. As it is observed, the vibration is attenuated until about $t = 50$ after which, the amplitude of vibration almost stays unchanged.

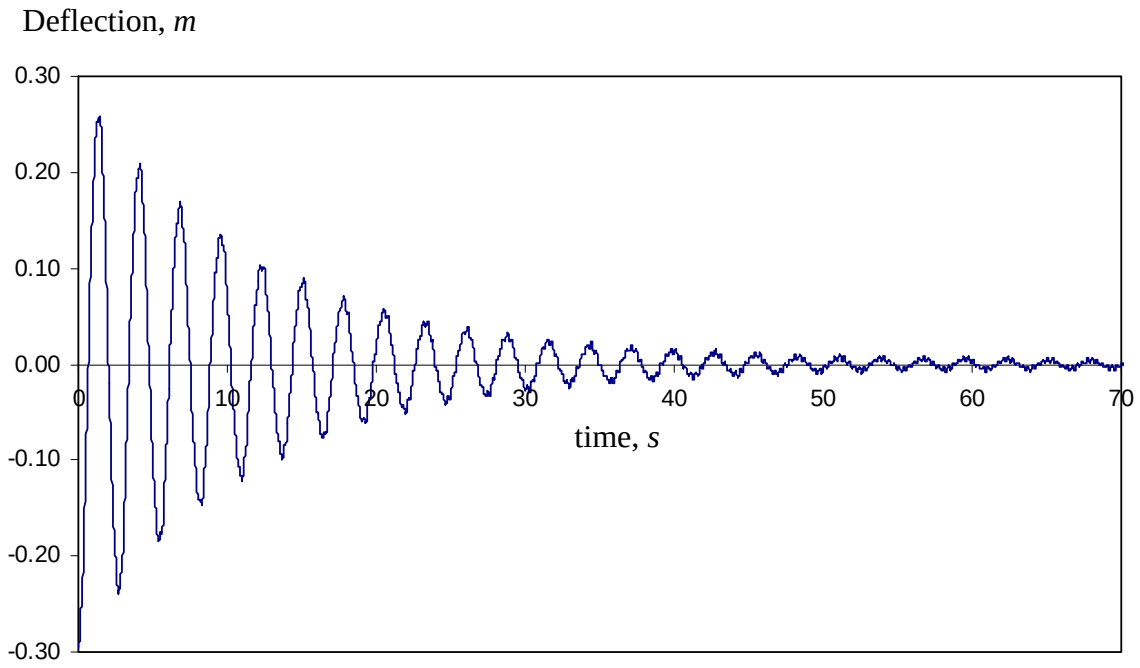

Figure 3-25 Tip deflection of a cantilevered beam versus time when the mass motion is synchronized according to the first scheme.

To understand why the beam's vibration is not attenuated completely, while it was completely attenuated for the pendulum problem, a more detailed study of the beam's response needs to be done. Figure 3-26 shows the tip's deflection over time for $60 < t < 75$. As it can be seen from the figure, vibration is affected by the second mode. The consequence of the presence of this mode is that the motion is not a regular periodical one (for instance, it is not close to a sinusoidal motion) and thus it's hard to synchronize the mass motion since the frequency and phase of vibration cannot be identified clearly. On the other hand, the effect of the second mode is small at the beginning of the motion (for $t < 50$) and it is possible to detect the frequency and phase of

motion and use them to synchronize the mass motion. This is why the motion is attenuated for $t < 50$ while for $t > 50$, where the second mode becomes more dominant, the synchronization cannot be done properly and vibration is not attenuated.

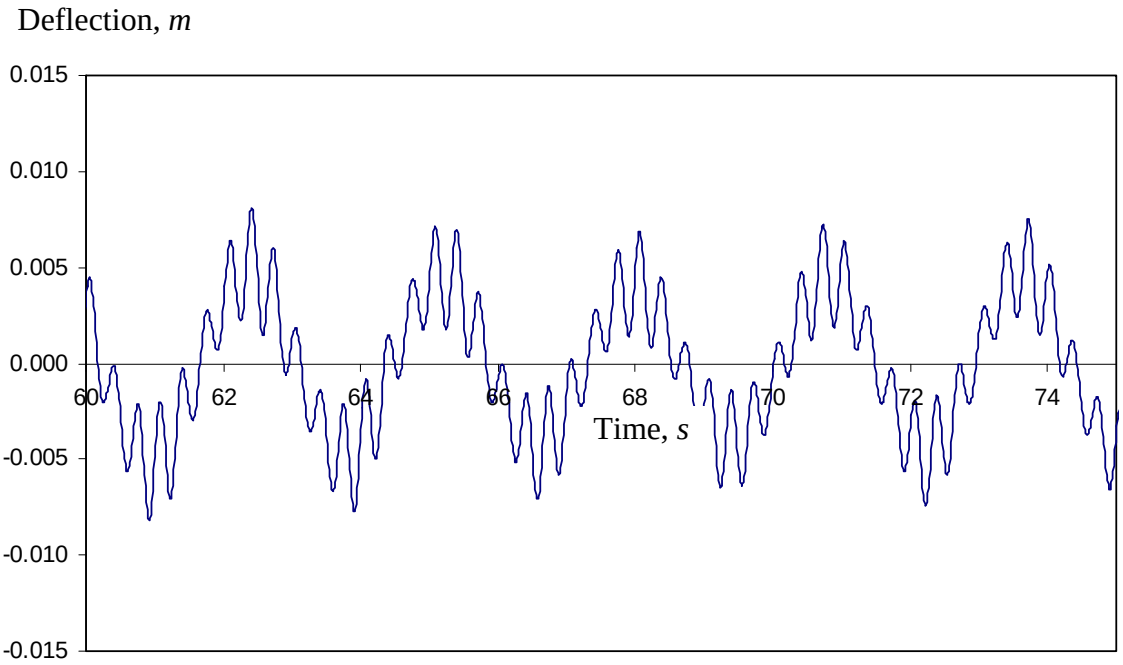

Figure 3-26 The same curve as that of Figure 3-25 for 60 < t < 75.

The synchronization strategy used in previous simulation (Figure 3-25 and 3-26) is based on the first scheme and using deflection. It is interesting to note that our simulations show no significant difference when the second or the third schemes are used. However, if the synchronization is based on the angle at the current location of the mass, then the beam's response changes as shown in Figure 3-27. A comparison of Figures 3-25 and 3-27 shows that vibration is attenuated more for Figure 3-25. This means that the deflection-based method results in more attenuation (and higher damping ratio) than the angle-based method. This can be explained by considering that the noise (due to the presence of the second mode) is more

pronounced in the time history of the angle, which in turn means that the identification of frequency and period is harder when history of angle is used.

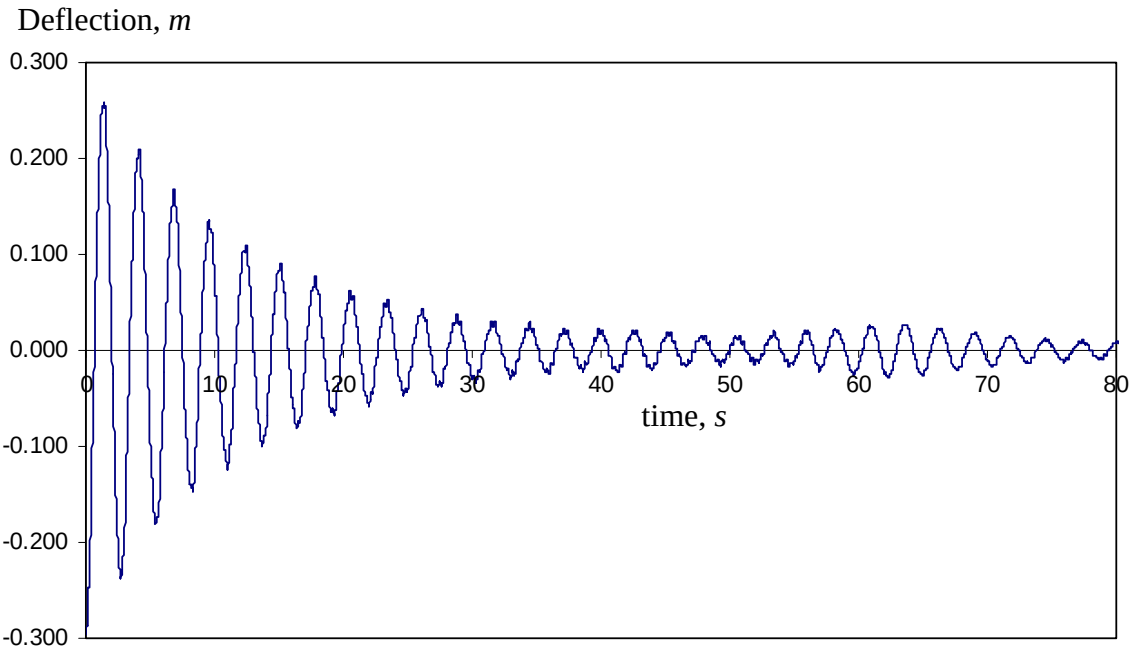

Figure 3-27 Tip deflection of a cantilevered beam versus time when the mass motion is synchronized according to the second scheme and using the angle.

As mentioned earlier, the results do not change much when the deflection-based synchronization method is used with three different schemes. However, when the angle-based method is used, the beam's response shows a small difference for the first and second schemes. Generally, the damping ratio is higher and the residual vibration is lower for the second scheme (the results are not shown for the sake of brevity).

The results shown so far in this section are obtained by modeling the beam without including the effect of any natural damping. If natural damping is taken into account, for instance by applying the Rayleigh damping coefficients, then it is observed that even inclusion of a relatively small natural damping results in a much smoother beam's response (the equivalent active

damping ratio for the natural damping is about 0.1%). This smoothness will in turn make the synchronization process possible for a longer period of time until the vibration of the beam is almost completely damped. Figure 3-28 shows a typical beam's response with the presence of natural damping. The Rayleigh parameters used for this analysis corresponds to a damping ratio of about 0.1% which means there is only a very small natural damping present. On the other

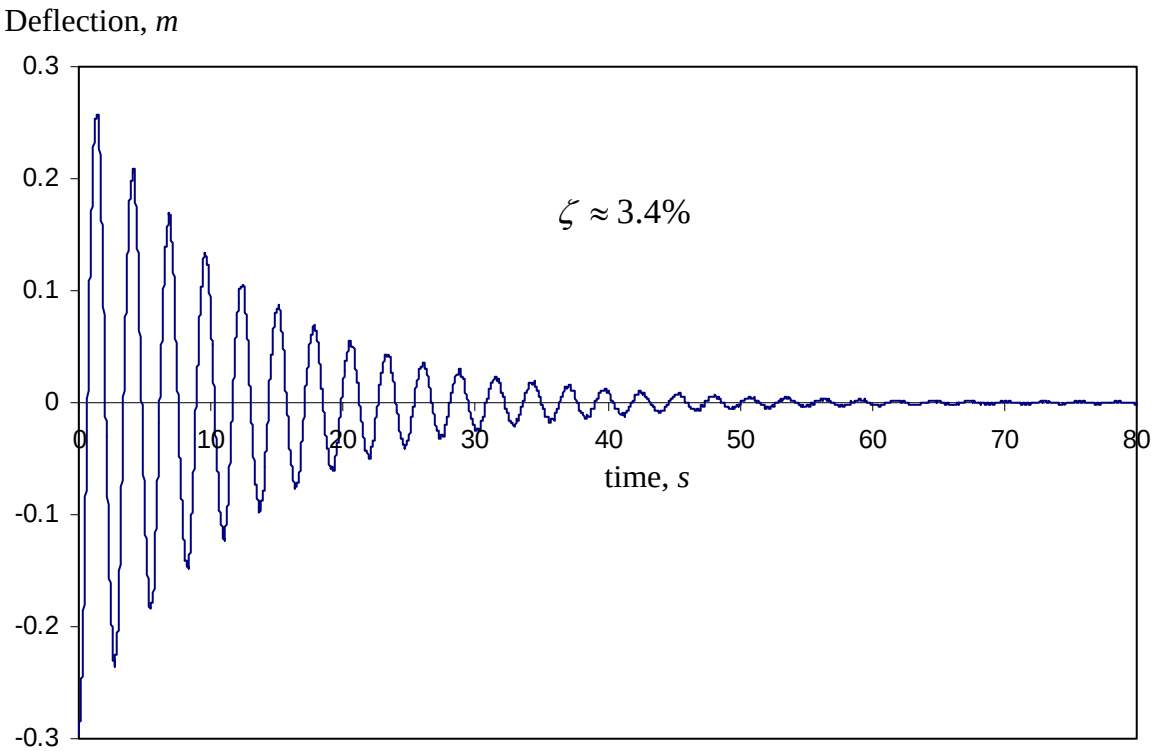

Figure 3-28 Tip deflection versus time when natural damping is included. The mass motion is synchronized according to the second scheme and using the deflection.

hand, the active damping ratio for this case, which is estimated by using the deflection history shown in Figure 3-28, is about 3.4%. Consequently, the damping effect coming from the natural damping is almost negligible compared to the damping effect from the moving mass; however,

the presence of natural damping will result in dissipation of the second mode in the beam's response. This eventually makes the synchronization process possible for a longer period of time.

From the vibration control point of view, it is interesting to investigate how the parameters s_0, ε and m affect the rate of vibration attenuation for the main beam which can help to optimize these parameters for obtaining the maximum damping-like effects. Figure 3-29 shows how the damping ratio is changing with the mass of the moving body, $\overline{m}$ (see Eq. (3.27)), for a constant $\bar{s}_0 = 0.83$ and $\varepsilon = 0.1$. As it is observed, the damping-like effect increases with increasing $\overline{m}$. This is what we expect since the Coriolis force, which is the force responsible for resisting the motion and producing damping-like effects, is directly proportional to $\overline{m}$. On the other hand, the slope of the curves decreases with increasing $\overline{m}$ which suggests that there is a maximum limit for ζ as $\overline{m}$ increases. This can be explained by considering that the increase in the mass of the body will not only increase the resisting Coriolis force, but it also increases the inertia of system making it harder to attenuate. The with-natural-damping curve in the figure is obtained by including a natural damping of approximately 0.1%.

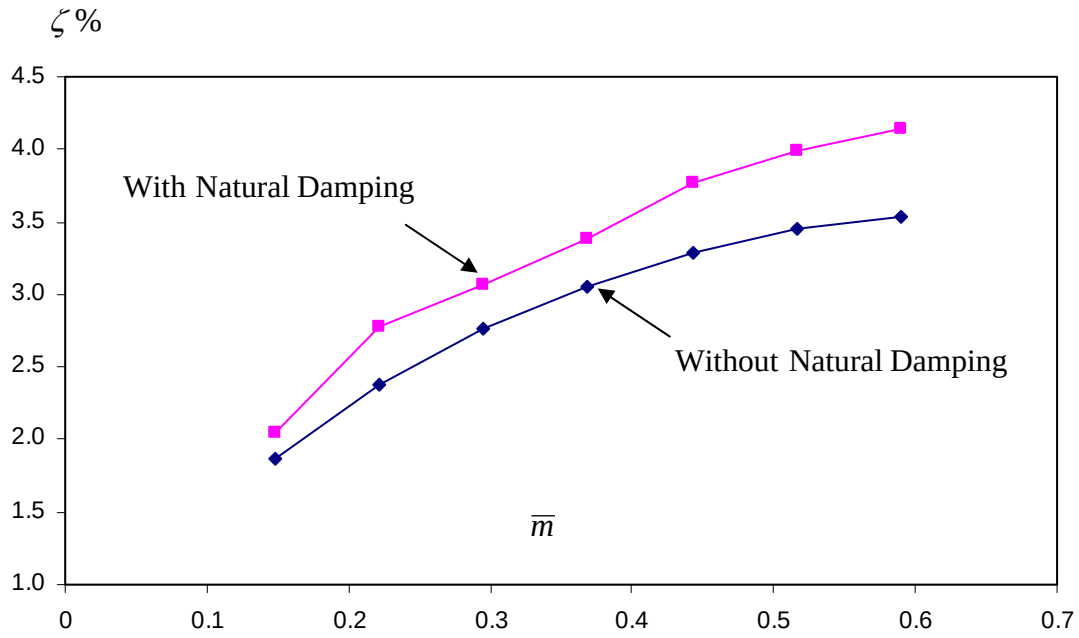

Figure 3-29 Variation of active damping ratio with the dimensionless mass of the moving body for a cantilevered beam.

The next parameter to study is the amplitude of mass vibration which, according to Eq. (3.29), is equal to εs_0. Figure 3-30 shows how this parameter, which is presented in the dimensionless form of $\varepsilon \bar{s}_0$, affects the damping ratio ζ. Based on these results, which are obtained by using a constant $\overline{m}$ of 0.37 and two values of s_0/L as shown in the figure, the damping ratio increases almost linearly with the amplitude εs_0. This was also expected since the Coriolis force is proportional to the velocity of mass, which, in turn, is proportional to the amplitude of mass motion εs_0. It is also noted that the results shown in Figure 3-30 are obtained by including a natural dapping of 0.1%.

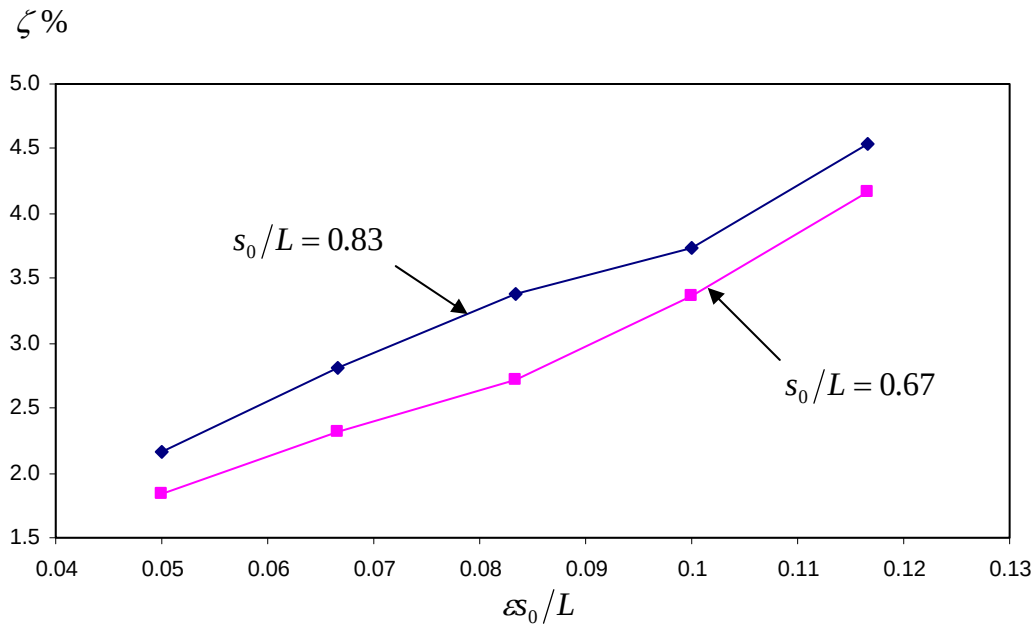

Figure 3-30 Variation of active damping ratio with the amplitude of mass motion $\bar{s}_0\varepsilon$.

As can be seen in Figure 3-30, the damping ratios obtained for $\bar{s}_0 = 0.83$ are higher than those obtained for $\bar{s}_0 = 0.67$. As a result, one would expect the beam's response to be more irregular (as in Figure 3-25 for example) for $\bar{s}_0 = 0.83$ since the beam's vibration is attenuated more rapidly in this case. However, simulations show that the curves for beam vibration over time is indeed smoother for $s_0/L = 0.83$. To explain this, first it should be noted that it is the presence of the second mode in the beam's response that makes it uneven. Secondly, according to the patterns of the first two vibration modes, which are shown in Figure 3-31, it is observed that the displacement of the second mode shape is zero at around $x = 0.8L$. Consequently, for $\bar{s}_0 = 0.83$ the mass is oscillating around a point where the effect from the second mode is less, which means the mass oscillation is disturbing (exciting) the second mode less effectively. Once the second mode is excited to a lesser extent, the beam's response will be smoother, which is what is

observed in the simulations. This effect also shows that the beam's response can be noticeably changed if the mass average location, s_0, changes. Consequently, the effect of this parameter on active damping ratio is studied next.

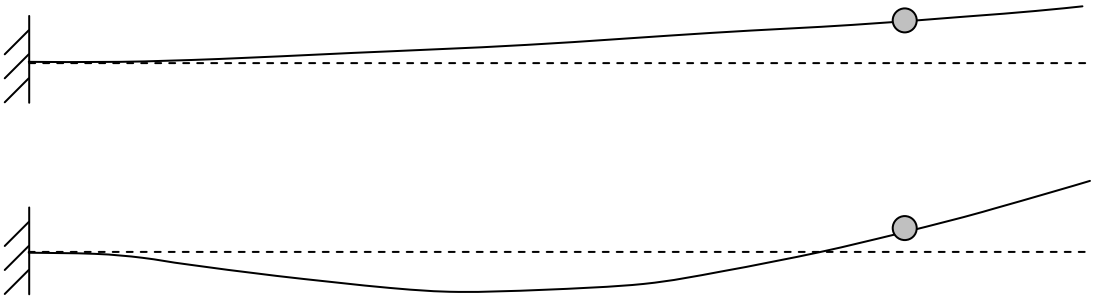

Figure 3-31 First and second vibration modes for a cantilevered beam.

To investigate how s_0 affects the damping ratio, the cases with a constant $\overline{m}$ of 0.37, two dimensionless amplitudes, $\bar{s}_0$, of 0.083 and 0.1 and a varying s_0. According to the results, which are shown in Figure 3-32, the damping ratio generally increases as the mass gets closer to the free end of the beam (or when s_0 increases). Again, this is what would be expected since the rotation (or the slope of the cantilever beam) is larger near the free end, which means the rate of rotation will also be larger. Eventually the resisting Coriolis force will therefore be bigger. Also, it is noted that the beam's response is smoother when s_0 increases. In other words, the presence of the second mode is less evident if the average location of mass oscillation gets closer to the free end of the beam.

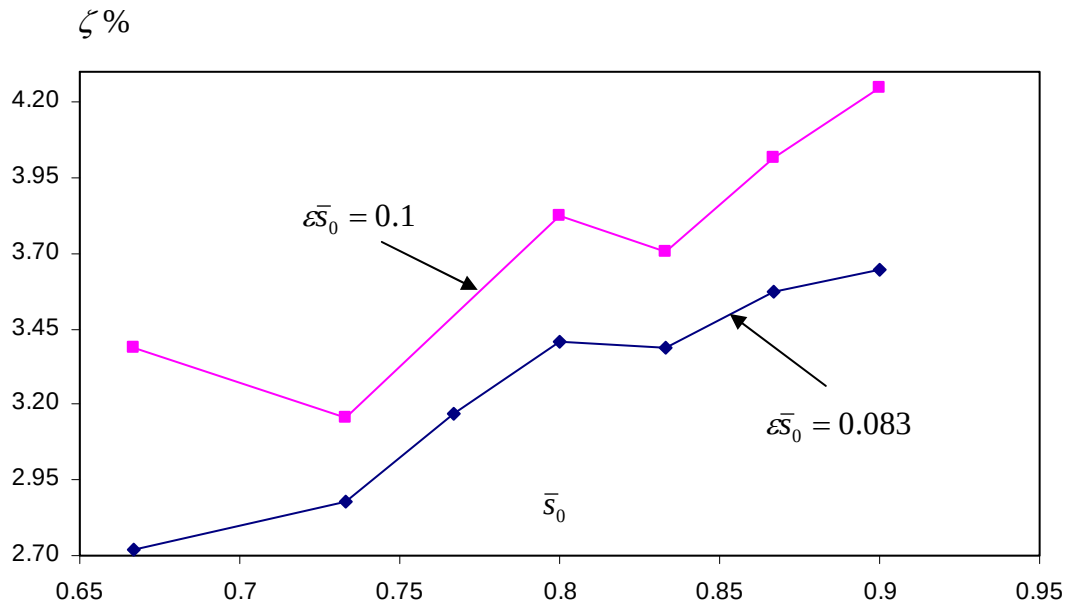

Figure 3-32 Variation of active damping ratio with mass average location $\bar{s}_0$.

3.3.2 Controlling Vibration of a Simply-Supported Beam

In this section, controlling vibration of the simply-supported beam shown in Figure 3-22 is attempted. The beam was initially deflected by applying a force at its center. Then, the force was removed to let the beam vibrate freely; the mass motion was then synchronized to control these vibrations. In the following examples, the length of the beam is 4 *m*, its parameters are such that the first natural period is about 2.5 *s* and the mass motion is given by Eq. (3.29). There are two main differences between this case and the previous one (the cantilever beam): firstly, the relationship between the natural frequencies is different for the simply supported beam and secondly, the modal shapes for the two beams are different. For instance, the second natural frequency of the simply supported beam is exactly 4 times the first natural frequency while this ratio is about 6.27 for the cantilever beam. As will be demonstrated later, the fact that the ratio of the second natural frequency over the first one is an integer number will lead to some issues in

the synchronization process as well as in the control process. In fact, it will be shown the mass motion, which is synchronized with the first natural frequency, is exciting the second mode since its frequency is almost half of the second natural frequency. In the following, the control process of this kind of beam will be investigated for different synchronization strategies and different parameters of mass motion.

As the first example, assume that the mass is fluctuating about the center of the beam, which means $s_0 = L/2$. In this case, since the beam's initial deflection as well as its modal shapes are symmetric with respect to the center line of the beam, the mass experiences the same angle change when it is on the left side as what it experiences in the right side. However, when it's on the left side (moving toward the rotation center) it causes amplification while it causes attenuation when it is on the right side (moving away from the rotation center). As a result, the attenuation and amplification cancels out and the mass motion does not change the beams vibration. Our analyses also show that vibration is almost fully periodic without any amplification or attenuation (the results are shown in Figure 3-33). In fact, as it is observed from the figure, vibration is slightly amplified in time. This is due to the fact that the nature of periodic relative mass motion makes the main system prone to amplification (Szyszkowski and Sharbati 2009).

On the other hand, if the mass moves about some point other than the center of the beam, then attenuation effects are observed. For instance, if the mass motion parameters are $\overline{m} = 0.26$, $s_0 = 0.45L$ and $\varepsilon s_0 = 0.05L$ then the beam's vibration attenuates with approximately a damping ratio of 0.65%, as shown in Figure 3-34. The deflection in the figure is for the mid-span point and nondimensionalized with respect to the length of the beam. Also, the synchronization strategy is based on the first scheme and using displacement.

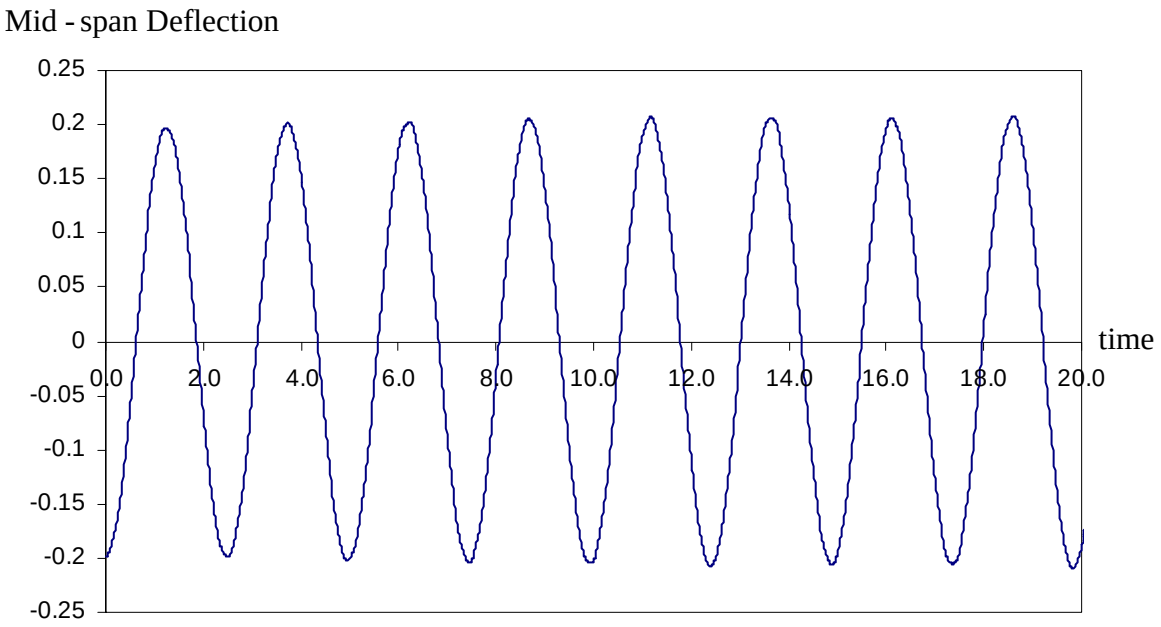

Figure 3-33 Simply-supported beam's response when the average mass location is $L/2$.

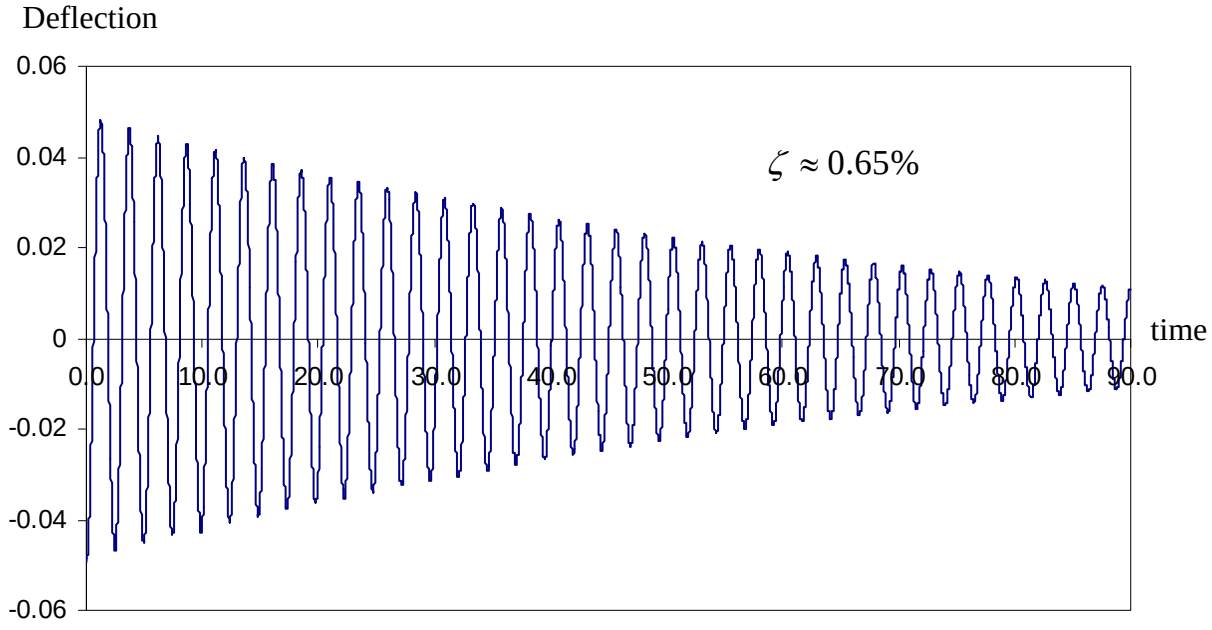

Figure 3-34 Dimensionless deflection of the beam's mid-span point versus time when mass motion is synchronized by using the first scheme.

As it is observed in the analysis shown in Figure 3-34, the damping ratio is relatively low. To maximize this damping-like effect, the influence of mass motion parameters on the damping ratio should be investigated. From the cantilever case, it is expected that the damping ratio increases by increasing the mass of the body, $\overline{m}$, and also by extending the mass motion range, εs_0. On the other hand, it is hard to predict the optimum mean position of the mass, s_0, for getting the maximum damping ratio. A set of analyses with a constant mass of $\overline{m} = 0.26$, amplitudes of $\varepsilon s_0 = 0.05L$ and $\varepsilon s_0 = 0.1L$, and varying s_0 have been done to show that the optimum s_0/L is between 0.2 and 0.3 (see Figure 3-35). These results also show that the damping ratio is almost doubled when the amplitude εs_0 is doubled. Furthermore, it is important to note that the results shown in Figure 3-35 are obtained by using the third synchronization

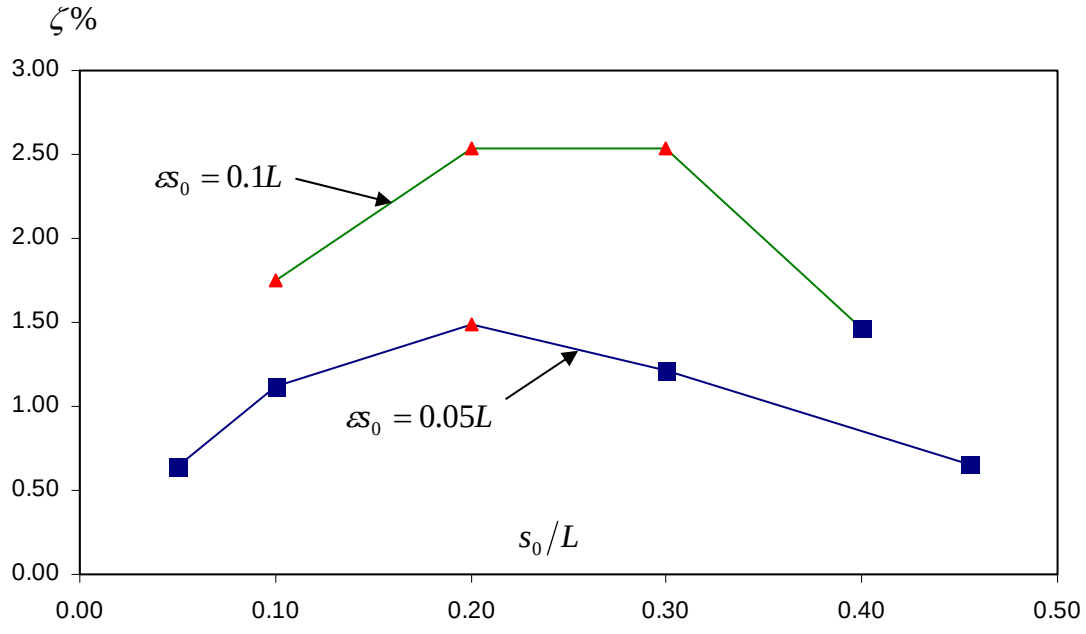

Figure 3-35 Variation of active damping ratio with the mean position of the mass s_0 for the simply supported beam.

scheme (mentioned previously in this section). In fact, our analyses show that no continuous attenuation of vibration is obtained when the first or second synchronization schemes are used (the synchronization is lost after the first few cycles).

Although a relatively acceptable damping ratio is obtained for this case, the beam's vibration is not completely damped due to a similar effect as that of the cantilever beam: the beam's vibration is slightly affected by the second mode which results in some irregularities in the beam's response. Like the cantilever beam, these irregularities are more pronounced as the time goes by since the first mode is reduced over time. This effect is shown in Figure 3-36, which is the beam's response versus time for $s_0 = 0.2L$ and $\varepsilon s_0 = 0.05L$. It is also noted that, in Figure 3-35, the cases where the vibration is not completely damped due to the effect of the second mode are marked by triangle points.

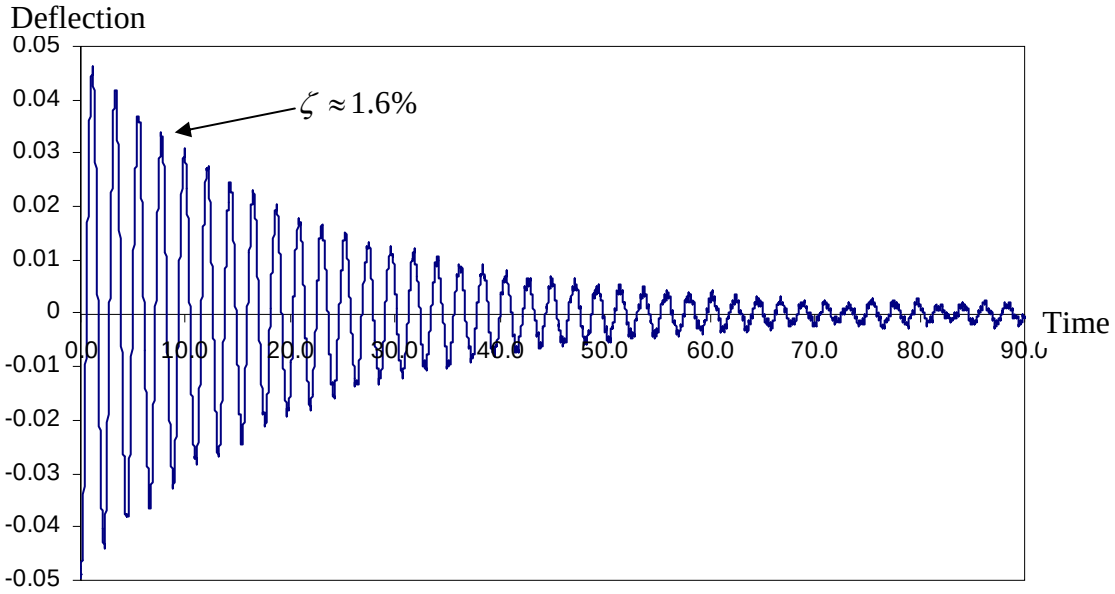

Figure 3-36 Dimensionless deflection of the beam's mid-span point versus time for $s_0 = 0.2L$ and $\varepsilon s_0 = 0.05L$.

Like the cantilevered beam case, one possible way to eliminate this effect of higher mode is to apply natural damping. However, our analyses show that for the simply supported beam, even using relatively high natural damping ratios, up to about 0.4%, will not eliminate the second mode and the residual vibration is still present in the beam's response (the corresponding results are not shown). To understand why this phenomenon occurs, the beam's response over time has been decomposed into its modal shape for both the cantilever and the simply supported beam. For the simply-supported beam, for instance, it is assumed that the beam's response can be expressed in terms of its modal shape (similar to Eq. (3.21)) as:

$$w(x,t)=\sum_{n}\Theta_{n}(t)\sin(n\pi x/L) \tag{3.30}$$

Then, since the beam's deflection at any given time, i.e. t_i, is known from the FEM analysis (i.e. $w(x,t_i)$ is known), the contribution of the k-th mode, $\Theta_k(t_i)$, in the beam's deflection can be calculated from:

$$\Theta_k(t_i)=\frac{\int_0^L w(x',t_i)\sin(k\pi x'/L)dx'}{\int_0^L \sin^2(k\pi x'/L)dx'}=\frac{2}{L}\int_0^L w(x',t_i)\sin(k\pi x'/L)dx' \tag{3.31}$$

It is noted that the integral in Eq. (3.31) should be calculated numerically since the beam's deflection at time t_i is only known at the nodal points from the FEM analysis. Also, this integration should be done for all time instants t_i and the desired number of modes (in this case for $k=1,2$). Once this is done, the history of $\Theta_k(t)$, which is the contribution of k-th mode in the beam's response, is obtained for all the desired modes. The same procedure could be used for the cantilevered beam except that the modal shapes of a cantilevered beam should be used in Eqs. (3.30) and (3.31).

This decomposition procedure has been done for both the cantilevered and simply supported beams in the presence of natural damping. Figure 3-37 shows these components, $\Theta_1(t)$ and $\Theta_2(t)$, for a typical cantilever beam analysis with mass motion parameters of $s_0 = 0.9L$, $\varepsilon s_0 = 0.09L$ and $\overline{m} = 0.37$. As can be seen in the figure, both the first and second

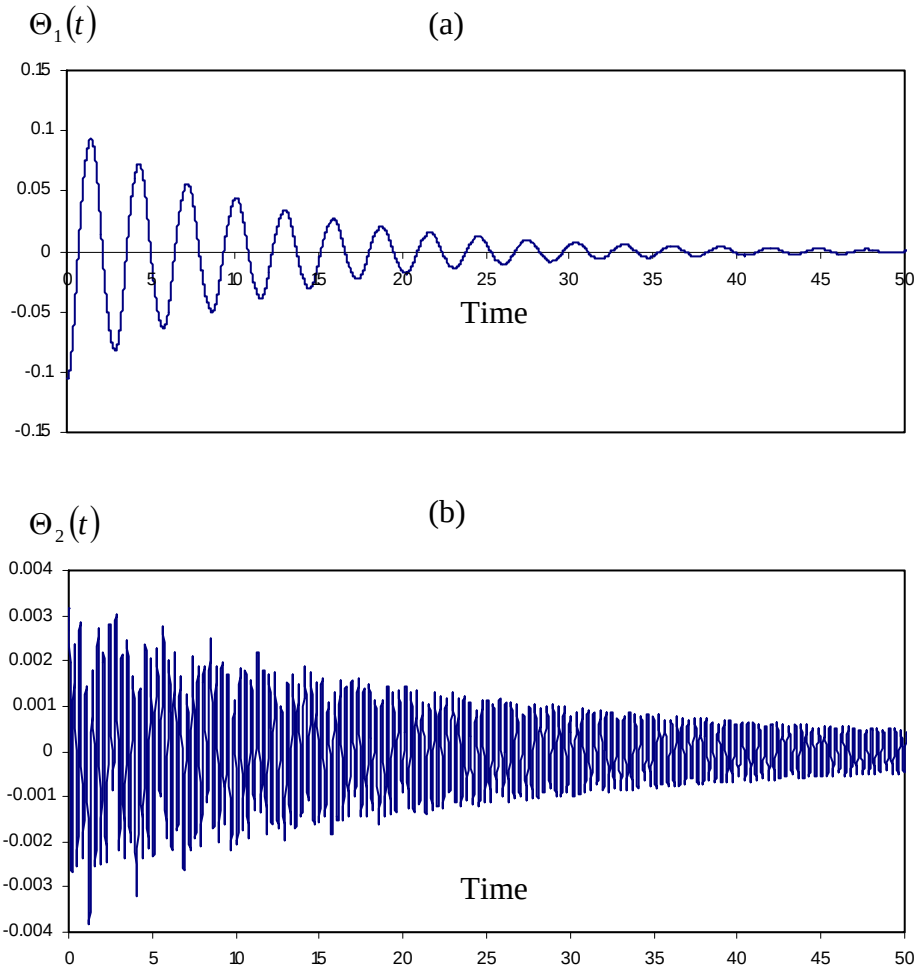

Figure 3-37 Contribution of the first and second modes in the response of a cantilever beam. (a) the first mode (b) the second mode.

modes are attenuating over time with a faster attenuation rate for the first mode. In fact, the first mode is attenuating over time mainly due to the mass motion (with $\zeta \approx 4\%$) while the second

mode is attenuating due to the natural damping (with $\zeta \approx 0.2\%$). Consequently, it is concluded that the mass motion, which is synchronized with the first frequency, will attenuate the first mode while it does not disturb (excite) the second mode which will then attenuate due to the natural damping.

For the simply supported beam on the other hand, the decomposition of vibration modes show that the second mode does not damp in time even in the presence of natural damping. As shown in Figure 3-38, which is the mode decomposition for $s_0 = 0.3L$, $\varepsilon s_0 = 0.1L$ and $\overline{m} = 0.26$, the first mode is attenuating with time ($\zeta \approx 2.3\%$) mainly due to mass motion. However, the second mode amplitude almost remains unchanged for $t > 25$ despite of the presence of natural damping (according to the Rayleigh parameters used to model natural damping, a damping ratio of 0.1% is expected). This means that the mass motion, which is synchronized with the first mode, is in fact exciting (or disturbing) the second mode. To explain this effect, it should first be noted that the mass motion frequency, which is almost twice the first natural frequency, is also about half of the second natural frequency (the second natural frequency is exactly four times the first for the simply supported beam). This means that the mass motion happens to be (roughly) synchronized with the second mode as well. However, this synchronization is not in correct phase since the phase adjustment in the synchronization procedure is only done for the first mode. On the other hand, it can be shown that this type of rough synchronization (in the absence of phase adjustment) can lead to the occurrence of parametric resonance, in which the system motion is attenuating and amplifying periodically.

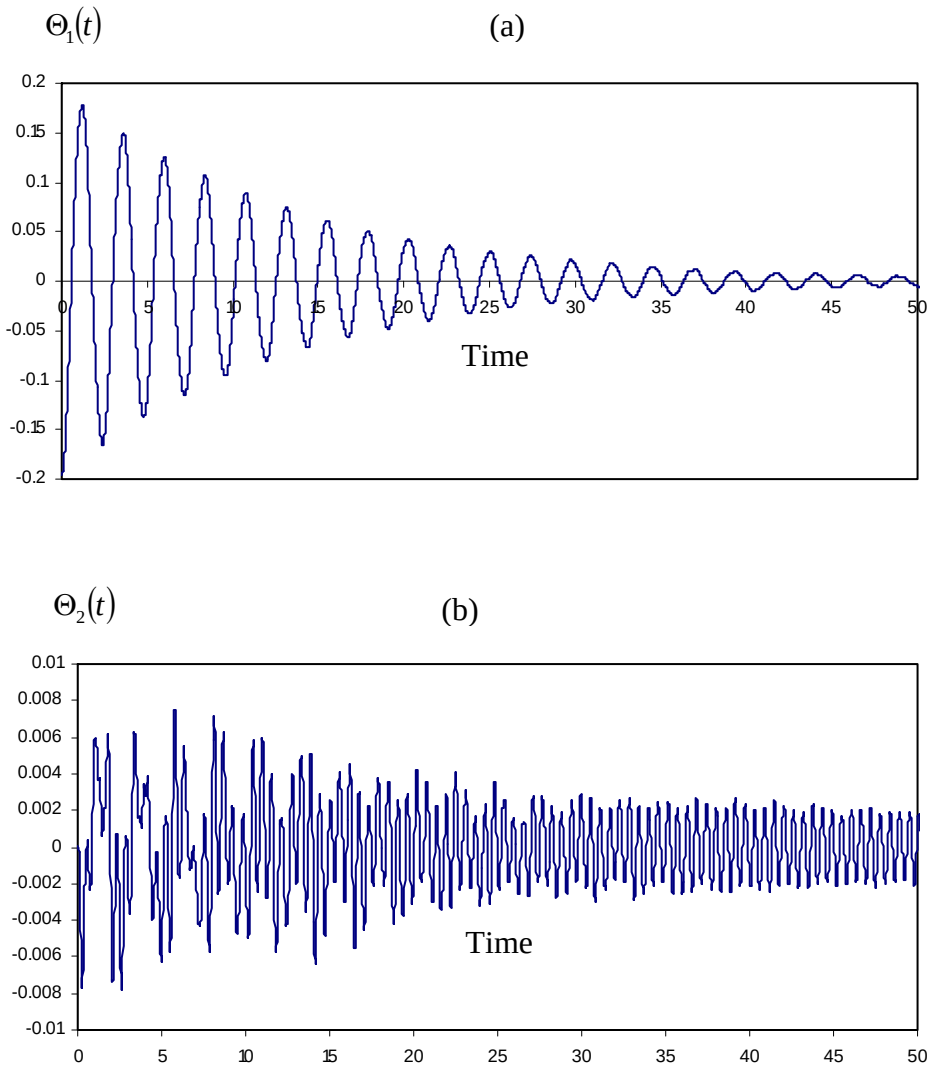

Figure 3-38 Contribution of the first and second modes in the response of a simply supported beam. (a) the first mode (b) the second mode.

While it was shown that the vibration will not be damped completely for the simply-supported beam (because of the second mode excitation), it is possible to set the mass motion parameters, in particular s_0 and ε, such that the second mode is excited minimally. For instance, for $s_0 = 0.4L$ and $\varepsilon s_0 = 0.1L$, the beam's response is very smooth and the second mode almost does not appear as shown in Figure 3-35. If $s_0 = 0.4L$ and $\varepsilon s_0 = 0.05L$ are used, the beam response will also be very smooth (but with a smaller active damping ratio). As a result, it seems that if

the mean position of the moving mass is somewhere around $0.4L$, the second mode excitation is minimized. Consequently, as illustrated in Figure 3-35, the maximum obtainable damping ratio for simply supported beam is around 1.5% for $s_0 = 0.4L$ and $\varepsilon s_0 = 0.1L$ (note that the triangle points in Figure 3-35 cannot be considered as vibration is not completely damped for these cases). In general, it looks possible to adjust mass motion parameters based on the shapes of different vibration modes such that vibration is effectively and smoothly attenuated. Furthermore, one can change the natural frequencies of the beam slightly, for instance by placing one or more masses at specific locations on the beam, such that the ratio of consecutive natural frequencies is no longer related by an even integer.

3.3.3 Controlling Vibration of a Simply-Supported Beam with a Rotary Inertia Mass at the Center

As indicated in previous sections, the relationship between different vibration modes of the beam, including the ratio of the natural frequencies and the shape of vibration modes, plays an important role on how the system responds and how challenging it is to attenuate vibration. As just shown in the previous section, for the simply supported beam, where the second natural frequency is an integer multiplier of the first one, the synchronization process is more challenging. In this section, a beam with the first and second natural frequencies close to one another (an almost bimodal case) is considered and will be shown to impose more issues in the synchronization process.

Consider a simply supported beam with a block attached at its center, as shown in Figure 3-39. This block allows us to introduce the rotational inertia, *J*, which can be used to control the modal shapes of the beam. The modal analysis of this beam shows that when the value of *J* increases, the first and second natural frequencies get closer until they are equal at a certain *J*.

This rotary inertia is nondimensionalized as $\bar{J} = J/(\rho AL^3/12)$ where $\rho AL^3/12$ approximates the beam's rotary inertia about its center. For instance, for a beam made of aluminum ($E = 78GPa$, $\rho = 2800\ kg/m^3$), with a length of 3 m and rectangular cross section of $57mm \times 5.7mm$, the first two natural frequencies are 1.094 Hz and 1.1 Hz for $J = 4.57\ kg.m^2$ (or $\bar{J} = 2.25$). This shows that the value of $\bar{J}$ should be relatively high in order to have the first two natural frequencies close together.

Next, the beam is initially deflected by applying and removing a force F not necessarily its center. Like before, it is aimed to control the beam's vibration by moving the mass as illustrated in Figure 3-39. Our analyses, however, show that the system response and also vibration control for this case are more difficult than for other cases. For instance, regardless of the synchronization scheme used, the beam's response for $s_0 = 0.3L$, $\varepsilon s_0 = 0.1L$ and $\bar{m} = 0.3$ (when the initial force is applied at the center of the beam) is noisy and that attenuation only occurs for a couple of first cycles. After these cycles, the beam's vibration amplifies and/or gets noisy to the extent that the frequency and phase cannot be detected by the program precisely enough leading to divergence of the solution. A sample case is shown in Figure 3-40 which is the beam's mid-span deflection versus time when the second scheme displacement-based strategy is used for synchronization. As it is observed, the vibration mainly amplifies for $t > 5$ and it diverges at around 13 s.

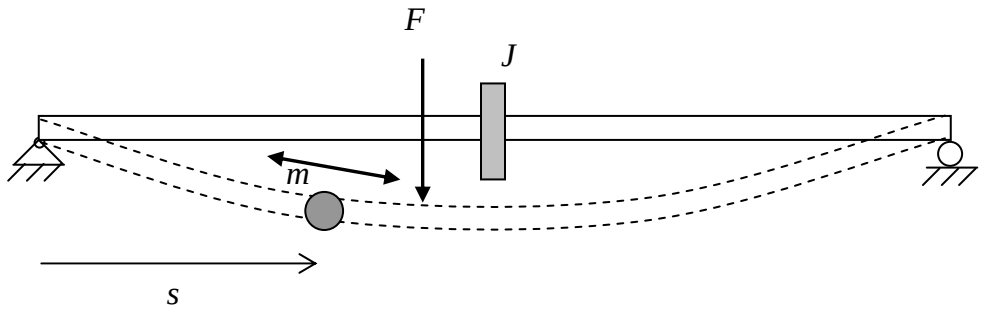

Figure 3-39 A simply supported beam with a mass positioned at its center. The other mass, *m*, is moving to control vibration of the beam.

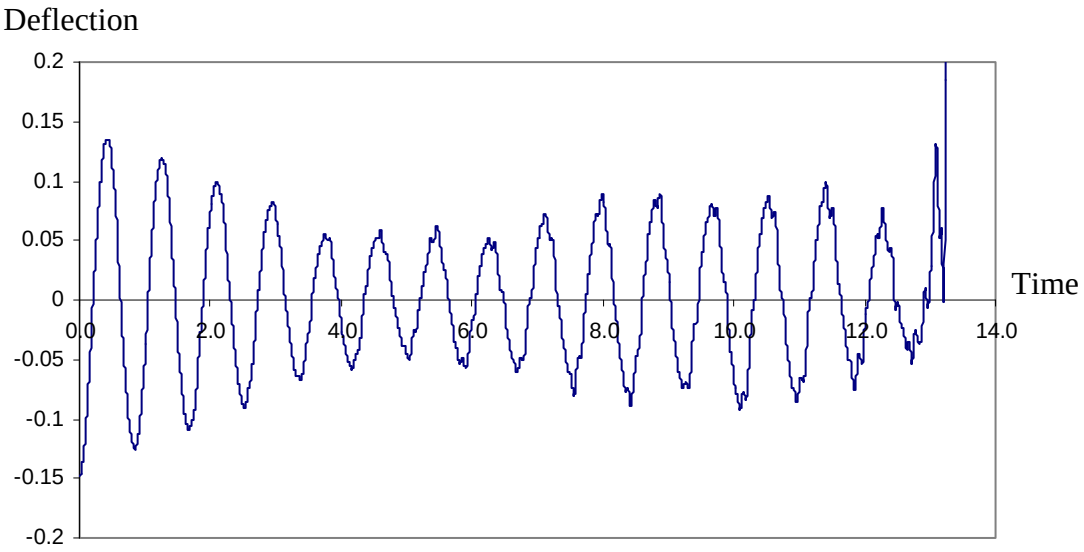

Figure 3-40 Dimensionless deflection of the beam's mid-span point versus time for $s_0 = 0.3L$, $\varepsilon s_0 = 0.1L$ and $\overline{m} = 0.3$.

Although the solution for the previous case was noisy, some continuous attenuation can be obtained if the other parameters of mass motion are used. For instance, for $s_0 = 0.3L$, $\varepsilon s_0 = 0.05L$ and $\overline{m} = 0.3$ the vibration, which is presented in Figure 3-41 in terms of mid-span deflection, shows a general attenuation trend. It is important to note that the result of Figure 3-41

is obtained by applying the third synchronization scheme while using the first scheme will not give any continuous attenuation. Also, it is noted that the force which causes the initial deflection is applied at the center of the beam for results of Figures 3-40 and 3-41.

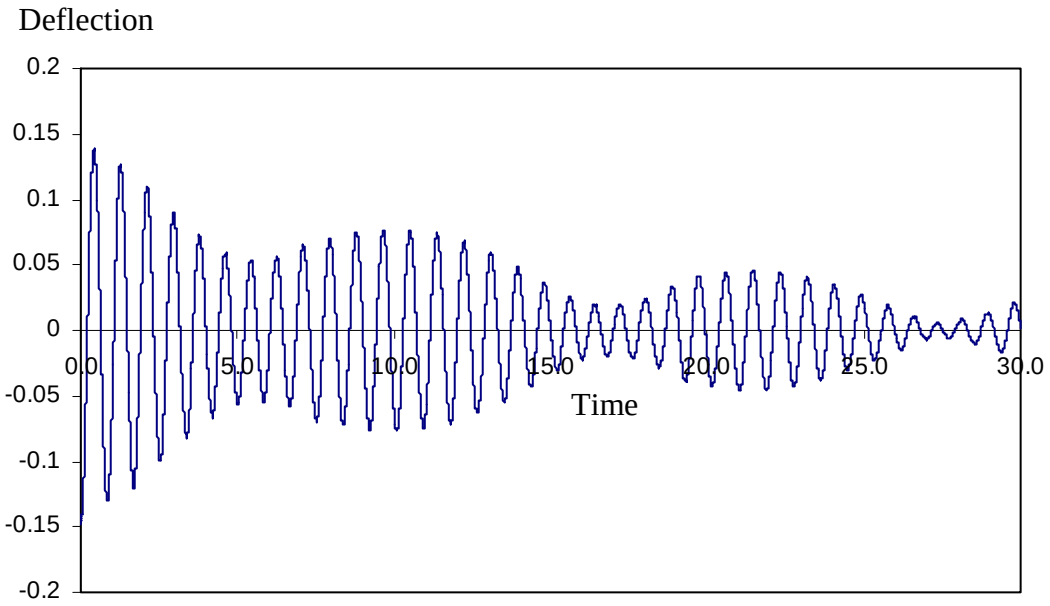

Figure 3-41 Dimensionless deflection of the beam's mid-span point versus time for $s_0 = 0.3L$, $\varepsilon s_0 = 0.05L$ and $\overline{m} = 0.3$.

While a continuous general attenuation is observed in Figure 3-41, a more detailed study of the solution reveals that the response is mainly affected by the first and third modes (the frequency of the noise in these results is close to the third natural frequency). The reason is that the beam's initial deflection is symmetric with respect to the beam's center; since the second mode shape is anti-symmetric with respect to this point, the second mode is not initially excited and subsequently does not affect the solution. On the other hand, if the initial force is applied somewhere off center, then the second mode is also excited. In this case, the vibration

attenuation process is more challenging as the solution is almost equally affected by the first two modes (since the first two natural frequencies are close). Figure 3-42, which presents a sample beam's response when the initial force is applied at $L/4$, indicates how the beam's response is getting more complicated when two modes of almost same frequencies are involved in the solution.

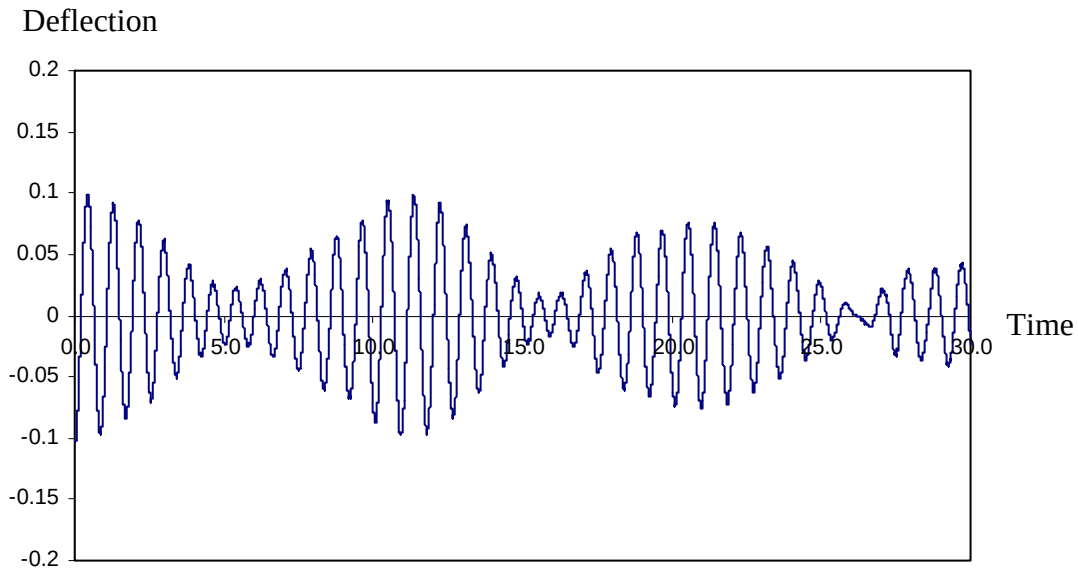

Figure 3-42 Dimensionless deflection of the beam's mid-span point versus time when the initial force is applied at $L/4$ and $s_0 = 0.3L$, $\varepsilon s_0 = 0.05L$ and $\overline{m} = 0.3$.

3.4 Controlling the Beam's Vibration by Using a Vertically Moving Mass

So far in previous results, the mass motion along the beam was used for controlling the beam's vibration. In this section, the possibility of controlling the beam's vibration by moving a mass perpendicular to the beam's axis is investigated. For this purpose, consider the simply-supported beam and moving mass structure as shown in Figure 3-43. It is assumed that the additional guide bar is clamped to the beam and is made of a light rigid material. Consequently, it will only undergo a rigid body rotation with its rotation being equal to the slope of the beam at

$s = s_L$. In fact, its motion will be similar to the oscillating pendulum of the previous chapter. Thus, the relative mass motion along its length, as shown in the figure, will be accompanied by rotation and can cause Coriolis type forces which can be utilized for control purposes similar to what was done in the pendulum problem. Like in the previous cases, it is assumed that an external force drives the mass motion along the guiding bar.

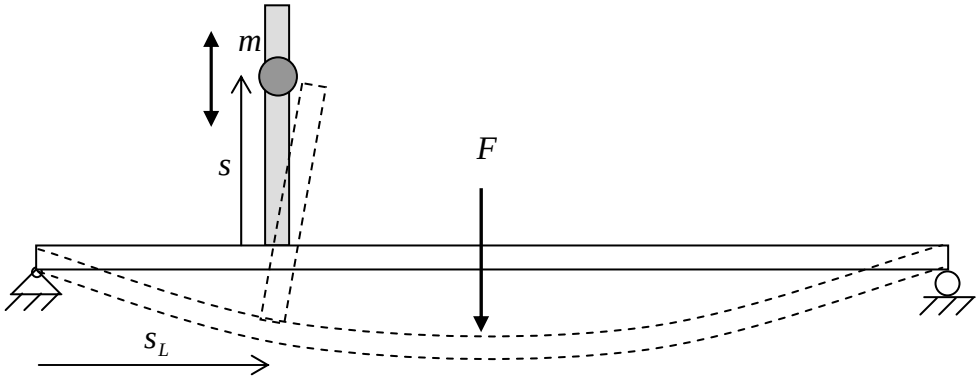

Figure 3-43 A simply supported beam with a mass moving perpendicular to its longitude axis.

To compare the results, this problem is handled analytically first. The dynamic equations of this system can be obtained by detaching the moving mass and the guiding bar, writing the dynamic equilibrium for the mass and remaining structure separately and then eliminating the interacting force between the mass and guiding bar. Doing so, the dynamic equation is obtained as:

$$EI\frac{\partial^4 w}{\partial x^4} + \rho A\frac{\partial^2 w}{\partial t^2} = -\rho Ag - m(2s\dot{s}\frac{\partial^2 w}{\partial t\partial x} + s^2\frac{\partial^3 w}{\partial x\partial^2 t})\delta'(x - s_L) \qquad (3.32)$$

where $\delta'(x-s)$ is the spatial derivative of the Dirac Delta function which is used to represent a concentrated moment applied to the beam. In order to solve this equation by using the infinite series (similar to what was done previously for the mass moving along the beam) the beam's

response should be defined according to Eq's. (3.21) and (3.22). Then, by substituting these equations into Eq. (3.32) the dynamic equation in terms of mode shapes is obtained as:

$$\rho A\sum_n \omega_n^2 \mathrm{X}_n(x)\Theta_n(t)+\rho A\sum_n \mathrm{X}_n(x)\ddot{\Theta}_n(t)=-\rho Ag$$
$$-m\left(2s\dot{s}\sum_n \mathrm{X}'_n(x)\dot{\Theta}_n(t)+s^2\sum_n \mathrm{X}'_n(x)\ddot{\Theta}_n(t)\right)\delta'(x-s_L) \qquad (3.33)$$

By using the same procedure as before, and employing the properties of Dirac's function, the differential equations for $\Theta_k(t)$ are obtained as:

$$\ddot{\Theta}_k(t)+\omega_k^2\Theta_k(t)=-g\frac{\beta_k}{\alpha_k}-\frac{m}{\rho A\alpha_k}\left(2s\dot{s}\sum_n\left(\mathrm{X}_k(s_L)\mathrm{X}''_n(s_L)+\mathrm{X}'_k(s_L)\mathrm{X}'_n(s_L)\right)\dot{\Theta}_n(t)\right.$$
$$\left.+s^2\sum_n\left(\mathrm{X}_k(s_L)\mathrm{X}''_n(s_L)+\mathrm{X}'_k(s_L)\mathrm{X}'_n(s_L)\right)\ddot{\Theta}_n(t)\right) \qquad (3.34)$$

As for the previous cases discussed in 3.2.3.3, this set of differential equations can be solved by using a numerical integration method like Runge-Kutta method. It is also noted that the dynamic equations for this case can be nondimensionalized similarly as before and according to Eq. (3.27).

The examples solved in this section are chosen such that they are comparable with those presented in 3.3.2. To this end, a simply supported beam with properties identical to those of 3.3.2 which was initially disturbed by applying a force in its center is considered. The mass motion is given by Eq. (3.29) and the synchronization procedure is implemented in the code used for numerical integration. The parameters used for the examples include different values of s_L and s_0. However, simulations show that the set of differential equations of (3.34) cannot be solved for all values of s_L and s_0. In fact, only for some particular values of the two parameters does the solution converge. For other values of s_L and s_0, the numerical solution diverges

regardless of the size of the time step used for integration. For instance, with $s_L = 0.4L$ and $s_0 < 0.2L$, the solution converges while for any $0 < s_L < 0.35L$ and almost any given s_0, the solution diverges quickly. For the case considered in 3.3.2 on the other hand, the differential equations obtained by application of infinite series (Eq. (3.24)) can be solved for all values of s_0.

One possible way to explain why the solution of Eq. (3.34) diverges (while it converges for Eq. (3.24)) is to write the equations in a matrix form of:

$$\tilde{A}\ddot{\vec{\Theta}} + \tilde{B}\dot{\vec{\Theta}} + \tilde{C}\vec{\Theta} = \vec{D} \qquad (3.35)$$

where components of the vectors $\vec{\Theta}$, $\dot{\vec{\Theta}}$ and $\ddot{\vec{\Theta}}$ are $\Theta_k(t)$, $\dot{\Theta}_k(t)$ and $\ddot{\Theta}_k(t)$, respectively, and matrices $\tilde{A}$, $\tilde{B}$, $\tilde{C}$ and vector $\vec{D}$ should be defined according to Eq. (3.34) or (3.24). From the numerical integration point of view, the structure of matrix $\tilde{A}$ plays an important role in the convergence. For the case of Eq. (3.24), this matrix is given by:

$$\tilde{A}_{ij} = \delta_{ij} - \frac{m\mathrm{X}_i(s)\mathrm{X}_j(s)}{\rho A \alpha_i} \qquad (3.36)$$

which can be shown to be symmetric. However, for the beam considered here, the matrix $\tilde{A}$ in view of Eq. (3.34) will be

$$\tilde{A}_{ij} = \delta_{ij} - \frac{ms^2}{\rho A \alpha_i}\left(\mathrm{X}_i(s_L)\mathrm{X}''_j(s_L) + \mathrm{X}'_i(s_L)\mathrm{X}'_j(s_L)\right) \qquad (3.37)$$

which is not symmetric. As a result, the numerical integration procedure is not stable and for most values of parameters s_L and s_0 and therefore diverges.

The divergence of the solution based on an infinite series shows that the method is not always reliable for analyzing the mass-beam interaction problems. This means that the FEM approach should be used for analyzing such problems with the solution converging once proper values of

time step and element size are used in the FEM model. This, in turn, shows the significance of using the proposed FEM approach for modeling such moving mass-beam interaction problems.

The problems in Figure 3-43 is handled numerically by slightly revising the proposed FEM approach. The revision includes neglecting the centripetal acceleration term in the formulation as the guiding bar is assumed to be rigid with no curvature. Also, it should be mentioned that the Coriolis force vector calculated in Eqs. (3.11), (3.17) and (3.18) is in local coordinate system and needs to undergo the proper transformation before being applied to the structure.

Figure 3-44 shows the results, in terms of mid-span deflection versus time, for the mass parameters of $m = 1$, $s_L = 0.25L$, $s_0 = 0.3L$ and $\varepsilon = 1/6$. The synchronization scheme 3 has been used and no natural damping is included. As it is observed, an active damping ratio of about 1.73% is achieved and the beam's response appears to be very smooth. Recall that the maximum acceptable damping ratio obtained previously for the same beam (but with the mass moving along the beam) was about 1.5% (see Figure 3-35).

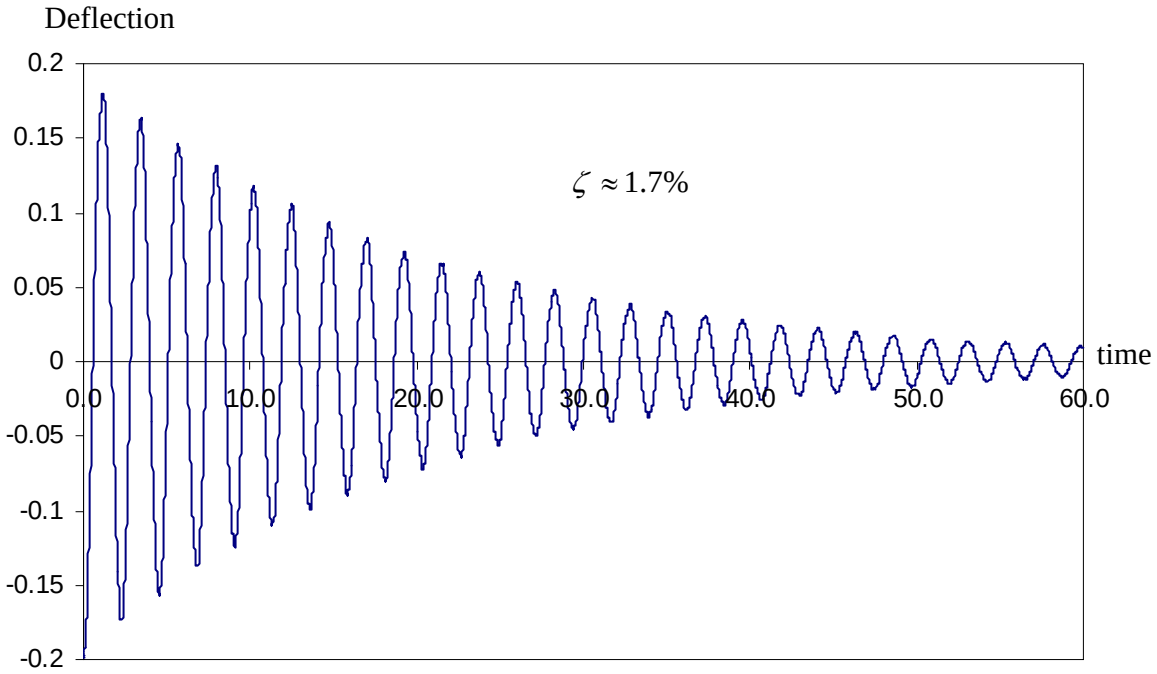

Figure 3-44 Beam's response when the mass moves perpendicular to the beam at $s_L = 0.25L$ with $s_0 = 0.3L$.

Like in the previous cases, it is desirable to adjust the mass motion parameters such that the damping-like effect of the mass motion increases. The parameters of the mass to adjust include m, s_L (measured horizontally), s_0 (measured vertically) and ε. From the previous results, it was shown that the damping ratio increases with m and ε as the Coriolis force magnitude is proportional to these parameters. On the other hand, no particular conclusion could be made for the effect of s_0 from these results. For this case, it is expected that the damping ratio increases with m and ε similarly as before. However, it appears that the damping ratio should also increase with s_0 since the resisting Coriolis force for this case is causing a resisting moment on the beam (typically $2ms\dot{s}\dot{\varphi}$). This means that the larger s_0 is, the bigger will be the resisting Coriolis moment resulting in a larger damping ratio. To verify this conclusion, a similar analysis to that of Figure 3-44 has been done except that $s_0 = 0.6L$ and $\varepsilon = 1/12$ have been used (the amplitude of mass motion is equal to the previous case i.e. $s_0\varepsilon = 0.6L/12 = 0.3L/12$). The results, shown in Figure 3-45, shows that the beam's response is considerably affected by higher modes of vibration resulting in the noisy curve shown in the figure. In fact, the mass oscillation is almost synchronized correctly with beam's vibration for the first 6 or 7 cycles; however, it is affecting the beam's vibration considerably (perhaps by affecting not only the first vibration mode but also the first few higher ones). This in turn results in irregular beam's response which eventually leads to loss of synchronization.

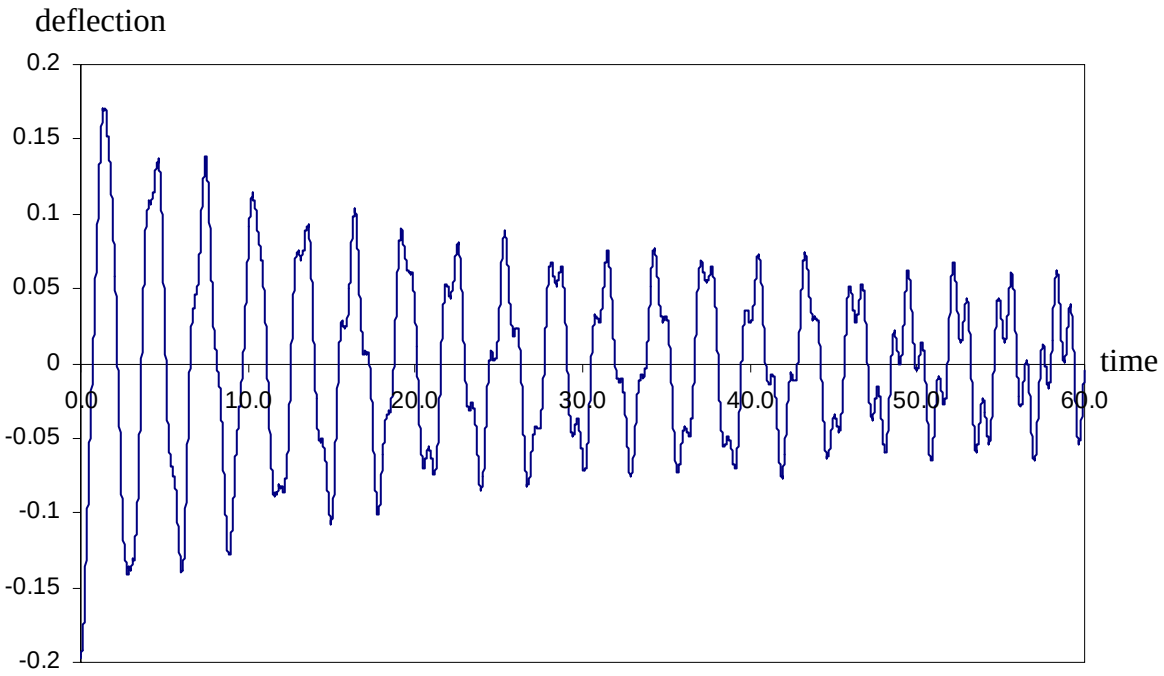

Figure 3-45 Beam's response when the mass moves perpendicular to the beam at $s_L = 0.25L$ with $s_0 = 0.6L$.

The last parameter which is expected to affect the active damping ratio is s_L, the horizontal location of mass motion. To investigate its effect, different analyses with different values of s_L have been done while s_0 and ε have been kept unchanged at $0.3L$ and $1/6$ respectively. The results are summarized in Figure 3-46 (the solution for $s_L = 0.25L$ has already been presented in Figure 3-44). As it is observed, while the damping ratio is about 1.8% for $s_L = 0.2L$ and $s_L = 0.15L$, the beam's response is not smooth and the synchronization will eventually be lost

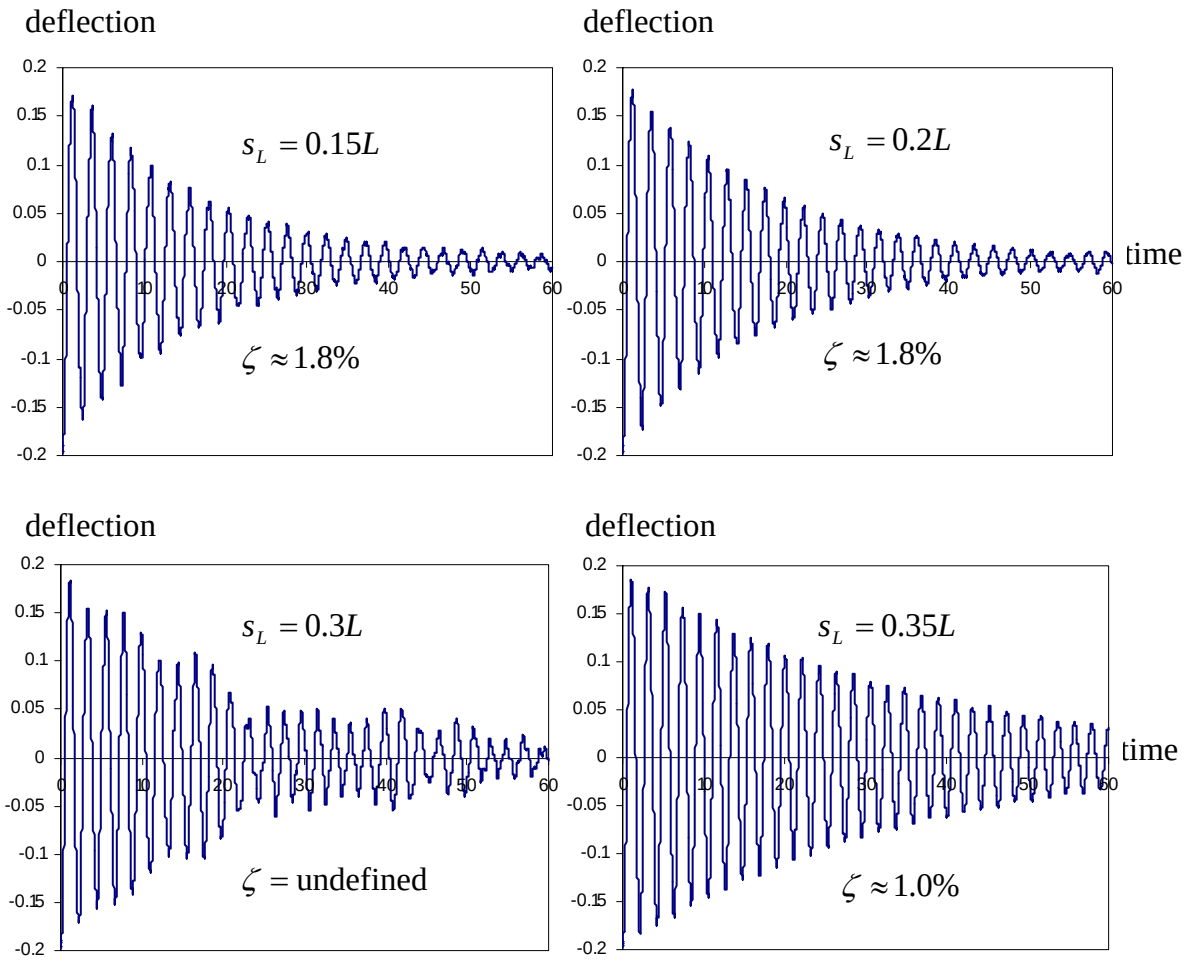

Figure 3-46 Results obtained for different values of s_L and $s_0 = 0.3L$ and $\varepsilon = 1/6$.

leading to some residual vibration. For $s_L = 0.35L$, the response is smooth; however, the damping ratio is relatively small. Finally for $s_L = 0.3L$, the response is considerably affected by higher modes which makes the synchronization procedure almost impossible.

It is also noted that using larger values of ε usually leads to higher attenuation effects for the first few cycles; however, the response will be noisier which makes the synchronization procedure harder. Eventually, after several cycles, the synchronization is lost and no continuous

attenuation is obtained afterwards. Considering all the results presented in this section, it can be concluded that the maximum obtainable damping ratio is about 1.7 % (for $s_0 = 0.3L,\ \varepsilon = 1/6$ and $s_L = 0.25L$) which is only slightly higher than what was obtained for the horizontally-moving mass considered previously (the highest damping ratio was 1.5%). On the other hand, it is important to note that, for this case, the beam's vibration will be completely damped (there will be no residual vibration left) while for the horizontally moving mass case there was a residual vibration left. In particular, inclusion of a very small natural damping will result in a very smooth attenuation of vibration which eventually leads to complete elimination of vibration. For instance, for $s_0 = 0.3L,\ \varepsilon = 1/6$ and $s_L = 0.25L$, including a natural damping of about 0.1% will result in a very smooth attenuation of vibration, with an overall damping ratio of 1.8%, which eventually leads to complete damping of vibration as shown in Figure 3-48.

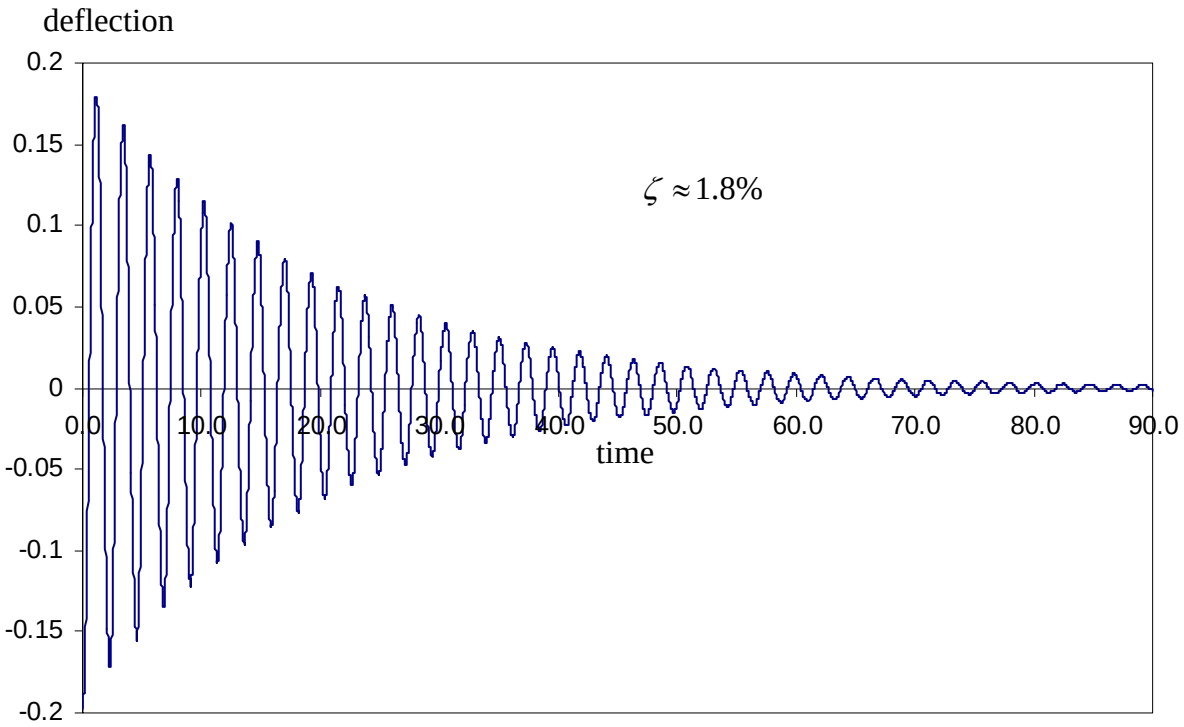

Figure 3-47 Beam's response for $s_L = 0.25L$, $s_0 = 0.3L$ and $\varepsilon = 1/6$ with inclusion of small natural damping.

While the simulations presented in this section showed that vibration for the simply-supported beam can be attenuated and completely eliminated by using a vertically moving mass, the maximum active damping ratio was around 1.8% which is relatively low, for instance, compared to that of cantilevered beam which was around 4%. A possible way to increase this active damping ratio is to use two vertically moving mass instead of one. For instance, as shown in Figure 3-48, two masses which are moving along the two guide bars perpendicular to the beam's axis, can be used for vibration control purposes. The horizontal location of the two guide bars can affect the beam's response considerably as will be shown later. It appears that one natural selection is to position the guide bars' symmetrically with respect to beam's center, as is the case in Figure 3-48.

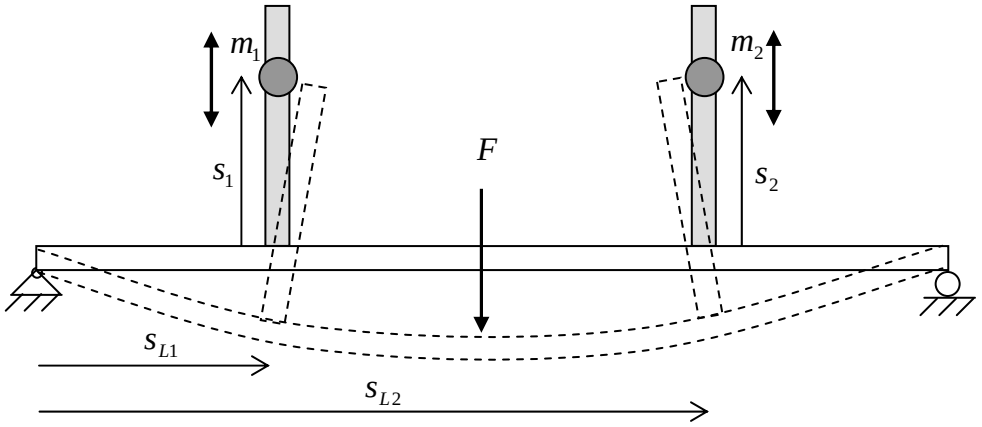

Figure 3-48 A simply supported beam with two masses moving perpendicular to its longitude axis.

For instance, assume that the mass motion parameters are $s_0 = 0.3L$ and $\varepsilon = 1/6$ and $m = 0.5$ for both masses while different values for s_{L1} and s_{L2} are tested. The results are summarized in Figure 3-49 where, for all the cases, the positions of the two guiding bars are

symmetric with respect to the center of the beam. As it is shown in the figure, the smoothest result is obtained for $s_{L1} = 0.2L$ and $s_{L1} = 0.8L$ where the damping ratio of around 2.1% is obtained (with inclusion of the natural damping). Note that the sum of the two masses for this case equals the mass for the previous case (Figure 3-48 for instance). Consequently, it can be concluded that using two smaller masses, which are positioned symmetrically with respect to the beam's center, can be more effective than using one larger mass.

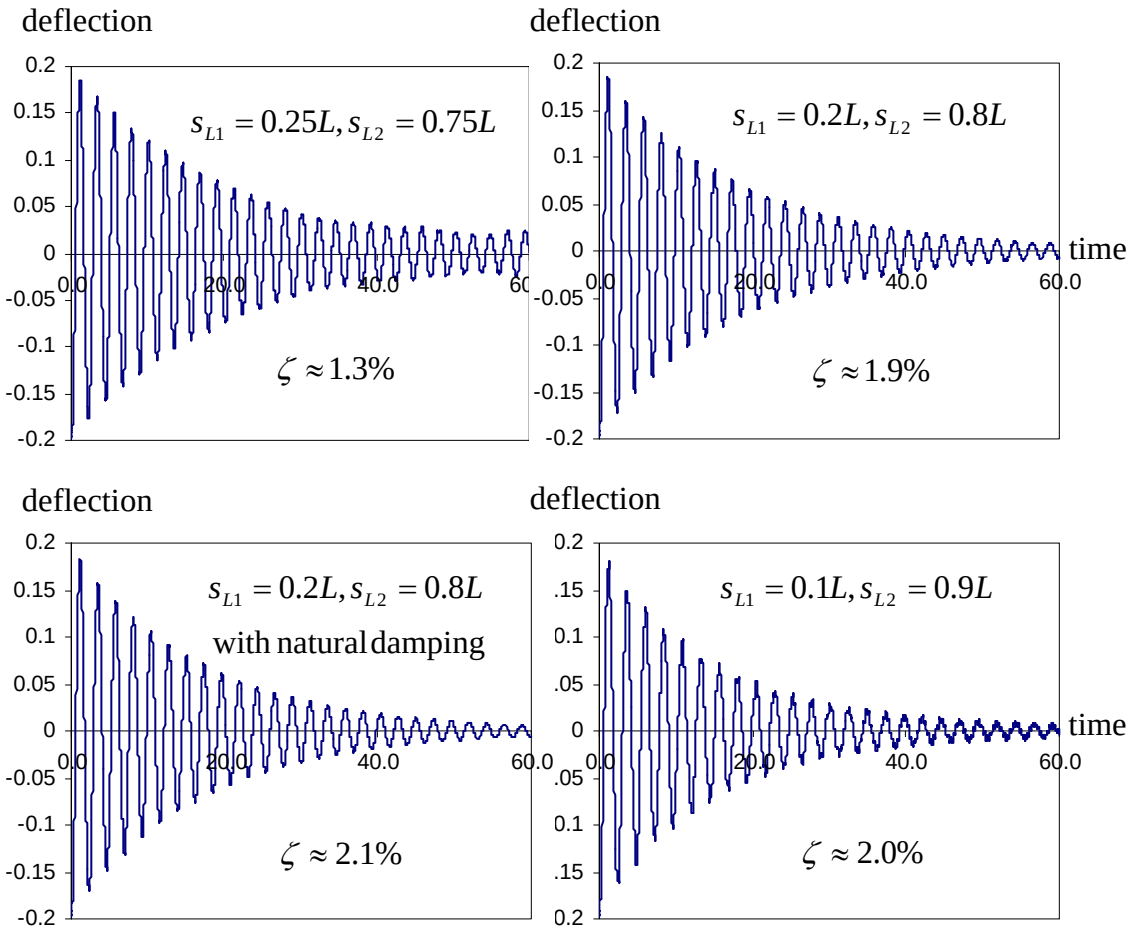

Figure 3-49 Comparison of the beam's response obtained by using two vertically moving masses with $s_0 = 0.3L$, $\varepsilon = 1/6$ and $m = 0.5$ for both.

The other parameters which can be adjusted for increasing the active damping ratio are mass motion amplitude, $s_0\varepsilon$, and averaged location, s_0. While the analyses show that changing the

averaged location doesn't improve the damping ratio, they show that increasing the amplitude can improve it. The maximum damping ratio that could be obtained is for $s_0 = 0.3L$, $\varepsilon = 1/3$, $m = 0.5$, $s_{L1} = 0.2L$ and $s_{L1} = 0.8L$. The result, shown in Figure 3-50, indicates a very smooth attenuation of vibration with the damping ratio of around 4.1%, which shows a dramatic increase.

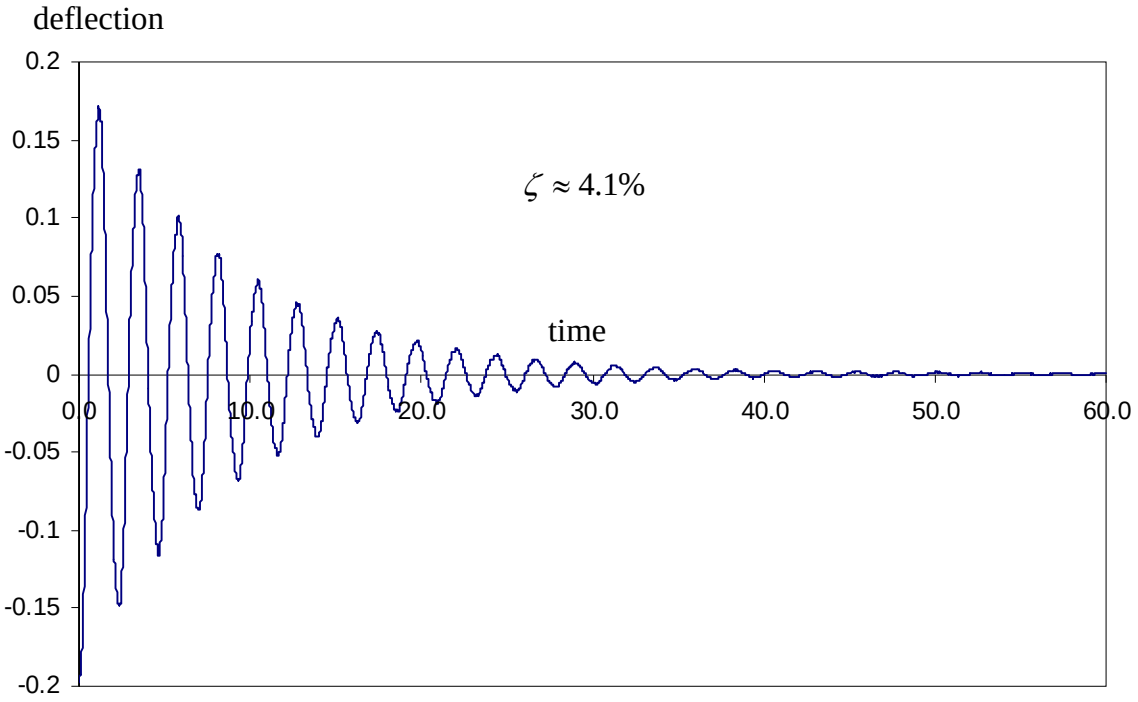

Figure 3-50 The beam's response obtained by using two vertically moving masses with $s_0 = 0.3L$, $\varepsilon = 1/3$ and $m = 0.5$ for both.

CHAPTER 4

CONTROLLING VIBRATION OF A FRAME

4.1 Introduction

In the previous chapters, the proposed vibration control method has been applied for controlling vibration of a pendulum as well as simple beams of different boundary conditions and properties. In this chapter, the method is applied to a more complicated structure, which is the frame structure shown in Figure 4-1. The frame can be initially excited by either force F_x or F_y or both. The vibration will then controlled by synchronizing motion of one or more masses as indicated in the figure. Masses m_1 and m_2 are placed as shown to control vibration of the first mode and mass m_3 is placed as shown to control second mode vibration (this will be explained in more details in the following sections). All the members of the frame are assumed identical

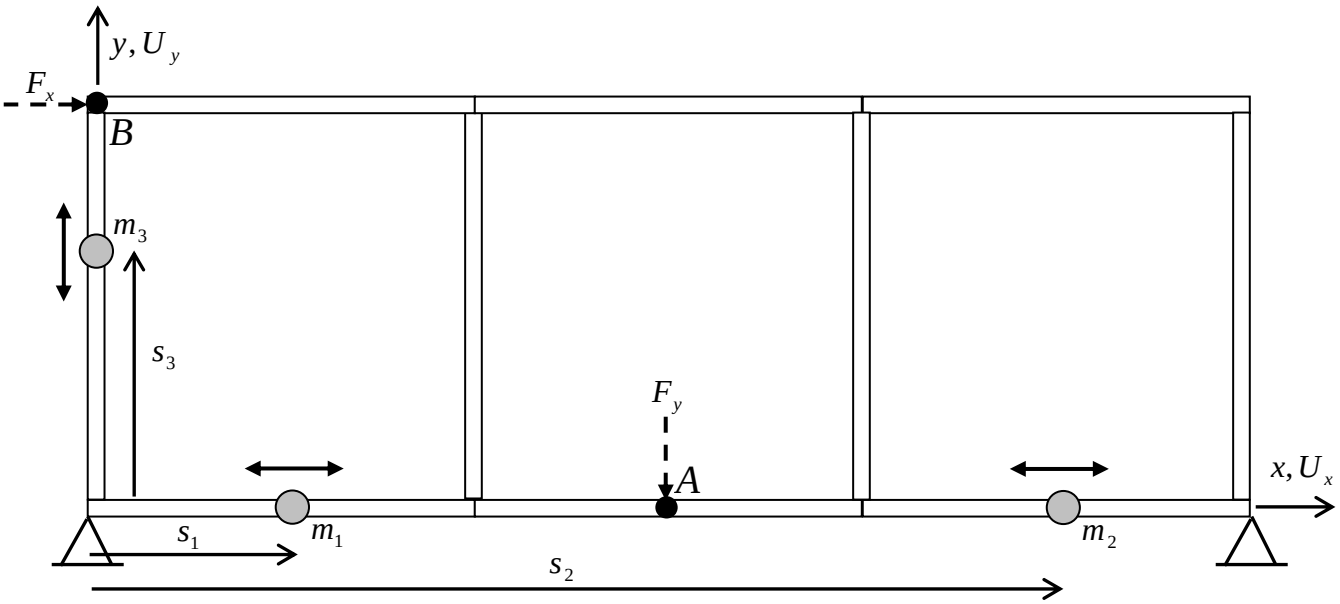

Figure 4-1 A typical frame structure with moving masses for controlling vibration.

, are welded to one another and pinned at the supports. The frame is made of aluminum, with Young's modulus of 70 *GPa* and density of 2700 kg/m^3. The cross section of frame members is a rectangle of width 58 *mm* and thickness 5.6 *mm*. The length of each member is *L*=1 *m*. The total mass of the frame is $m_f = 8.77\,kg$.

Figure 4-2 shows the first four vibration modes for a typical case. The corresponding frequencies are 2.7, 3.2, 6.1 and 11.7 Hz. As it is observed, the first mode is mainly bending of the horizontal sides while the second mode is the shear of the entire frame in the horizontal direction (or can be assumed as the bending of the vertical sides). The rest of the modes are mainly bending of the horizontal sides in higher modes.

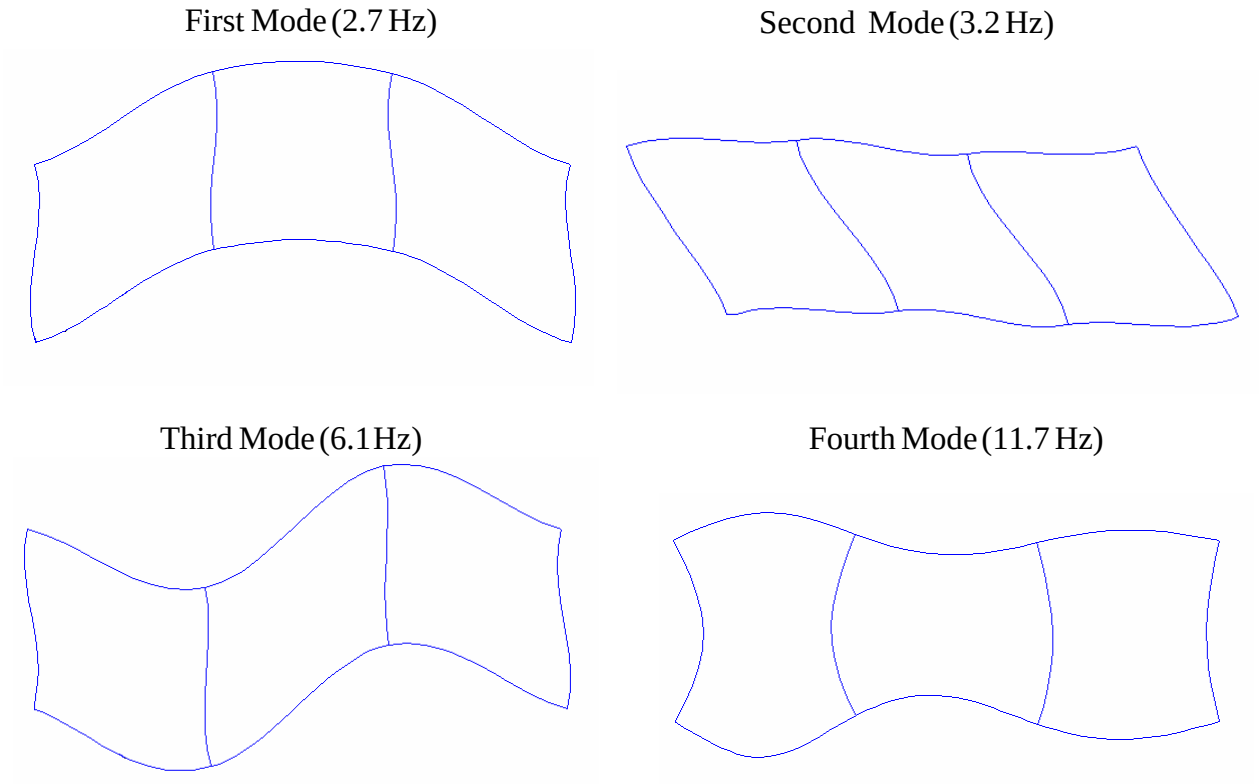

Figure 4-2 First four frequencies and vibration modes for the frame structure.

The main difference between the frame of Figure 4-1 and a simply supported beam considered before, lies on how the vibration modes and frequencies are distributed. For instance, for a typical frame considered in this section, the first two natural frequencies are close (within 20% of one another) while the first two natural frequencies for the simply supported (and cantilevered) beams are considerably different. Consequently, it is important to investigate whether synchronizing the mass motion for controlling one mode can affect (or excite) the other one. The other important factor on how the mass or masses should move to attenuate vibrations in different modes is how the shapes of these vibration modes are.

According to the shape modes presented in Figure 4-2, it is expected that mainly the first mode be initially excited and dominate the response when the force F_y (shown in Figure 4-1) is used to disturb the frame. On the other hand, when force F_x is initially applied, it is expected that the second mode mainly dominates the response. Furthermore, based on the values of the first four natural frequencies, it can be concluded that the response will be mainly affected by the first two modes while the contribution of the third and higher modes will be much less since their corresponding frequencies are relatively large. As a result, it appears that moving the mass along horizontal sides of the frame should attenuate vibration induced by applying force F_y, while moving it on vertical sides should attenuate vibration induced by force F_x. In other words, the mass motion on horizontal sides should control the first mode of vibration and the mass motion along vertical sides should control the second mode. This idea will be tested in the following sections through different numerical examples.

4.2 Controlling Vibration of the Frame Excited by F_x

The frame shown in Figure 4-2 is initially excited by the force F_y only. As discussed earlier, with such an initial disturbance, the frame will vibrate mainly in the first mode; therefore, it may be effective to move the mass m_1 horizontally. It is assumed that the mass of m_1 is 0.44 *kg* or $\overline{m}_1 = 0.05$, where $\overline{m}_1 = m_1 / m_f$ is the dimensionless mass of the moving body with respect to the total mass of the frame. The pattern of mass motion is similar to that of the previous sections:

$$s_1 = s_1^0 \left(1 - \varepsilon_1 \sin\left(\omega_m t + \Delta\psi\right)\right) \tag{4.1}$$

where different values of s_1^0 and ε_1 will be used. Figure 4-3 shows the frame's vertical displacement at point A, U_y^A, obtained for $s_1^0 = 0.5L$ and $\varepsilon_1 = 0.5$. As it is observed, attenuation rate is small and the frame's response is not smooth due to the effect of higher vibration modes. Similar to what was discussed in the previous chapter for the beam, the effect of the higher modes makes the synchronization procedure hard which, in turn, decreases the attenuation effects and can eventually lead to loss of mass synchronization. On the other hand, by including even a small natural damping, i.e. with an equivalent damping ratio of $\zeta = 0.1\%$, the frame response will be smoother and the attenuation effect increases considerably. This is shown in Figure 4-4 where the frame response for the same analysis as that of Figure 4-3 is done except that natural damping (by using the Rayleigh damping) is included. As it is observed, the vibration is smoothly attenuated with a damping ratio of around 0.7%. If the analysis is done for a longer period of time, which is not shown in the figure, it is observed that the vibration will be eventually eliminated completely.

Apart from increasing the attenuation effects, including natural damping is also effective in complete elimination of vibration. For example, the response of Figure 4-3 shows the presence of

a residual vibration (vibration does not attenuate further after about 25 seconds). However, the vibration is completely damped for the response of Figure 4-4. It is also noted that, for the result of Figure 4-3, the percentage of residual vibration (the average amplitude of residual vibration over initial amplitude of vibration) is about 16%.

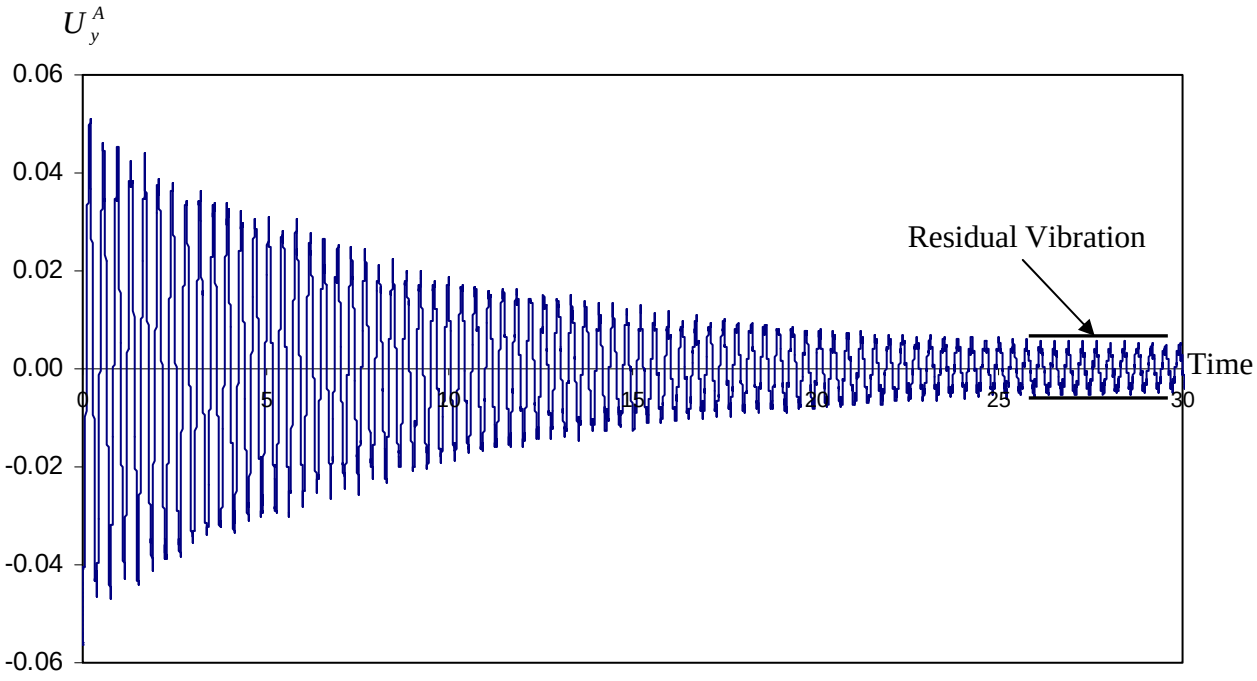

Figure 4-3 Displacement U_y^A when the frame is initially excited by force F_y (no natural damping).

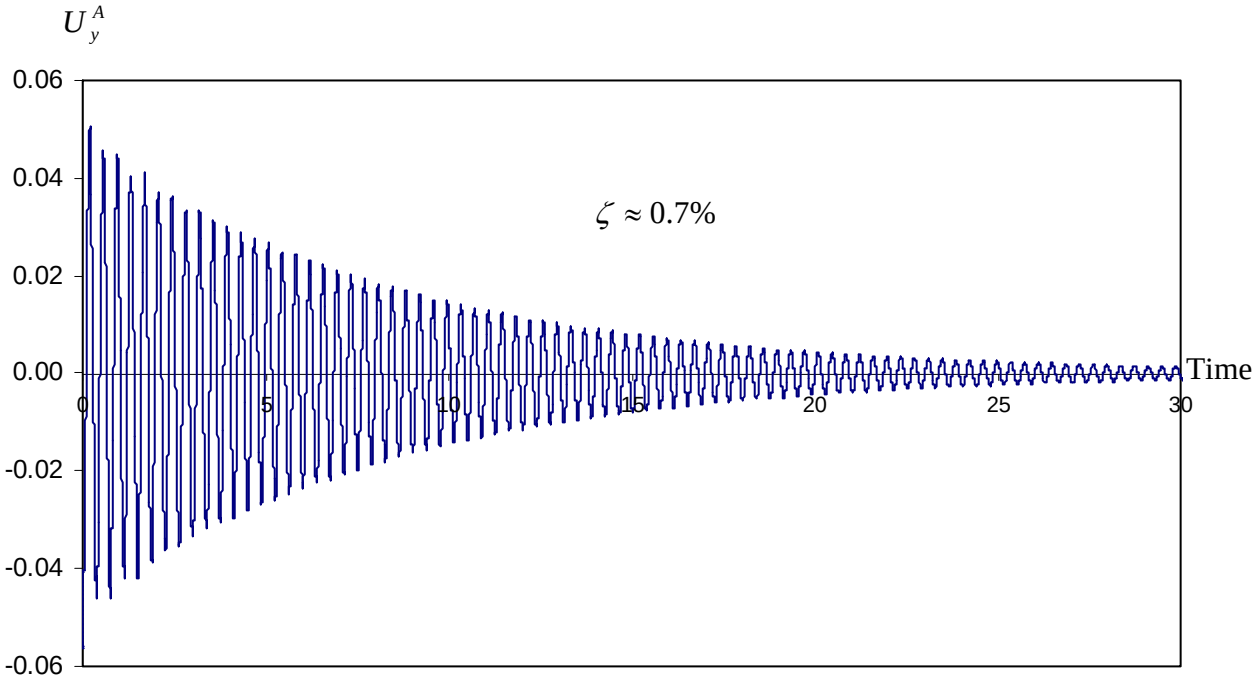

Figure 4-4 Displacement U_y^A when the frame is initially excited by force F_y (with natural damping).

From the control point of view, it is desirable to maximize the attenuation effect, i.e. to increase the active damping ratio. For this purpose, similarly to the beam problem, different values of the mass motion parameters, including s_0 and ε, are used and the corresponding results be compared in Table 4-1. The residual vibration percentage mentioned in the table shows the amplitude of residual vibration after about 25 seconds over the initial vibration amplitude. It is also noted that the active damping ratio in Table 4-1 is calculated by averaging it over the first 20 seconds. According to the table, the maximum damping ratio with no residual vibration occurs at $s_0 = 3L/4$ and $\varepsilon = 1/2$. It is also observed that increasing the mass motion amplitude, εs_0, does not always lead to an increase in the damping ratio. In general, increasing εs_0 from a particular value makes the frame's response noisy which eventually leads to the presence of residual vibration. It is also noted that increasing the mass of the moving body, for instance to

$\overline{m}_1 = 0.1$, will have a similar effect where the damping ratio increases but the response is noisier (and there is residual vibration).

Table 4-1 Active damping ratio obtained for different values of s_0 and ε when the first mode is mainly excited.

s_1^0	$\varepsilon_1 s_1^0$	ζ %	Response Type	Residual Vibration %
L/2	L/4	0.70	Smooth	0.00
L/2	3L/8	0.85	Noisy	0.89
L/2	L/2	1.28	Noisy	3.21
3L/4	L/4	0.88	Smooth	0.00
3L/4	3L/8	0.80	Noisy	0.94
3L/4	L/2	1.02	Very Noisy	3.56

4.3 Controlling Vibration of the Frame Excited by F_y

In this section, the frame shown in Figure 4-1 is assumed to be initially excited by the force F_x which as mentioned previously results in excitation of mostly the second mode (and also the response will be dominated by this mode) and mass m_3 is moved vertically for controlling the frame vibration. Like the previous section, different values of the mass motion parameters, i.e. s_3^0 and ε_3, will be examined. For instance, Figure 4-5 shows the frame response represented by the horizontal displacement U_x^B, for $s_3^0 = 3L/4$ and $\varepsilon_3 = 0.25$. As it is observed, vibration is attenuated with an equivalent damping ratio of around 0.7%. The result shown in Figure 4-5 is obtained without including any natural damping.

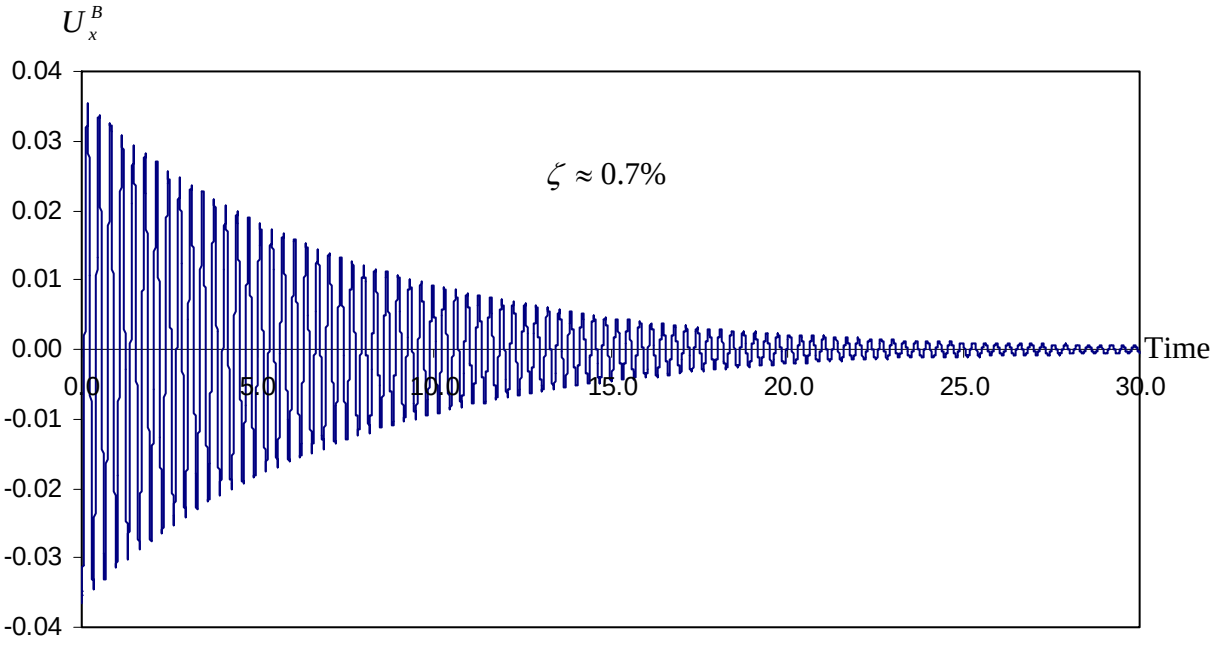

Figure 4-5 Frame response when the second mode is initially excited.

Like the previous cases, the effects of different mass motion parameters on the damping ratio and vibration attenuation has been investigated. Table 4-2 summarizes some of the results obtained by using different values s_3^0 and ε_3 where the mass of the moving body is constant at $\overline{m}_3 = 0.05$. As it is observed from the table, the damping ratio is relatively small for these values (the maximum occurs at $s_3^0 = 3L/4$ and $\varepsilon_3 = 1/3$ where $\zeta = 0.77\%$). Also, the results in the table show that the damping ratio does not generally increase when the mass motion amplitude, εs_0, increases. In fact, similar to section 4.2, the increase in εs_0 can make the response noisier which eventually results in the presence of residual vibration.

Table 4-2 Active damping ratio obtained for different values of s_3^0 and ε_3 when the second mode is mainly excited.

s_3^0	$\varepsilon_3 s_3^0$	$\overline{m}_3$	Natural Damping	ζ %	Response Type	Residual Vibration %
L/2	L/8	0.05	No	0.43	Smooth	0.00
L/2	3L/16	0.05	No	0.54	Smooth	0.00
L/2	L/4	0.05	No	0.52	Noisy	27.40
L/2	3L/8	0.05	No	0.58	Noisy	21.90
3L/4	L/8	0.05	No	0.46	Smooth	0.00
3L/4	3L/16	0.05	No	0.70	Smooth	0.00
3L/4	L/4	0.05	No	0.77	Smooth	0.00
3L/4	L/4	0.05	Yes	1.00	Smooth	0.00
3L/4	L/4	0.1	Yes	1.62	Smooth	0.00
3L/4	L/4	0.2	Yes	2.97	Smooth	0.00

Including a small natural damping, around 0.1% for instance, smoothens the response which, in turn, increases the damping ratio (as shown in the table, for $s_3^0 = 3L/4$ and $\varepsilon_3 = 1/3$ the damping ratio raises to 1%). Finally, it should be noted that unlike the case of section 4.2, increasing the mass of the moving body can actually increase the active damping ratio without leading to the presence of residual vibration. According to Table 4-2, the active damping ratio can be increased up to 2.97%, by using $\overline{m}_3$ of 0.2, without having any residual vibration in the response. Apparently, moving a large mass vertically does not disturb the first mode as much as a horizontally moving mass affects the second mode. Consequently, larger masses can be used for vibration control of the second mode which in turn leads to achieving larger damping ratios for this case.

4.4 Using Two Masses to Control Vibration of the First Mode

Based on the results of the last two sections, the attenuation rate obtained from the moving masses was relatively low for vibration control of the first mode (the maximum damping ratio was about only 0.8%). One possible way to improve the attenuation effect is to use more than one mass for control purposes. Assume that the frame is initially excited by applying force F_y and then vibration is controlled by moving masses m_1 and m_2 along the horizontal side as shown in Figure 4-6. It is also assumed that similar to Eq. (4.1), the motions of the masses are given by:

$$s_1 = s_1^0\left(1-\varepsilon_1 \sin\left(\omega_m^1 t + \Delta\psi_1\right)\right) \tag{4.2}$$

$$s_2 = s_2^0\left(1-\varepsilon_2 \sin\left(\omega_m^2 t + \Delta\psi_2\right)\right) \tag{4.3}$$

where s_i^0 and ε_i are the mass motion averaged location and non-dimensional amplitude for the *i*th mass, respectively.

To investigate the possibility of increasing the attenuation effects by using two masses, different values of mass motions parameters, including s_i^0 and ε_i, as well as different values of $\overline{m}_1$ and $\overline{m}_2$, the dimensionless masses of the moving bodies, need to be tested. Since the initial deformation of the frame, as well as the first vibration mode, as shown in Figure 4-2, are symmetric with respect to the center of the frame, it seems natural to select the mass motion parameters such that their motion is also symmetric with respect to the frame's center. This means that the sum of averaged mass locations should be equal to the length of frame's horizontal side, i.e. $s_1^0 + s_2^0 = 3L$, and the mass motion amplitudes be the same, i.e. $s_1^0\varepsilon_1 = s_2^0\varepsilon_2$.

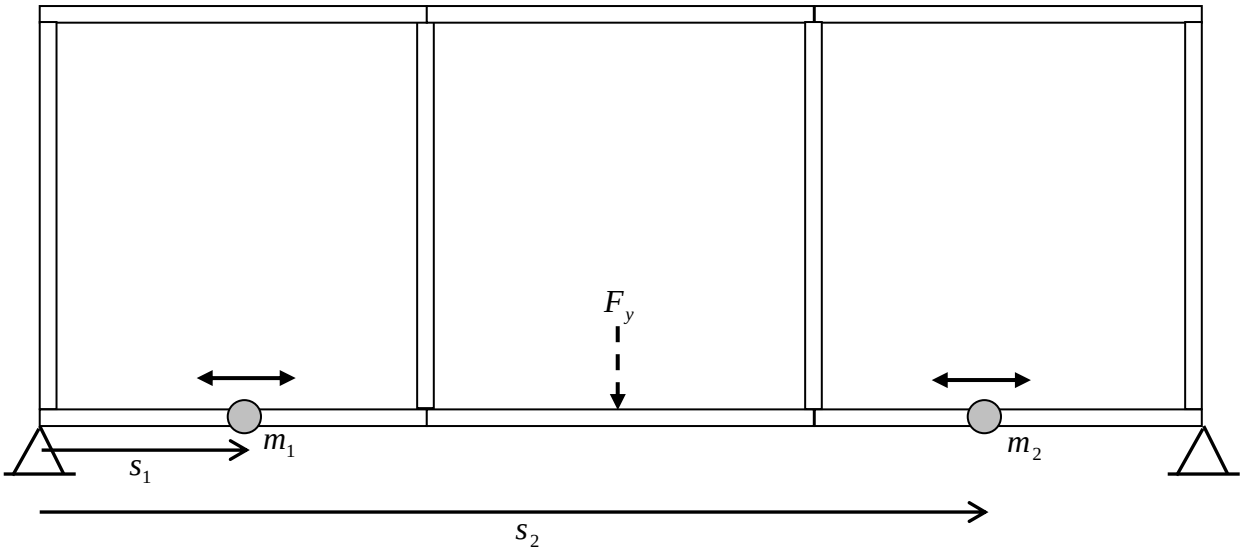

Figure 4-6 Moving two masses horizontally for controlling vibration caused by force F_y.

Also, the mass of the two moving bodies has been selected to be the same, i.e. $\overline{m}_1 = \overline{m}_2$. Table 4-3 shows some of the results obtained by using different mass parameters and including natural damping. As it is observed, the frame's response is not smooth and in most cases there is a residual vibration left. For the only case where vibration is completely damped, i.e. for $s_1^0 = L$ and $s_2^0 = 2L$, the active damping ratio is relatively low.

Table 4-3 Active damping ratio obtained for different values of mass motion parameters when two masses are used.

$\overline{m}_1$ or $\overline{m}_2$	s_1^0	$s_1^0 \varepsilon_1$	s_2^0	$s_2^0 \varepsilon_2$	ζ	Response type	Residual vibration
0.05	3L/4	L/4	9L/4	L/4	1.40	Noisy	7.5
0.05	L	L/4	2L	L/4	1.04	Noisy	0.0
0.05	L/2	L/4	2.5L	L/4	1.02	Noisy	23.0
0.1	L	L/8	2L	L/8	0.92	Noisy	19.6
0.05	3L/4	L/4	2.5L	L/4	1.09	Noisy	7.0
0.05	L/2	L/4	L	L/4	0.99	Noisy	18.0

The results obtained when the mass motions are symmetric with respect to the frame's center are not satisfactory, similarly as asymmetric masses' motions are not symmetric. For instance, as shown in Table 4-3, for $s_1^0 = 3L/4$ and $s_2^0 = 2.5L$ there is residual vibration and the active damping ratio is also small. Even for a case where the two masses are moving to the left of the frame's center, with $s_1^0 = L/2$ and $s_2^0 = L$, the response is not smooth and residual vibration exists.

It is important to note that the results shown in Table 4-3 were obtained by using the first synchronization scheme mentioned in chapter 3. On the other hand, using the second or the third scheme for synchronization did not improve the results, i.e. does not lead to results with higher active damping ratios. One may conclude that the reason is that the first two natural frequencies are close, i.e. the second natural frequency is only about 20% higher than the first one. Therefore, the response is affected by both the first and the second modes, which makes it irregular; thus, the synchronization is either lost or not sufficient for obtaining desired attenuation effects.

To test this conclusion, a stationary mass will be added to the frame such that the first two natural frequencies are no longer close. For example, placing a mass at the center of the bottom horizontals side will change (decrease) the first natural frequency while it barely changes the second one. For instance, placing a mass of $\overline{m}_s = 0.5$ will result in a first natural frequency of about 1.7 Hz and a second natural frequency of 3.2 Hz (i.e. the second natural frequency is about 90% higher than the first one).

Table 4-4 Active damping ratio obtained for different values of mass motion parameters when a stationary mass is placed at the frame's center.

$\overline{m}_1$ and $\overline{m}_2$	s_1^0	$s_1^0\varepsilon_1$	s_2^0	$s_2^0\varepsilon_2$	ζ	Response type	Residual vibration	Synchronization Type
0.05	L	L/4	2L	L/4	0.63	Smooth	0.0	First
0.1	L	L/4	2L	L/4	0.99	Smooth	0.0	First
0.1	L	L/2	2L	L/2	-	Not Converged	-	First
0.2	L	L/4	2L	L/4	1.66	Noisy	15.9	First
0.2	L	L/4	2L	L/4	2.00	Smooth	0.0	Third
0.3	L	L/4	2L	L/4	2.69	Smooth	0.0	Third

The attenuation effects with the stationary mass of $\overline{m}_s = 0.5$ placed at the center of the horizontal side obtained for $s_1^0 = L$, $s_2^0 = 2L$ and $s_i^0\varepsilon_i = L/4$ and $L/2$ are summarized in Table 4-4. By comparing the results shown in this table with those of Table 4-3 it can be observed that the frame response is smoother when the stationary mass is placed at the frame's center since the frequencies are more well separated. It is also observed that higher active damping ratios can be obtained by increasing the mass of moving bodies. However, for larger values of $\overline{m}_1$ and $\overline{m}_2$ where the damping ratio is higher, using the first synchronization scheme leads to the presence of residual vibration in frame's response. In other words, since the attenuation rate is higher for larger $\overline{m}_1$ and $\overline{m}_2$, the first synchronization scheme fails to keep the mass motion and frame's vibration synchronized, which eventually leads to presence of residual vibration. On the other hand, simulations show that the third scheme can successfully keep the synchronization of the mass motion and the frame vibration. Consequently, larger masses can be used for vibration control when the third scheme is applied, which eventually leads to obtaining relatively high damping ratio. For instance, Figure 4-7 shows the frame's response, in terms of vertical

displacement U_y^A versus time for $\overline{m}_1 = \overline{m}_2 = 0.3$, $s_1^0 = L$ and $s_2^0 = 2L$. As it is observed from the figure, vibration is smoothly attenuated with a relatively high rate.

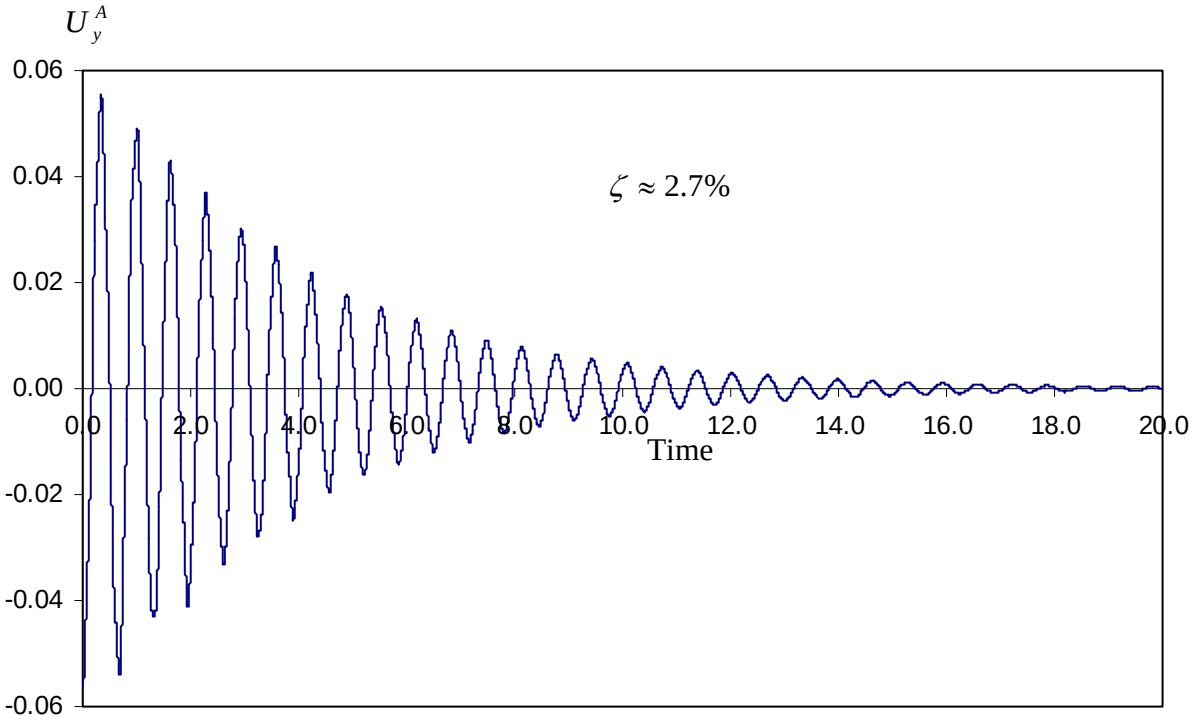

Figure 4-7 Frame's response when a stationary mass is placed at its center and the first mode is excited.

According to the results summarized in Table 4-4, it is important to note that the active damping ratio cannot be increased more by increasing the mass motion's amplitude further than $s_0^i \varepsilon^i = 0.1L$. In fact, the FEM solution diverges if any values higher than $0.1L$ is used for the mass motion's amplitude. It is also very important to note that if the analyses shown in Table 4-4 are repeated with using only one mass for vibration control, the results are different. In fact, the FEM solution either diverges (for larger values of $\overline{m}_1$) or leads to results with a relatively small

active damping ratio (for smaller values of $\overline{m}_1$). This means that using two moving masses is necessary for obtaining a smooth attenuation with relatively high damping ratios.

4.5 Controlling Two Vibration Modes for the Frame

So far in the previous sections, the frame was initially excited either mostly in the first mode or mostly in the second mode. In this section, the possibility of controlling the frame's vibration when both modes are comparably excited by forces F_x and F_y is investigated. Figure 4-8 shows such a frame and four masses m_1 to m_4 for controlling its vibration. It is also noted that no stationary mass is used for the analyses of this section. According to the results shown in Table 4-2, the maximum attenuation effect for controlling vibration of the second mode is obtained for mass motion parameters of $s_3^0 = 3L/4$ and $\varepsilon_3 = 1/4$. Consequently, these values will be used in this section for motion of masses m_1 and m_2 (see Figure 4-8). As will be shown later, the main challenge in this section will be on controlling vibration in the first mode. As a result, different values of mass motion parameters for m_3 and m_4 will be investigated.

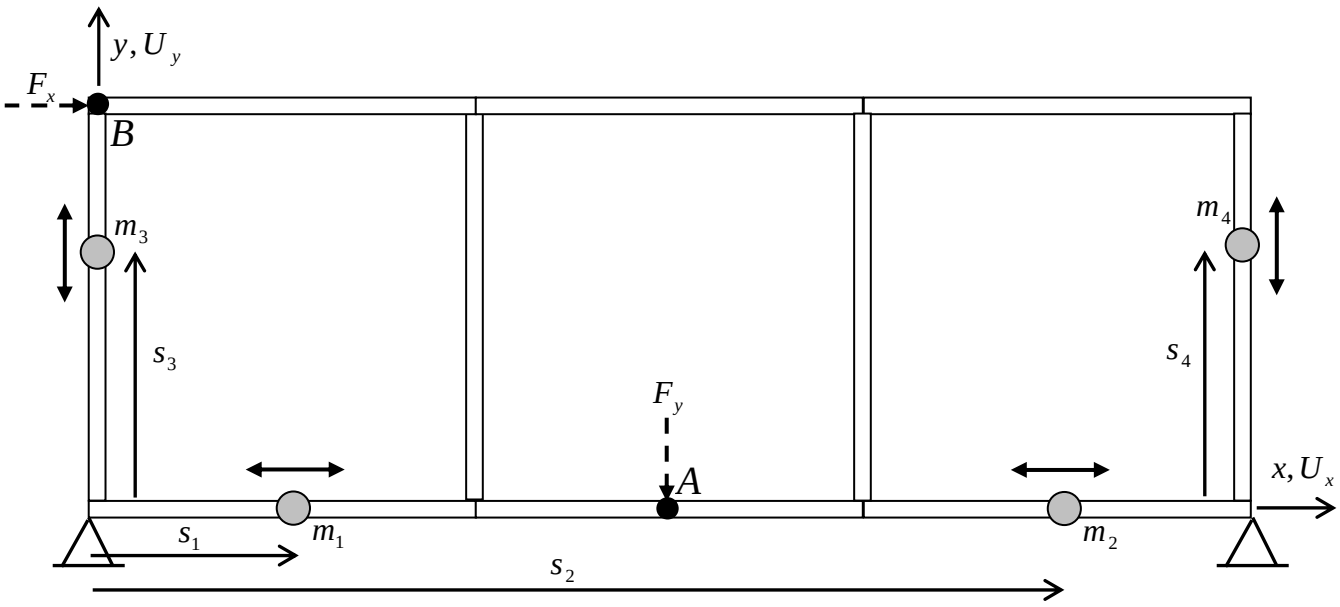

Figure 4-8 A frame initially excited in the first and second modes by forces F_x and F_y.

In the first set of analyses, three masses including m_3 and m_4 (for controlling vibration due to second mode) and m_1 (for controlling vibration of the first mode) will be used. The simulations show that including a relatively small natural damping is essential for obtaining a smooth response. Consequently, natural damping, with an equivalent damping ratio of about 0.1%, is included in all the results presenting in this section.

Figure 4-9 shows a sample frame response obtained for $\overline{m}_1 = \overline{m}_3 = \overline{m}_4 = 0.05$, $s_1^0 = s_3^0 = s_4^0 = 3L/4$, $\varepsilon_3 = \varepsilon_4 = 0.25$ and $\varepsilon_1 = 1/3$. The response is presented by two plots: vertical displacement of point A, U_y^A, versus time and horizontal displacement of point B, U_x^B, versus time. According to the figure, it can be observed that the U_y^A is fluctuating in time with almost the same frequency as the first natural frequency, which is about 2.6Hz. On the other hand, fluctuation of U_x^B in time has almost the same frequency as the second natural frequency,

which is about 3Hz. Consequently, it is concluded that U_y^A is representing vibration in the first mode while U_x^B is representing vibration in the second mode.

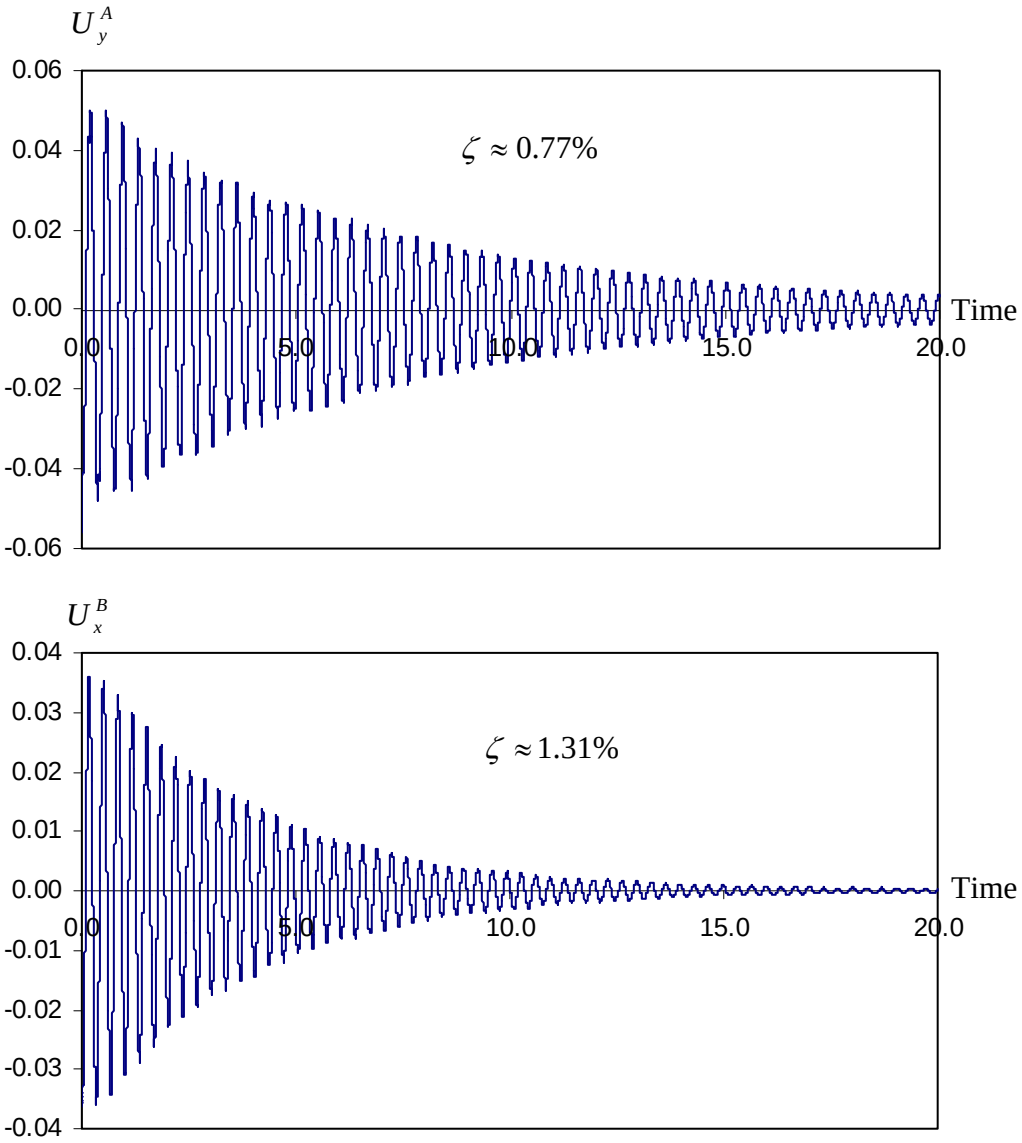

Figure 4-9 Frame's response when the first two modes are initially excited and three masses are used for controlling vibration.

Table 4-5 Results obtained for vibration control of two modes by using three masses.

	Case Number	1	2	3	4	5	6	7	8	9
	$\overline{m}_3$ and $\overline{m}_4$	0.025	0.025	0.025	0.025	0.025	0.05	0.05	0.1	0.1
	s_3^0 and s_4^0	3L/4	3L/4	3L/4	3L/4	3L/4	3L/4	3L/4	3L/4	3L/4
	$\varepsilon_3 s_3^0$ and $\varepsilon_4 s_4^0$	3L/16	3L/16	3L/16	3L/16	3L/16	3L/16	3L/16	3L/16	3L/16
	$\overline{m}_1$	0.05	0.05	0.05	0.05	0.05	0.05	0.05	0.05	0.1
	s_1^0	L/2	3L/4	3L/4	L	L/2	L/2	3L/4	3L/4	3L/4
	$\varepsilon_1 s_1^0$	L/4	L/4	L/4	L/4	3L/8	3L/8	L/4	L/4	L/4
	Synchronization scheme	Third	First	Third	Third	Third	Third	Third	Third	Third
First Mode	ζ	0.71	0.58	0.80	0.63	0.83	0.47	0.77	0.86	1.32
First Mode	Response type	Smooth	Noisy	Smooth	Smooth	Smooth	Smooth	Smooth	Smooth	Noisy
First Mode	Residual Vibration	0.00	7.00	0.00	0.00	0.00	0.00	0.00	0.00	2.60
Second Mode	ζ	0.84	0.71	0.84	0.83	0.81	0.63	1.31	1.91	1.92
Second Mode	Response type	Smooth	Smooth	Smooth	Smooth	Smooth	Noisy	Smooth	Smooth	Smooth
Second Mode	Residual Vibration	0.00	0.00	0.00	0.00	0.00	8.00	0.00	0.00	0.00

Table 4-5 summarizes the results obtained by using three masses. The active damping ratio for the first and second modes are obtained by considering the vertical and horizontal displacements (as shown in Figure 4-9), respectively. According to these results, some important conclusions can be made:

– The active damping ratio is generally lower for the first mode. In order to increase this ratio, different values of s_1^0, ε_1 and $\overline{m}_1$ have been used. However, none of them leads to a smooth attenuation of vibration with active damping ratio higher than 1%.

The second mode on the other hand, is attenuated with a relatively high damping ratio even though only one set of values is used for s_3^0, ε_3, s_4^0 and ε_4.

- The mass motion parameters used for case 6 differs with those of case 7 only in values of s_1^0 and ε_1. While this change affected (increased) the damping ratio for the first mode, it is interesting to note that it also affected (increased) the damping ratio for the second mode dramatically. On the other hand, comparison of cases 7 and 8 in the table (which only differ in values of s_3^0, ε_3, s_4^0 and ε_4) show that the change in motion parameters of m_3 and m_4 not only affects active damping ratio of the second mode, but it also affects the active damping ratio of the first mode. To summarize, it can be concluded that controlling vibration of the first mode (by using mass m_1) is not completely independent from controlling vibration of the second mode (by using masses m_3 and m_4).
- The best (maximum) attenuation effect obtained for the second mode corresponds to case 8 in the table. For this case however, the active damping ratio of the first mode is relatively small. To increase this ratio, one method is to increase $\overline{m}_1$, which is done in case 9. As it is observed from the table, while the damping ratio of the first mode increases to 1.32 %, there is a residual vibration and the frame's response is not smooth as shown in Figure 4-10. Based on these analyses, it appears that using one mass for controlling vibration of the first mode is not sufficient.
- Comparing the results for case 2 and 3 in the table shows that using the third scheme for synchronization procedure leads to much smoother and higher rate of vibration

attenuation. This has been proved through more numerical simulations which are not presented in Table 4-5 for the sake of brevity.

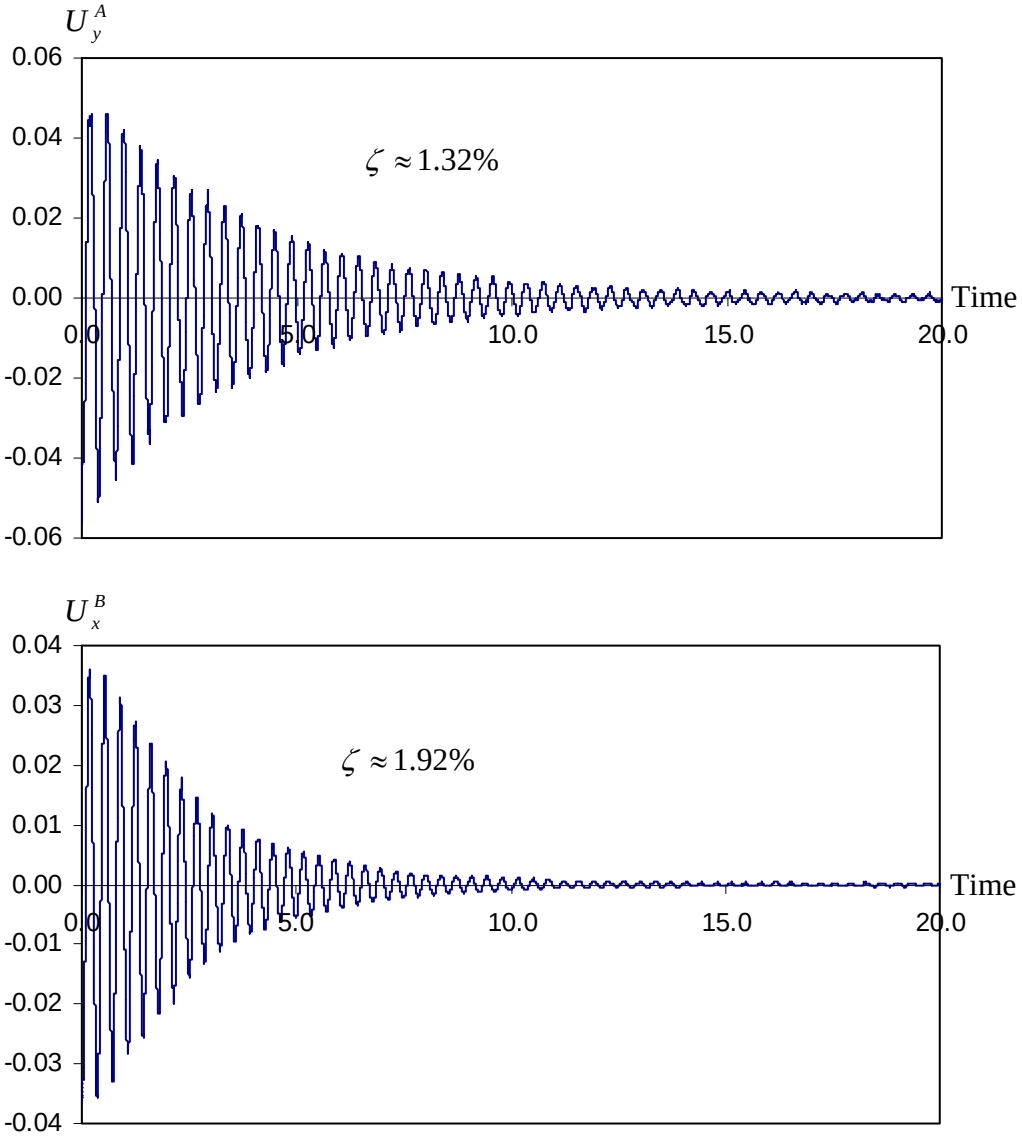

Figure 4-10 Frame's response corresponding to best attenuation effect test when three masses are used.

In order to increase the attenuation effect, especially for controlling vibration of the first mode, one way is to use four moving masses. As shown in Figure 4-8, masses m_1 and m_2 are

moving horizontally to control vibration of the first mode while masses m_3 and m_4 are moving vertically to control vibration of the second mode. Table 4-6 summarizes the results obtained by using different values for mass motion parameters $\overline{m}_i$, s_i^0 and ε_i. All the results presented in the table are obtained by using the third synchronization scheme. Also, the results of case 9 from

Table 4-6 Results obtained for vibration control of two modes by using four masses.

	Case Number	1	2	3	4	5	6	7
	$\overline{m}_3$ and $\overline{m}_4$	0.025	0.025	0.025	0.05	0.1	0.1	0.1
	s_3^0 and s_4^0	3L/4	3L/4	3L/4	3L/4	3L/4	3L/4	3L/4
	$\varepsilon_3 s_3^0$ and $\varepsilon_4 s_4^0$	3L/16	3L/16	3L/16	3L/16	3L/16	3L/16	3L/16
	$\overline{m}_1$	0.025	0.05	0.025	0.05	0.05	0.1	0.1
	$\overline{m}_2$	0.025	0.05	0.025	0.05	0.05	0.1	0
	s_1^0	L/2	L/2	L/2	3L/4	3L/4	3L/4	3L/4
	$\varepsilon_1 s_1^0$	L/4	L/4	L/4	L/4	L/4	L/4	L/4
	s_2^0	5L/2	5L/2	5L/2	9L/4	9L/4	9L/4	-
	$\varepsilon_2 s_2^0$	L/4	L/4	L/4	L/4	L/4	L/4	-
	Natural Damping Included	No	No	Yes	Yes	Yes	Yes	Yes
First Mode	ζ	0.55	0.73	0.72	1.44	1.42	2.23	1.32
	Response type	Noisy	Noisy	Smooth	Smooth	Smooth	Smooth	Noisy
	Residual Vibration	0.0	17.0	0.0	0.0	0.0	0.0	2.6
Second Mode	ζ	0.72	0.72	0.83	1.40	2.27	2.22	1.92
	Response type	Smooth	Smooth	Smooth	Smooth	Smooth	Smooth	Smooth
	Residual Vibration	0.0	0.0	0.0	0.0	0.0	0.0	0.0

Table 4-5 are repeated in Table 4-6 (case number 7) in order to have a better comparison. The following conclusions can be made by investigating the results of Tables 4-6:

- In case 7 of the results shown in the table, one mass of $\overline{m}_1 = 0.1$ is moving on the left side of the frame while in case 5, two masses of $\overline{m}_1 = \overline{m}_2 = 0.05$ are moving symmetrically with respect to the frame's center. Comparison of these results show that the frame response is smoother, with no remaining residual vibration, and the attenuation rate is higher when two masses are moving symmetrically. It is also interesting to note that moving two horizontally-moving masses instead of one increases the active damping ratio both for the first and the second mode.
- Comparison of the results of case 2 and 4 indicates the importance of selecting the location of mass motion in obtaining more attenuation effect. While the mass motion amplitude and the masses of the moving bodies for m_1 and m_2 are the same for the two cases, the difference in averaged mass position, s_1^0 and s_2^0, changes the frame response from noisy to smooth and also increases the attenuation effects.
- Comparing the results of case 1 and 3, where the mass motion parameters are the same but natural damping is included only in case 3, and also considering the result of case 2, shows that including natural damping smooth the frame response as well as increases the attenuation effects. This conclusion has also been made for the beam's problem in Chapter 3.

The highest attenuation rate for both modes is obtained for case 6 where the frame's response is smooth and the active damping ratio is relatively high. This is also shown in Figure 4-11 where the frame's response, in terms of vertical displacement of the point A, U_y^A, and horizontal

displacement of point B, U_x^B, is presented. As it is observed from the curves in the figure, both vertical and horizontal displacements are attenuating smoothly over time with a relatively high rate.

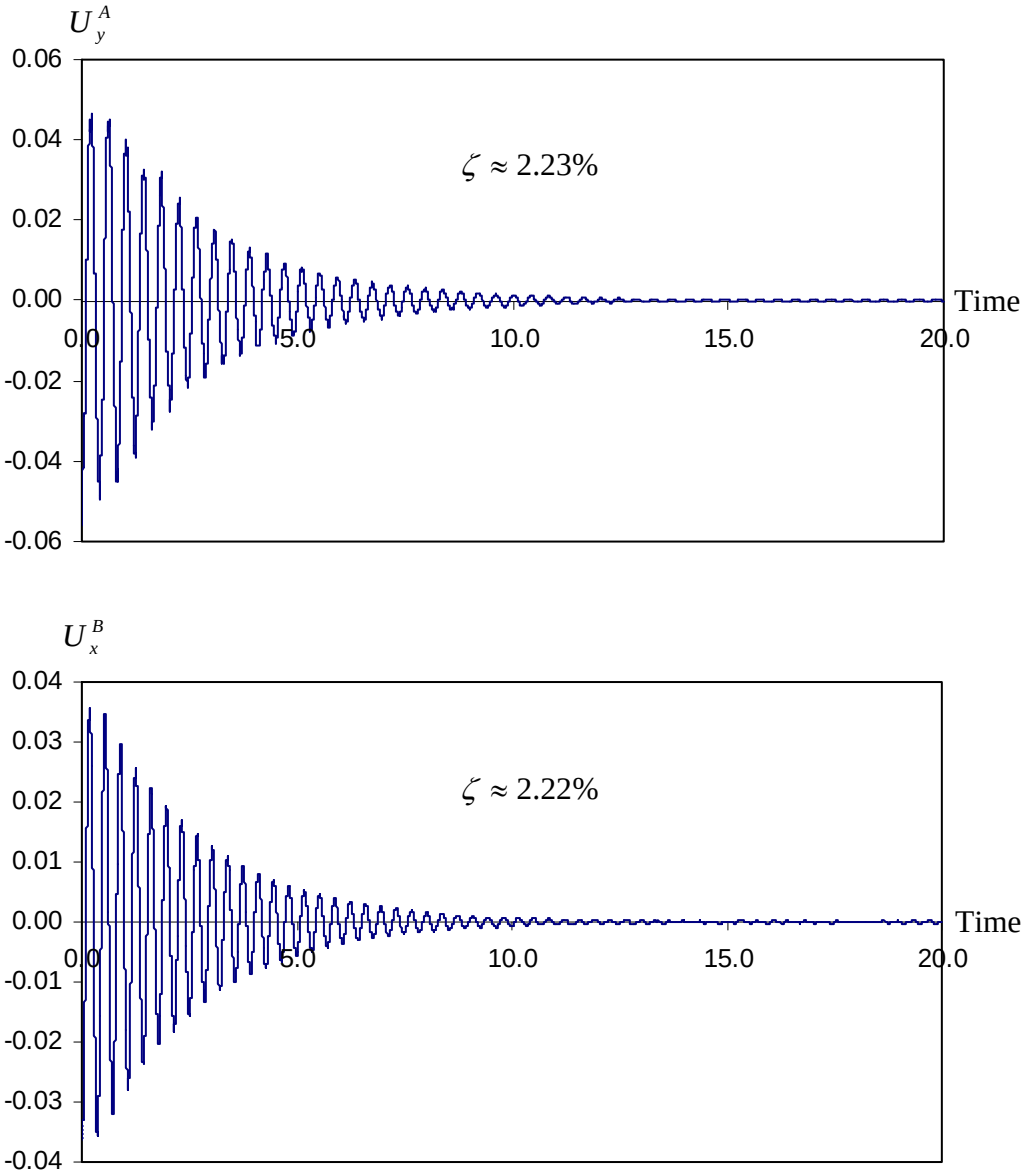

Figure 4-11 Frame's response corresponding to best attenuation effect test when four masses are used.

CHAPTER 5

CONCLUSIONS AND RECOMMENDATIONS

5.1 Overall Summary and Contributions

Relative movement of some parts of a vibrating mechanical structure can cause amplification or attenuation of the vibration amplitudes. It has been shown previously, in Szyszkowski and Stilling (2005), that this relative movement can be utilized for controlling oscillation of a pendulum. In that work, vibration of a physical pendulum which is oscillating about a pivot has been controlled by moving a mass along its length. Since the dynamic equations of this system were straight forward, the pendulum response to any relative mass motion could be obtained by directly integrating these equations. Then, it has been shown that the Coriolis acceleration induced to the moving mass due to its relative motion was 'physically' responsible for attenuation or amplification effects of the moving mass. By considering this conclusion, the mass motion pattern was then adjusted such that it continuously attenuated the pendulum's oscillations. However, this procedure has been shown to be challenging as the relative mass motion is normally associated with self-excited vibrations, i.e., they tend to amplify the structure's vibration (also referred to as the parametric resonance).

This research is an extension of the previous work on the pendulum, Stilling (2000). The first objective was to formulate and devise a method for modeling the moving mass-structure problems which can be applied for more complicated structures than the pendulum. In order to provide a proper computational tool, the standard Finite Element Method (FEM) formulation was extended in such a way that it includes all the relative mass motion effects. In some of the previous works available in the literature, modeling of such moving mass problems has been done mainly by other numerical methods like using infinite series, but also by applying FEM.

However, in most of these FEM works, the effect of the mass relative motion was not considered ‘completely’, for instance the effect of mass Coriolis acceleration was generally omitted. On the other hand, in a few works where the mass relative motion was ‘completely’ modeled, the FEM methodology was not suitable for control purposes (for instance they are mainly for cases with constant velocity of the mass).

The FEM approach proposed in the thesis was first verified on the pendulum’s case and then was applied for simulating the moving mass-beam and the moving mass-frame problems. Also for these problems the approach was verified by comparing the results obtained to those available in the literature. All the procedures required for securing accuracy, such as the element size, time step, etc, were established in this phase as well. The next objective of the research was to devise a mass motion pattern such that vibration of the main structure is continuously attenuated. As it has been shown in the research, this is more challenging for beams and frames, since the mass motion may affect by more than one vibration mode in such structures. By using the fact that the mass Coriolis acceleration is responsible for attenuation effects, as well as investigating different mass motion patterns, the mass motion pattern which results in the best continuous attenuation effects has been proposed for each structure.

5.2 Conclusions

The following conclusions can be made based on the results presented in thesis:

5.2.1 General conclusions

- It is shown (in chapters 2 and 3 of the thesis) that the proposed FEM approach is capable of modeling the moving mass-structure interaction accurately. However, the required time step should generally be much smaller, i.e. about 20 times smaller than that required for dynamic problems with no relative mass motion. Also, the element size

should be much smaller than normal dynamic analysis in order to render the mass relative motion accurately.

- As indicated in chapter 2 and 3 of the thesis, simulations show that properly including the effect of Coriolis acceleration may be essential for correct modeling of the moving mass problems (the solution is considerably different when this effect is not included). This effect is modeled by introducing the Coriolis force vector which is applied only to the element traversed by the mass.
- The three different patterns proposed for applying the Coriolis force vector are compared against one another and it is shown that the results obtained by using them are close as long as the element size is relatively small. It is also noted that since the element size should be small for obtaining sufficient accuracy, this condition is normally satisfied.
- The general scheme suggested for synchronizing the mass motion with the structure's vibration is proven to be effective. If this synchronization is not done properly, then the beating phenomenon, in which vibration attenuates and amplifies periodically, occurs in the structure.
- The three proposed synchronization schemes are compared against one another and their effectiveness is shown to be generally close. However, for some cases (like the beam and frame problems) only the third scheme, mentioned in section 3.3, is capable of giving results with high and continuous attenuation rate.

5.2.2 Conclusions for the pendulum problem

- Generally, the proposed control approach is capable of effectively and continuously attenuating the pendulum's vibration. Compared to the beam and frame structures, the attenuation of vibration is smoother and its rate is higher for the pendulum since the moving mass-pendulum structure has only one vibration mode.
- It is shown that the equivalent active damping ratio due to the mass motion increases almost linearly with the amplitude of mass motion, doesn't change much with the mass average position and increases with the mass of the moving body. For the case considered in the thesis, the maximum active damping ratio for the pendulum was about 8.2%.

5.2.3 Conclusions for the beam problem

- The results obtained by the proposed FEM approach are in agreement with those obtained by using infinite series. However, for some cases, the numerical integration for the infinite series method diverges and no solution is obtained which shows the significance of using FEM for modeling of such moving mass problems.
- It is indicated that including the mass Coriolis and centripetal accelerations can affect the response of the beam considerably. In particular, the effect of mass centripetal acceleration increases with the velocity of the moving mass while the Coriolis effect increases up to a particular velocity and then decreases. It is also concluded that for relatively low velocities, which is normally the case for control problems (as considered in this research) including the Coriolis effect is more important than including the centripetal effect.

- Comparison of the results obtained for different beams, i.e. cantilevered beam, simply supported beam, etc, shows that the control process can be different for each case. The reason lies in the difference in frequency spectrum of the beams. In particular, it is indicated that attenuation is more challenging to achieve when the first few natural frequencies are close. Also, the control process can be difficult when the ratio of the natural frequencies is an integer, like for the simply supported beam in section 3.3.2.
- For the cantilevered beam, it is shown that vibration cannot be damped completely due to the presence of the second mode in the response. On the other hand, if a relatively small natural damping is included (an equivalent damping ratio of about 0.1% was used in the numerical model) vibration is completely eliminated with an effective damping ratio of about 3.4%.
- For the problems considered in this research (where the first natural frequency is almost the same as for the pendulum problem) the maximum active damping ratio obtained for the cantilevered beam is about 4.5%. Also, the damping ratio increases almost linearly with mass motion amplitude and increases, with a trend that goes asymptotically to a particular maximum, with mass of the moving body. Finally, results show that active damping ratio is generally larger when the mass moves closer to the free end of the beam.
- For the simply supported beam, it is shown that the mass motion for controlling the first mode is exciting the second mode and thus vibration is not attenuated completely even with inclusion of natural damping. This is a result of the integer ratio of the second natural frequency over the first one. To overcome this issue, the mass motion parameters should be adjusted such that the second mode is excited minimally. Doing

so, the vibration can be completely eliminated and the maximum obtainable damping ratio is about 1.5%.

- Another method proposed for complete elimination of vibration for the simply supported beam is to attach one or two vertical rigid guiding bars (perpendicular to the longitude axis of the beam) to the beam and move the mass along these guiding bars. Analyses show that the method can raise the damping ratio up to 1.8% when one bar is used and up to 4.1% when two are used.
- A particular case of the simply supported beam where the first and second natural frequencies are very close (this difference can be adjusted by a rotary inertia mass placed at its center) is also investigated. It was shown that controlling vibration is more challenging for this case as vibration is dominated by two modes (of almost equal natural frequencies) at the same time. In fact, for this beam, which is essentially a bi-modal structure, no satisfactory vibration control was achieved and further investigations are required.

5.2.3 Conclusions for the frame problem

- The proposed composite beam element can be used for the analysis of a frame response to moving mass (or masses) and then uses the mass motion for control purposes. However, since the frequency spectrum of the frame is different than that of the beam, the conclusions which can be made for the frame are somewhat different than those of the beam.

- It is shown that the control process of the frame structure considered here, with the first two natural frequencies close to one another, is different when the first, second or both vibration modes are initially excited. This is why these cases are studied separately.
- For the frame considered here, when the first mode is excited initially and one mass is used for control process, the maximum obtainable damping ratio is about 0.8% which is rather low. When the second mode is initially excited, higher damping ratios, up to 3.0%, can be achieved.
- In order to improve attenuation effects for vibration control of the first mode, it is proposed that more than one moving mass be used. Moreover, a stationary mass should be placed at the center of the frame's lower member to differentiate the first two natural frequencies. Doing so leads to smoother responses and eventually higher active damping ratios, up to 2.7%, was obtained.
- For the case where both the first and second modes are initially excited, one approach is to use three masses and the other is to use four masses. When three masses are used, the maximum obtainable active damping ratio (for the frame considered here) is 0.9% for the first mode and 1.9% for the second mode. When four masses are used, the damping ratios of the first and second modes are both 2.2%.
- It is shown that frame response is very sensitive to the mass motion parameters, especially when more than one mass is used for control purposes. Consequently, the mass motion parameters should be adjusted carefully.

5.3 Recommendations for Future Works

The following suggestions are made for further works related to this research:

- So far the mass motion pattern was limited to a sinusoidal one. For obtaining possible higher attenuation effects and also smoother responses, other mass motion patterns can be examined.
- The proposed vibration control approach can be used for other more complicated structures. One may start with, for instance, controlling flexural vibration of a two dimensional plate, which can be modeled by using shell elements. The FEM formulation presented here can be extended to a shell element on which a mass is moving in two dimensions or can be applied directly by simply using the current beam elements (real or fictitious) along the path of mass motion on the plate.
- In this research, the focus was on proposing a mass motion pattern such that vibration is attenuated continuously. In practice, any part of the equipment may be moved to provide the desired effects. Then, there will be a need for devising a system that controls the parts' motion according to the required pattern. As a next step, one may devise a smart self-controlled system in which vibrations of the structure are identified as the input, and the selected masses are moved on the structure as the output such that vibration is autonomously reduced.
- In all the analyses done in the research, it is assumed that the mass follows the planned pattern of motion precisely. In real applications, there might be some deviations from the pattern of motion due to inevitable imperfection of the actuators or controlling motors. Therefore, it is important to perform a sensitivity analysis in which the variation of the structure's response to small deviation in the planned mass motion pattern is investigated.

– In this research, the FEM approach was verified by comparing its results with those available in the literature. For further verification, an experiment can be devised where dynamic response of a moving mass-structure is investigated. For example, a relatively inexpensive experiment can be done on a very flexible beam (and a relatively long vibration period) along which a small mass is sliding and the deflection measured on particular points of the beam can be compared to what the FEM is predicting.

LIST OF REFERENCES

Esmailzadeh, E. and Ghorashi, M.(1995). Vibration analysis of beams traversed by uniform partially distributed moving masses. *Journal of Sound and Vibration*, 184 (1): 9.

Foda, M.A. and Abduljabbar, Z. (1998). A dynamic green function formulation for the response of a beam structure to a moving mass. *Journal of Sound and Vibration*, 210(3): 295.

Garinei, A. and Risitano, G. (2008). Vibration of railway bridges for high speed trains under moving loads varying in time. *Engineering Structures*, 30(3): 724.

Henchi, K. and Fafard (1997), M. Dynamic behavior of multi-span beams under moving loads. *Journal of Sound and Vibration*, 199(1): 33.

Ichikawa, M., Miyakawa, Y. and Matsuda, A. (2000). Vibration analysis of the continuous beam subjected to a moving mass. *Journal of Sound and Vibration*, 230(3): 493.

Jiang, R.J., Au, F.T.K. and Cheung, Y.K. (2003). Identification of masses moving on multi-span beams based on a genetic algorithm. *Computers & Structures*, 81: 2137.

Kryloff, A. N. (1905). Uber die erzwungenen Schwingungen von gleichformigen elastischen Staben . *Mathematische Annalen*, 61: 211.

Lou , P. (2004). A vehicle-track-bridge interaction element considering vehicle's pitching effect. *Finite Element in Analysis and Design*, 41: 397.

Michaltsos, G.T. and Kounadism, A.N. (2001). The effects of centripetal and Coriolis forces on the dynamic response of light bridges under moving loads, *Journal of Vibration and Control*, 7: 315.

Nguyen, V.H. and Duhamel, D. (2006). Finite element procedure for nonlinear structures in moving coordinates. part 1: infinite bar under moving axial loads. *Computes & Structures*, 84: 1368.

Nikkhoo, A., Rofooei, F.R. and Shadnam, M.R. (2007). Dynamic behavior and modal control of beams under moving mass. *Journal of Sound and Vibration*, 306: 712.

Rieker, J. R. and Trethewey, M.W. (1999). Finite element analysis of an elastic beam structure subjected to a moving distributed mass train. *Mechanical Systems and Signal Processing*, 13(1): 31.

Sadiku, S. and Leipholz, H.H.E. (1987). On the dynamics of elastic systems with moving concentrated masses. *Ingenieur-Archiv*, 57: 223.

Schneider, H.J., Elf, H.P. and Kolle, P. (1983). Modeling of traveling-loads and time-dependent mass with ADINA. *Computers & Structures*, 17(5-6): 749.

Siddiqui, S.A.Q., Golnaraghi, M.F. and Heppler, G.R.(2003). Large free vibration of a beam carrying a moving mass. *International Journal of Non-linear Mechanics*, 38: 1481.

Stanisic, M. M. (1985). On a new theory of the dynamic behavior of the structures carrying moving masses. *Ingenieur-Archiv*, 55: 176.

Stilling, D.S.D. (2000). Vibration attenuation by mass redistribution. PhD thesis, University of Saskatchewan, Saskatoon, Saskatchewan.

Stilling, D.S.D. and Szyszkowski, W. (2002). Controlling angular oscillations through mass reconfiguration: a variable length pendulum case. *International Journal of Non-Linear Mechanics*, 37:89.

Szyszkowski, W. and Sharbati, E. (2009). On the fem modeling of mechanical systems controlled by relative motion of a member; a pendulum-mass interaction test case. *Finite Element in Analysis and Design*, 45: 730.

Szyszkowski, W. and Stilling, D.S.D. (2005). On damping properties of a frictionless physical pendulum with a moving mass. *International Journal of Non-Linear Mechanics*, 40:669.

Timoshenko S.P. (1911). Erzwungene schwingungen prismatischer stabe. *Zeitsch. f. Mathematik u. Physik*, 59(2): 163.

Watanabe, K., Awano, H. and Nishinari, K.(1997). The resonant frequency of a reciprocating load on an elastic beam. *Journal of Sound and Vibration*, 200(5): 621.

Xu, X., Xu, W. and Genin, J. (1997). A non-linear moving mass problem. *Journal of Sound and Vibration*, 204(3): 495.

Yang, Y.B. and Wu, Y.S.(2001). A versatile element for analyzing vehicle-bridge interaction response, *Engineering Structures*, 23: 452.

Yang, Y. B., Yau, J.D. and Wu, Y.S. (2004). *Vehicle-bridge interaction dynamics with applications to high-speed railways*, World Scientific Publishing Co. Pte. Ltd.

Yang, Y.B. and Lin, C.W. (2005). Vehicle-bridge interaction dynamics and potential applications. *Journal of Sound and Vibration*, 284: 205.

Zheng, D.Y., Cheung, Y.K., Au, F.T.K. and Cheng, Y.S. (1997). Vibration of multi-span non-uniform beams under moving loads by using modified beam vibration functions. *Journal of Sound and Vibration*, 212(3): 455.